

# **A cell line-based co-culture model of the inflamed intestinal mucosa and its application for safety and efficacy testing of nanomaterials**

Dissertation

Zur Erlangung des Grades des

Doktors der Naturwissenschaften

der Naturwissenschaftlich-Technischen Fakultät III

Chemie, Pharmazie, Bio- und Werkstoffwissenschaften

der Universität des Saarlandes

von

Julia Susewind

Saarbrücken

2015

Tag des Kolloquiums: 20.07.2015

Dekan: Prof. Dr.-Ing. Dirk Bähre

Berichterstatter: Prof. Dr. Claus-Michael Lehr  
Prof. Dr. Manfred Schmitt

Vorsitz: Prof. Dr. Uli Kazmaier

Akad. Mitarbeiterin: Dr. Jessica Hoppstädter

Die vorliegende Arbeit entstand auf Anregung und unter Anleitung von

Herrn Prof. Dr. Claus-Michael Lehr

am Lehrstuhl für

Biopharmazie und Pharmazeutische Technologie

an der

Universität des Saarlandes

"I meant," said Ipslore bitterly, "what is there in this world that makes living worthwhile?" Death thought about it. "CATS," he said eventually, "CATS ARE NICE."

Terry Pratchett, *Sourcery*

---

## Table of contents

Table of contents .....	1
Short summary .....	4
Kurzzusammenfassung .....	5
1 Introduction.....	6
1.1 Intestinal mucosa and inflammatory bowel disease .....	6
1.2 Treatment of IBD .....	9
1.3 <i>In vivo</i> models for IBD.....	11
1.4 Epithelial <i>in vitro</i> models .....	12
1.5 <i>In vitro</i> co-culture models of the intestine.....	13
1.6 Nanoparticles.....	16
1.7 Aim .....	17
2 Replacement of primary cells by cell lines in a 3D co-culture model of the inflamed intestinal mucosa .....	20
2.1 Introduction.....	21
2.2 Materials and Methods .....	24
2.2.1 Cell culture .....	24
2.2.2 Isolation of primary macrophages and dendritic cells.....	26
2.2.3 Three dimensional triple culture of epithelial cells, macrophages and dendritic cells.....	26
2.2.4 Transepithelial electrical resistance (TEER) .....	27
2.2.5 IL-8 measurement .....	27
2.2.6 Transmission electron microscopy (TEM).....	27
2.2.7 Immunostaining for confocal laser scanning microscopy (CLSM) .....	28
2.2.8 Statistical analysis .....	29
2.3 Results .....	29
2.3.1 Replacement of primary cells by cell lines .....	29
2.3.2 Morphological analysis of the cell line-based triple culture model with TEM and CLSM.....	33
2.3.3 Improvement of the triple culture model using the Caco-2 clone HTB37.....	36
2.4 Discussion .....	40
2.5 Conclusion.....	45
3 Cytotoxicity measurements of nanoparticles in the cell line-based co-culture model.....	46
3.1 Introduction.....	47
3.2 Materials and Methods .....	50

---

3.2.1	Nanoparticles (NPs).....	50
3.2.2	NP preparation and characterization.....	50
3.2.3	Cell culture .....	52
3.2.4	Triple culture of the intestinal mucosa.....	52
3.2.5	Cell viability measurement via lactate dehydrogenase (LDH) and Alamar Blue assay .....	53
3.2.6	Influence of Ag ions on cell viability .....	54
3.2.7	Transmission electron microscopy (TEM) .....	54
3.2.8	TEER.....	54
3.2.9	Cytokine measurement (IL-8) on the protein level via FACS.....	54
3.2.10	Cytokine measurement (IL-8 and TNF- $\alpha$ ) on the mRNA level via Real-time PCR .....	55
3.2.11	Statistical analysis .....	56
3.3	Results .....	57
3.3.1	NP characterization .....	57
3.3.2	Cell viability measurement – LDH and Alamar Blue assay.....	58
3.3.3	Assessment of Caco-2 cell integrity via TEER measurement.....	62
3.3.4	Impact of NPs on inflammatory response .....	63
3.3.5	Uptake of NPs .....	66
3.4	Discussion .....	67
3.5	Conclusion.....	73
4	Application of the cell line-based co-culture model for efficacy testing of anti-inflammatory formulations.....	74
4.1	Introduction.....	75
4.2	Materials and Methods .....	78
4.2.1	NP preparation by nanoprecipitation.....	78
4.2.2	PLGA MP preparation by nano spray drying.....	79
4.2.3	Determination of particle size and size distribution .....	80
4.2.4	Determination of encapsulation efficiency and optimal loading .....	80
4.2.5	Stability of NPs and MPs in cell culture media .....	82
4.2.6	<i>In vitro</i> drug release .....	82
4.2.7	Cell culture .....	83
4.2.8	Triple culture of the inflamed intestinal mucosa .....	83
4.2.9	LDH assay.....	84
4.2.10	TEER.....	84
4.2.11	IL-8 measurement .....	84
4.2.12	Immunostaining of the triple culture for CLSM .....	84

---

4.2.13	Statistical analysis .....	85
4.3	Results .....	85
4.3.1	Encapsulation efficiency and optimal loading.....	85
4.3.2	Size and size distribution of NPs and MPs.....	87
4.3.3	Stability of NPs and MPs in cell culture media .....	90
4.3.4	<i>In vitro</i> drug release studies.....	92
4.3.5	NP and MP cytotoxicity measurements.....	93
4.3.6	Dose finding experiments with Bu and CyA .....	95
4.3.7	Efficacy studies with Bu-loaded NPs and MPs.....	97
4.3.8	Efficacy studies with CyA-loaded NPs and MPs .....	101
4.3.9	Deposition of NPs and MPs in the triple culture model.....	104
4.4	Discussion .....	107
4.5	Conclusion.....	113
	Summary and outlook .....	114
	References .....	116
	Abbreviations .....	130
	List of publications .....	132
	Curriculum Vitae .....	134
	Danksagung .....	135

---

## Short summary

*In vitro* cell culture models are an important alternative for animal testing, as they are less ethically questionable and avoid the problem of non-representative results due to species differences. A previously established 3D co-culture model of the inflamed intestinal mucosa consisting of human epithelial and primary immune cells was further developed by replacing primary cells by two human monocytic cell lines in order to have a stable and more reproducible system, which shows a well preserved ultrastructure and good barrier properties.

With this model the safety of different nanoparticles (NPs) was investigated and it was shown that Ag NPs show a high cytotoxicity. Co-culture models incubated with Au NPs showed an inflammatory response although no toxic effects were measurable. Furthermore, differences between inflamed and non-inflamed co-cultures and Caco-2 monocultures were shown with the result that Caco-2 cells are more sensitive to toxic Ag NPs than the co-culture models.

For the treatment of inflammatory bowel disease (IBD) nano- and microparticulate drug delivery systems (DDS) were developed, containing anti-inflammatory compounds budesonide and cyclosporine A. The anti-inflammatory effect of the formulations on the inflamed co-culture was shown by TEER and IL-8 measurement.

In summary, the further developed co-culture model is a useful tool for safety testing of nanomaterials and can be used to test anti-inflammatory effects of DDS for the treatment of IBD.

---

## **Kurzzusammenfassung**

*In vitro* Modelle sind eine wichtige Alternative zu Tierversuchen, da sie ethisch weniger fragwürdig sind und nicht-repräsentative Ergebnisse aufgrund von Spezies-Unterschieden vermeiden. Ein 3D Co-Kultur Modell der entzündeten Darmmukosa, bestehend aus menschlichen Epithel- und primären Immunzellen wurde entworfen, welches in der vorliegenden Arbeit weiterentwickelt wurde, indem die Primärzellen durch Zelllinien ersetzt wurden, um ein reproduzierbareres Modell zu erhalten.

Mit diesem Modell wurde die Sicherheit verschiedener Nanomaterialien untersucht und es wurde gezeigt, dass Ag NP zytotoxisch wirken. Zell-Modelle, inkubiert mit Au NP, zeigten eine entzündliche Antwort, obwohl keine Toxizität gemessen werden konnte. Zusätzlich wurde gezeigt, dass Caco-2 Monokulturen empfindlicher gegenüber toxischen Ag NP sind als die Co-Kultur Modelle.

Für die Behandlung entzündlicher Darmerkrankungen wurden nano- und mikropartikuläre Arzneistoffträgersysteme entwickelt, die die anti-entzündlichen Verbindungen Budesonide und Ciclosporin A enthalten. Der anti-entzündliche Effekt dieser Partikel wurde im entzündeten Co-Kultur Modell des Darms durch TEER und Zytokin Messungen gezeigt.

Dies zeigt: Das weiterentwickelte Co-Kultur Modell ist ein nützliches Werkzeug für Sicherheitstests von Nanomaterialien. Darüber hinaus kann es genutzt werden, um anti-entzündliche Effekte von Arzneistoffträgersystemen für die Behandlung entzündlicher Darmerkrankungen zu testen.

---

# 1 Introduction

## 1.1 Intestinal mucosa and inflammatory bowel disease

Approximately  $10^{14}$  microorganisms from 1000 different species, corresponding to 10-fold the number of cells in the human body, are located in the human gastrointestinal (GI) tract. At birth the human intestine is a sterile area and bacterial colonization only begins during the delivery process [1]. The intestinal epithelium with its huge surface area ( $\sim 100\text{m}^2$ ) forms a physiological barrier [2], and probiotic bacteria in the GI tract contribute to this barrier function through e.g. effects on epithelial tight junction proteins, prevention of epithelial apoptosis, increased production of intestinal mucus or increased stimulation of defensin production [1].

Nowadays, inflammatory bowel diseases (IBD) such as Crohn's disease (CD) and ulcerative colitis (UC) are serious and incurable diseases. In the US, about 1-2 million people are affected by such diseases [3]. Patients in particular with CD often need surgical intervention, and their mortality rate is greater than that of the general population. However, the prognosis of IBD patients in general is not so easy to determine [4], and in fact, differentiation between diseases may also prove difficult. Both CD and UC affect parts of the GI tract and the colonic mucosa. They both show similar symptoms (such as diarrhea, fever, muscle aches, abdominal pain, weight loss or bloody stool) and lead to an increased risk of colon cancer [5]. However, while CD can cause inflammation anywhere in the lining of the GI tract, UC is characterized by a long-lasting inflammation specifically in the large intestine [6] (Figure 1.1). So far the detailed pathogenic mechanisms of IBD remain to be fully elucidated, although worldwide a strong correlation between IBD and environmental factors has been detected [7]. Furthermore, genetics, immune dysfunction and changes in the microbiome could be reasons for the appearance of IBD [8].

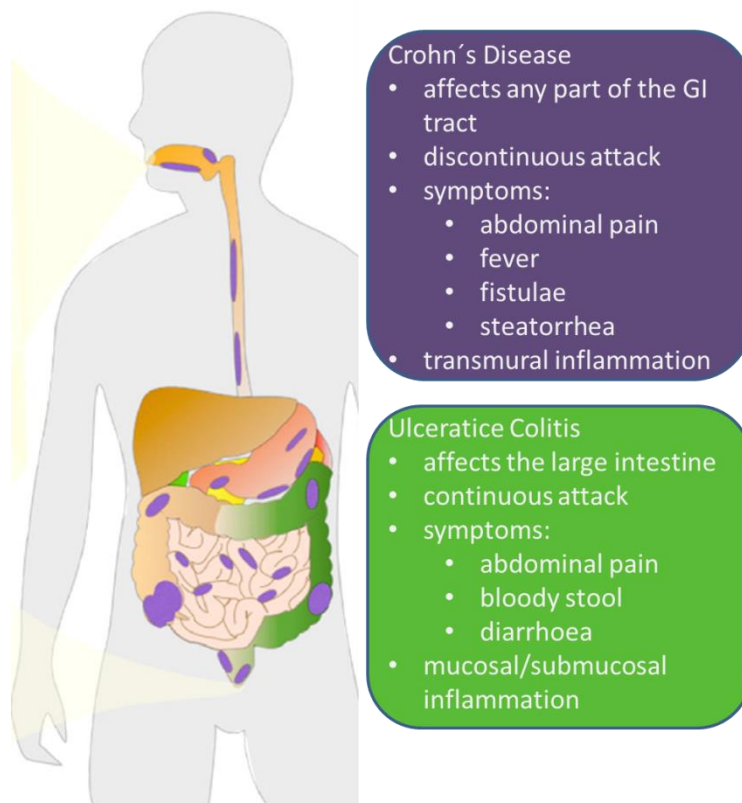


**Figure 1.1: Disease areas and symptoms of CD and UC** (based on Lautenschläger et al. [9]).

The state of IBD highlights the important role of the microbiome in gut barrier function - in IBD patients an excessive, cell-mediated inflammation is induced in response to normal bacterial microflora antigens; as a result, an abnormal permeability and gut barrier function can be observed in affected and non-affected GI areas [10].

In the light of the abnormal response to normal gut contents seen in IBD, diet control is quite important for IBD patients as a means to control their disease symptoms. The removal of specific foods, suspected to worsen patients conditions, is an important factor for dietary optimization [11]. The importance of diet is highlighted by the fact that IBD occur more frequently in western countries, where diet control is a problem, than in underdeveloped regions. Western food, with large amounts of animal fat and proteins and comparatively less fiber, may influence the gut microbiome and could increase the risk of IBD [12]. However, the other possibility is that people in more industrialized countries are

exposed to fewer microorganisms because of the higher hygienic standards in such areas, and as a result the immune system is not able to tolerate too many microorganisms. Smoking also influences the development of IBD. It was shown that smoking increases the risk of extra-intestinal manifestations in CD [13], [14]. Surprisingly, smoking seems to protect people from UC, which is largely a disease of non-smokers [15]. However, so far the reason for this unusual association remains unclear [16], and scientific studies have failed to confirm a beneficial effect of smoking for UC patients [17].

With respect to the treatment of IBD, several changes in the GI tract must be considered. Firstly, the transit time through the intestine varies between healthy and diseased persons. In healthy persons the transit time through the small intestine is approximately 4 hours, and varies in the colon between 6 and 70 hours [18]. Contrary to this, the transit time in IBD patients is twice as fast as in healthy persons due to the occurrence of diarrhea, which, as mentioned, is a common symptom of this disease [19]; this significantly faster transit time makes it very difficult to target drug formulations for IBD treatment to the affected regions of the GI tract. Another difference is the colonic pH value: in UC and CD patients this is significantly lower than in healthy persons. The intestinal pH is influenced by microbial fermentation, intestinal volume and transit times [20] – all these are factors which are disrupted during IBD. Furthermore, the mucosal integrity is altered by the IBD-associated inflammation as is the mucosal metabolism [21]. Additionally, mucus production is higher in diseased tissue [22], which also makes it difficult for drug treatment formulations to reach the inflamed area. Therefore, the evaluation of new strategies in the treatment of IBD is a point of extreme importance.

## 1.2 Treatment of IBD

So far there is no medical cure for IBD, and a lifetime of drug therapy for the maintenance of life quality is often necessary. A group of anti-inflammatory drugs including 5-aminosalicylic acid (5-ASA) is commonly used for the therapy of mild types of IBD [23]. When this therapy fails patients are often treated with other drugs such as infliximab, which is a chimeric monoclonal antibody directed against the inflammation-related cytokine tumor necrosis factor- $\alpha$  (TNF- $\alpha$ ). Such antibodies increase the production of anti-inflammatory cytokines including interleukin-4 (IL-4), IL-5 and IL-10, which in turn inhibit production of pro-inflammatory cytokines. Corticosteroids are also used as more effective drugs in severe forms of IBD. Biological drugs (such as antibodies), 5-ASA and immunosuppressants can each be effective in their own way. However, under some circumstances medication fails and patients require surgery. In many cases this may consist of a colectomy, in which parts of or the entire large intestine is removed. After removal cases of UC may be cured, however, CD can still recur after this type of surgery [6].

With respect to medical treatments serious side effects can occur. Many drugs can induce side effects ranging from mild to severe in nature; this may even include mortality in some cases. Corticosteroids often induce hypertension, osteoporosis and glaucoma as well as many other effects. Treatment with immunosuppressants leads to an increased susceptibility to infections and malignoma. Therefore it is important to attempt to achieve and to maintain a balance between effective IBD treatment and the risk of occurrence of adverse drug reactions. The ability to treat IBD with anti-inflammatory agents at an effective dose, which does not induce any side effects, would be the ideal situation [9].

Oral treatment of IBD with anti-inflammatory drugs or antibodies has shown success against inflammation [24]. The limitation of such treatments however is that drugs are transported non-specifically to cells of the human body, which can also lead to several side effects such as headache, vomiting or diarrhea, all of which have the potential to

worsen patient conditions [6]. Therefore it is important not only to be able to deliver drugs at an effective and safe dose, but also to develop drug delivery systems (DDS) for the transport of drugs to the specific target site. For this purpose nano- and microparticulate DDS are often used. These can accumulate in the inflamed tissue and release the drug specifically at the target site, as shown in Figure 1.2. As mentioned previously the GI tract in IBD patients shows disrupted barrier properties and increased mucus production, which makes it easier for the particles to accumulate in such affected areas. Furthermore, immune competent cells such as macrophages and dendritic cells are able to penetrate and migrate through the disrupted barrier, and take up the particles.

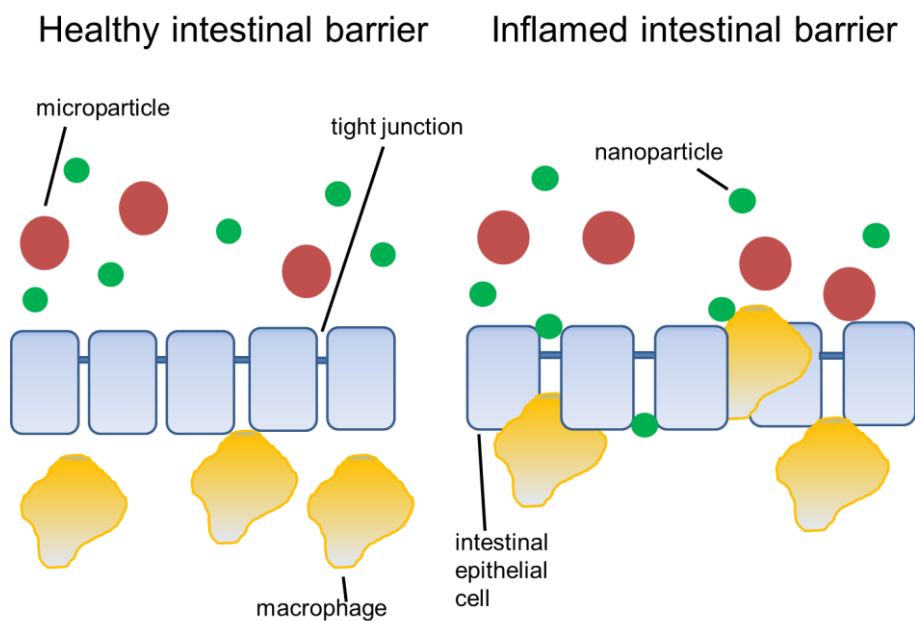


**Figure 1.2: Mechanism of particle accumulation in the inflamed intestinal mucosa.** Particles may accumulate between epithelial cells, because tight junctions are disrupted, or be taken up by macrophages (based on Collnot et al. [25]).

The use of nano- and microparticles is therefore an excellent strategy in the treatment of IBD, as an improvement of drug efficacy and colonic uptake can be seen to result from inflammation site-specific targeting. A better bioavailability in the diseased tissue and a

reduction of side effects resulting from non-specific delivery are also seen. Additionally, lower drug concentrations are needed in particulate systems as compared to conventional formulations, also reducing the risk of adverse drug effects [25].

Before such DDS can be used for human IBD patients, it is important to test their efficacy and of course their safety in biological models. There are several animal models that can be used for investigations related to IBD.

### **1.3 *In vivo* models for IBD**

The term “IBD animal model” is defined as a model which is characterized by chronic or relapsing inflammation of the GI tract with features resembling human IBD [26]. Two models are very often used for this purpose, because of their high reproducibility: the DSS model and the TNBS model. In the first case, dextran sodium sulfate (DSS) is given to mice orally in their drinking water for five days. Afterwards mice show typical symptoms of IBD such as weight loss, diarrhea or bloody stool. Inflammation can be analyzed e.g. by histological methods or measurement of inflammatory markers including IL-8 and TNF- $\alpha$  [27]. The DSS model is mostly used for investigations of UC, while the TNBS model is more often used for CD. In the case of the TNBS model, rodents are treated intra-rectally with 2,4,6-trinitrobenzene sulfonic acid (TNBS), which is dissolved in alcohol to induce gut inflammation and barrier disruption [28]. While DSS and TNBS are able to readily induce symptoms of IBD in model species, many animals die during the experimental time, which makes these chemically-induced models in fact rather variable and unpredictable. As an alternative, genetically-modified IL-10 knockout mice have been established. In this model animals develop a time-dependent IBD-like disorder in the colon [29]. Unfortunately this model is more expensive and shows a higher sensitivity than the chemically induced models.

It can therefore be seen that serious problems and difficulties exist with respect to IBD in *in vivo* experiments. Additionally the interpretation of data from animal testing is often

further complicated by the species differences between rodents and humans. *In vivo* testing in animals in general is also more expensive and ethically questionable in comparison to *in vitro* studies. Furthermore, the new REACH (Registration, Evaluation, Authorization and Restriction of Chemical substances) regulations, which also cover nanomaterials, greatly increase the number of substances which must be tested thus overwhelming the capacities of *in vivo* animal testing.

#### **1.4 Epithelial *in vitro* models**

Cell culture-based *in vitro* models are a very important alternative to animal testing. They are often used for studying the processes of drug absorption, distribution, metabolism and excretion (ADME). The epithelial cell line Caco-2, a human colon adenocarcinoma cell line, which, having been used for the last 20 years as a means to mimic the GI epithelium, is an established cell culture model of the human intestinal barrier [30]. A study that compared 20 different intestinal cell lines found that Caco-2 cells show the highest correlation to the *in vivo* situation [31]. On permeable cell culture supports Caco-2 cells grow in a monolayer and show a cylindrical polarized morphology with microvilli on the apical side. They express small intestinal enzymes, transport proteins and functional tight junctions [32]. In such a system, the permeable supports on which cells are grown generally consist of 10  $\mu\text{m}$  thick polyester or polycarbonate membranes, which are incorporated into culture plate insert systems. Such insert systems result in division of the cell culture plate well into an apical compartment, which mimics the intestinal lumen, and a basolateral compartment, which represents the blood side. To investigate the tightness of the Caco-2 monolayer representing the epithelial barrier, the transepithelial electrical resistance (TEER) can be measured in these systems, giving readings with the units of  $\Omega\cdot\text{cm}^2$ . The tighter the epithelium, the higher is the measured TEER value.

Epithelial cells constitute the major cell type in the intestinal mucosa and cover the majority of the intestinal surface ( $\sim 250\text{ m}^2$ ). Thus they are the main interface for

interaction and absorption, and as such the Caco-2 monolayer system has consequently been accepted by regulatory authorities as an *in vitro* model to predict oral drug bioavailability. The Caco-2 *in vitro* model is a very useful means to investigate the absorption and permeation of small drug molecules because Caco-2 cells grow into monolayers with a differentiated phenotype with many functions of the small intestinal villus epithelium [33].

However, one cell type alone cannot mimic the behavior of a whole tissue. Therefore, while Caco-2 monolayers are a very important tool for drug absorption and bioavailability studies, there are some limitations to this model with respect to its use in other applications. An important limiting factor in the case of safety testing for example is the lack of immune competent cells (e.g. macrophages and dendritic cells), which play a key role in the response to exposure to toxic materials (such as certain nanoparticles). Furthermore, the presence of immune cells is very important for studies concerning inflammation, as they are responsible for the production of pro-inflammatory cytokines such as IL-8, IL-6 or TNF- $\alpha$ . Therefore, the development of novel co-culture systems, consisting of two or more cell types, is very important for *in vitro* testing of nanomaterials or drug delivery systems.

### **1.5 *In vitro* co-culture models of the intestine**

Several co-culture models have already been established and are well described in literature. A lot of these models are related to the lungs and respiratory tract, as for example the model from Rothen-Rutishauser et al., which consists of epithelial cells (A549), macrophages and dendritic cells, and is designed to study the interaction of lung tissue with nanoparticles (NPs) [34]. This model was even further developed by using primary alveolar type I cells to present a more realistic alveolar barrier [35].

Regarding intestinal co-cultures, several models have been established in order to investigate the penetration of drugs or NPs, many of which include M-cells and goblet

cells. M-cells play a role in the uptake and delivery of NPs or other substances, whereas goblet cells produce mucus (in far greater quantities than Caco-2 cells alone), which also influences the permeability of the epithelial layer. In a typical example of such a co-culture Des Rieux et al. developed a model of Caco-2 cells with M-cells. In order to produce such a model Caco-2 cells were seeded in the apical compartment of a transwell filter insert and Raji B cells were introduced into the basolateral compartment [36]. These cells release soluble mediators which are responsible for differentiation of Caco-2 to M-cells. Des Rieux et al. further improved this model by inverting the insert with the Caco-2 cells to get closer contact between the two cell types, making such a model physiologically more relevant for permeability studies with NPs because it leads to more efficient cell differentiation [37].

A similar model was established by Antunes and colleagues, who combined Caco-2 and Raji B cells with the mucus-producing cell line HT29. They developed one model with Caco-2 and HT29 cells seeded in the apical and Raji B cells in the basolateral compartment and one model in which the converse was true. With both models they performed permeability studies which showed that such a triple culture model leads to more reliable results than *in vitro* models with one or even two cell types because it could be seen that insulin permeation was faster in the triple culture models [38].

Araújo et al. established a similar model with Caco-2, HT29-MTX and Raji B cells with a seeding ratio of 90:10 between Caco-2 and HT29-MTX cells in order to closely mimic the physiological proportion of each cell [39]. Yet further studies have shown that the seeding day is important for such co-culture systems: when Caco-2 cells were grown for 21 days and HT29-MTX cells were seeded after different time points, it was found that after earlier seeding more goblet cells were present, which influenced the permeability of luciferase yellow and rhodamine123 [40]. The latest co-culture system with Caco-2, HT29-MTX and Raji B cells was established in 2014 by Schimpel et al., who also performed permeability studies with drugs and NPs and could show that goblet and M-cells have a huge influence in these studies [41].

As already mentioned all these models were developed for the purpose of permeability testing: there are even more co-culture models of the intestine in existence for other purposes. A model with Caco-2 cells in the apical compartment and lymphoblastoid TK6 cells in the basolateral compartment of transwell inserts was established for modelling the role of intestinal first-pass effects (such as absorption and metabolism) in the genotoxicity of orally-delivered drugs [42]. Other models with human submucosa and HT29-CI.16E as epithelial cells have been used to investigate the role of the human enteric nervous system in the control of the intestinal lumen organization and proliferation [43], while models with Caco-2 cells and peripheral blood mononuclear cells (PBMCs) in different compartments of a transwell system have been employed to determine reactivity to non-toxic bacterial signals [44]. Holland-Gunz et al. seeded enteric glial and nerve cells from rats in a collagen layer with HT29 enterocytes on top to prepare a basic model suitable for placement on cover slips [45].

Yet further models have been established for cytotoxicity testing, such as one model with Caco-2 cells in the apical compartment and PBMCs in the basolateral compartment of a transwell system. Toxicity studies performed with arsenic showed that the release of the pro-inflammatory marker TNF- $\alpha$  was increased, more in the basolateral compartment with PBMCs than in the apical compartment with the Caco-2 cells which proves how important immune competent cells are for pro-inflammatory reactions. This model was also inflamed with bacteria-derived lipopolysaccharides (LPS), which showed an even further increase in the amount of produced TNF- $\alpha$  [46].

As has been discussed, the ability to mimic a state of inflammation is a very important factor for IBD models. There are some fundamental differences between healthy and inflamed tissue as for example epithelial barrier disruption. Bisping et al. established a co-culture model with epithelial cells (Caco-2 or primary cells) together with PBMCs from healthy persons, or from IBD patients. The models containing cells from IBD patients released significantly more Interferon- $\gamma$  (IFN- $\gamma$ ), a pro-inflammatory marker, than the models containing cells from healthy persons [47]. In addition to IFN- $\gamma$ , other pro-

inflammatory cytokines can also be up-regulated in a state of inflammation leading to several measurable inflammatory markers. As the epithelial barrier is disrupted in inflammatory states, TEER values of the epithelial barrier can also be monitored. A decreasing TEER value can be used as an indicator of inflammation, as was observed in the co-culture model of Tanoue et al. after inflammation with LPS [43]. Other co-culture models available for IBD include a model with T84 epithelial cells, CCD186 myofibroblasts and lamina propria mononuclear cells, designed for the investigation of the interaction between cell types and evaluation of their role in barrier integrity [48], and a model with Caco-2 and THP-1 cells, which showed a disrupted epithelial barrier, low TEER values and high TNF- $\alpha$  release from activated THP-1 cells [49].

However, despite the existence of these numerous models, so far only one model has demonstrated good barrier properties suitable for NP translocation studies. This model combines the Caco-2 intestinal epithelial cell line with primary blood-derived dendritic cells and macrophages embedded in a collagen type I gel [50] and was developed in our research group. In this setup also a reversible inflammation could be induced by addition of the pro-inflammatory cytokine IL-1 $\beta$ , and the model was successfully applied to the testing of anti-inflammatory formulations, such as NPs, for the treatment of IBD [51]. Due to the presence of immune cells, this model should also be a useful tool to test cytotoxicity of NPs, which is a very important point, because NPs are frequently used in food packages, sun creams and wound healing products.

## **1.6 Nanoparticles**

NPs by definition have a size between 1 and 100 nanometers, and differ from other materials as a result of their large relative surface area. Because of this huge surface area they can show differences in properties such as reactivity, strength and electrical characteristics relative to other materials [53]. Furthermore, interaction of NPs with

biological media and cells is different to that of micro- and macrostructured materials as absorption pathways and cellular internalization differ.

Currently, nanoparticles can be found in many consumer products. They serve for example as surface coatings in paints, in food packages or in sun cream. Research on NP-associated toxicity has been focused for a long time on airborne particles. However, a large fraction of these particles never reaches the deeper lung, as particles impact in the throat and upper airways and are removed from the bronchi by mucociliary clearance, to be swallowed afterwards. Thus, such NPs in fact gain access to the GI tract. More importantly, engineered nanomaterials are also employed in food packaging or as additives in various food products. As already mentioned, they are also used in innovative drug delivery systems as they can passively or actively target drugs to their site of action and can protect their cargo from degradation [52].

There is still a huge concern about the safety of nanomaterials. Engineered nanomaterials can often be found in textiles and can end up in soils or wastewater [54]. Other nanomaterials are also used in construction and related infrastructure industries [55] and many NPs are used as food supply through novel applications, nutrient and bioactive absorption, improved colors and flavors or food packaging [56]. All these points make it very important to know more about the possible toxicity of nanomaterials, especially after reaching the GI tract.

## **1.7 Aim**

The first step of this work was to further develop the co-culture model of the inflamed intestinal mucosa, as established by Leonard et al. [50], by replacing the utilized primary immune cells with cell lines. Primary cells show a high variability, as they are isolated from different patients' blood samples. Additionally the isolation of the cells for every experiment is time consuming and expensive. The use of cell lines in such a model would therefore make the model more reproducible and easier to use. For this purpose THP-1

cells were stimulated with phorbol-12-myristate-13-acetate (PMA) in order to facilitate differentiation to macrophage-like cells; MUTZ-3 cells were used as dendritic-like cells and both were co-cultivated in a collagen layer with Caco-2 cells on top in order to mimic the intestinal mucosa (Figure 1.3).

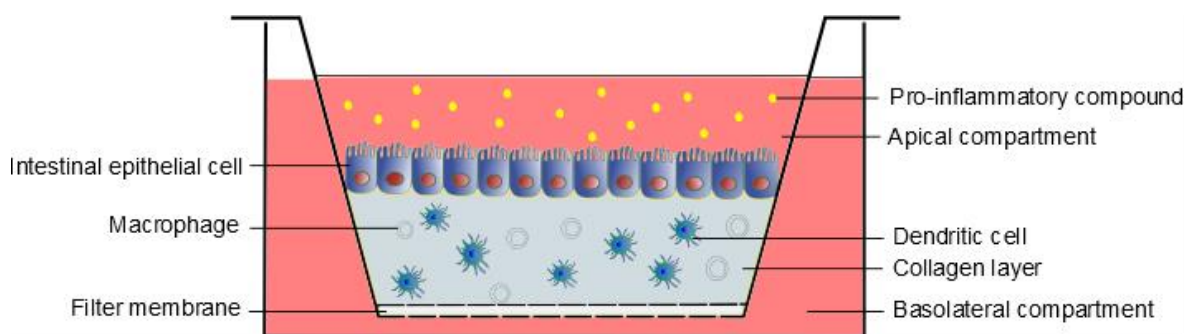


**Figure 1.3: Experimental setup of the co-culture of the inflamed intestinal mucosa.** Dendritic cells and macrophages are embedded in the collagen layer. Epithelial cells are seeded on top of the collagen. The model can be inflamed by adding of IL-1 $\beta$  into the apical compartment.

Following replacement of the primary cells by cell lines, it was tested whether the model showed the same behavior as previously, in order to see if the replacement of the cells was successful. Therefore, IL-1 $\beta$  was used as an inflammatory stimulus. Barrier properties (TEER) and release of the pro-inflammatory cytokine IL-8 were monitored and compared between the previously developed, primary cell containing model and the newly developed, cell line-based model.

As a second task the newly-established co-culture model was used to test the cytotoxicity of different engineered NPs. Ag, TiO<sub>2</sub> and two differently-sized Au NPs were tested in different concentrations with 24 hours incubation times. These particles are often used in food packages, tooth paste or in the medical field; they therefore have a high degree of exposure, which makes it very important to test the safety of these particular engineered nanomaterials. Cytotoxicity was measured by cell membrane damage (LDH assay),

mitochondrial activity (Alamar Blue assay), membrane integrity (TEER) and inflammation (IL-8 and TNF- $\alpha$  release). The results of inflamed and non-inflamed co-culture were compared to the results with a non-inflamed Caco-2 monoculture, to observe if they react differently due to the presence of immune cells and to determine whether the co-culture model showed a more realistic result than a model containing just one cell type.

The last part of this thesis shows another investigated application of the further developed *in vitro* system: the efficacy of drug loaded nano- and microparticles was tested within this model, in the context of local anti-inflammatory drug therapy. Budesonide- and cyclosporine A- (two anti-inflammatory drugs) loaded nano- and microparticles prepared by spray-drying and nanoprecipitation (PhD thesis, Christina Draheim) were used to treat the inflamed co-culture. The anti-inflammatory effect was determined by TEER and IL-8 measurements. Results were compared to culture treatment with free drug solution and blank nano- and microparticles. Confocal images showed the accumulation behavior of the particles in the cell culture model.

Therefore, the overall aim of this thesis was to show the successful further establishment of the co-culture model of the inflamed intestinal mucosa, constituted of cell lines, to use it as a tool to test not only the cytotoxicity of nanomaterials, but also the efficacy of nanomedicines.

---

## 2 Replacement of primary cells by cell lines in a 3D co-culture model of the inflamed intestinal mucosa

Parts of this chapter have been published in:

**J. Susewind**, C. de Souza Carvalho-Wodarz, U. Repnik, E.-M. Collnot, N. Schneider-Daum, G. W. Griffiths, and C.-M. Lehr, “A 3D co-culture of three human cell lines to model the inflamed intestinal mucosa for safety testing of nanomaterials,” *Nanotoxicology*, vol. 5390, pp. 1–10, 2015.

Julia Susewind made the following contributions to this publication: performed all cell culture experiments, measured TEER and IL-8 data, made confocal images, analyzed all data and wrote the manuscript.

## 2.1 Introduction

*In vitro* cell culture models are very important tools for safety testing, permeability studies and efficacy studies of newly developed drugs. There are a lot of established *in vitro* models for many purposes. For the intestine the most frequently used and well-established model is the Caco-2 cell model, which is commercially available. As already mentioned in the first chapter, this is a human colon adenocarcinoma cell line, which has been used for the last 20 years as model for the intestinal barrier [30]. The most frequently used Caco-2 clone is clone C2BBE1. The clone HTB37 is the parental Caco-2 clone, from which the cell line Caco-2 C2BBE1 was cloned in 1988 by limiting dilution. Caco-2 cells exhibit structural and functional differentiation patterns typical of enterocytes: the surface of the cell layer is covered by brush border microvilli, tight junctions are formed between the cells and a polarization of the cell monolayer can be seen [57]. The brush border of these cells is comparable to the human colon and contains microvillar proteins such as villin, fimbrin and sucrose-isomaltase [58]. In a comparison of different colon carcinoma cell lines, it was found that Caco-2 cells exhibit a better morphological and functional differentiation to enterocyte cells than the other tested cell lines [31]. Caco-2 cells can be grown on permeable filter supports in cell culture plates that form an apical and a basolateral compartment to better mimic the *in vivo* conditions of the intestinal lumen and blood side respectively. These supports also allow the free access of ions and nutrition to both sides of the epithelial monolayer, which leads to an even further improvement in morphological and functional differentiation. Furthermore, this enables the model to be used in transport and toxicity studies. The integrity of the cell monolayer can be measured via TEER with an EVOM (epithelial voltohmmeter) and ultrastructural morphological analysis can be performed via electron microscopy [30].

A limitation of the Caco-2 cell model is that it is not a good tool for absorption or toxicity studies of small molecules or entities, such as nanoparticles. Furthermore, *in vivo* interactions of molecules with the intestinal mucosa are not limited to enterocytes. For this

reason, it is also important to look at other cell types. Specialized epithelial cells, the so-called M-cells, and antigen presenting cells have shown a great ability to internalize nano- and microparticles. Many NPs are first taken up by phagocytes of the immune system (e.g. macrophages). These interactions between immune system and nanomaterials can lead to inflammatory reactions. Immune cells recognize NPs by their surface properties and mount an inflammatory response which includes the release of cytokines [59]. Although the immune system's task is to protect the body from foreign substances, the immune response against the NPs can lead to toxicity [60]. Thus monocultures of epithelial cell lines are not sufficient to mimic this complex interplay of cells and particles. The predictive power of *in vitro* models could be enhanced in a co-culture setting of innate immune cells and epithelial cells.

Another point that has to be considered for *in vitro* models of IBD is the inflammation status. In IBD patients several regions of the human intestine show inflamed areas. This should also be addressed in an appropriate *in vitro* model. Caco-2 cells alone cannot mimic this inflammation because other cell types, such as immune cells, play key roles in this process. Therefore, a 3D co-culture of the inflamed intestinal mucosa was developed by Leonard et al. [50] with Caco-2 cells together with primary blood mononuclear cells (PBMCs), which were isolated from blood samples and differentiated to macrophages and dendritic cells. The immune cells were seeded in a collagen layer with Caco-2 cells as epithelial barrier on top. It could be shown that this model exhibits good barrier properties after a growth time of 21 days. After inflammation with IL-1 $\beta$  a decrease of TEER and an increase in production of IL-8, a pro-inflammatory cytokine, could be measured. Furthermore, the inflammation was reversible - it could be shown that after removal of IL-1 $\beta$  a decrease of IL-8 release and increase of TEER back to the starting value before inflammation occurred [50]. However, there are some limitations of this model related to the use of primary cells. These cells have to be isolated from buffy coats, which is an expensive and time-consuming procedure. An even more important point is that the blood comes from different patients with different conditions of the cells, which is a problem for

the reproducibility of the model. Cell lines offer an advantage over primary cells in this respect, as they are a homogeneous population. Therefore our aim was to replace the primary cells in the previously developed triple culture model with cell lines. Two human monocytic cell lines were chosen for this purpose: THP-1 and MUTZ-3.

MUTZ-3 is a CD34<sup>+</sup> human myeloid leukemia-derived cell line that is commercially available. A comparison with other human cell lines such as KG1 (myeloblasts from bone marrow) and THP-1 (monocytes from blood), which are also able to form a dendritic cell-like phenotype after stimulation, showed that this cell line shows the best DC-like phenotype [61] [62]. Other human (HL-60) or mouse (D1, J774, Raw264.7) cell lines are also able to acquire a dendritic cell-like phenotype [63], but their functional and transcriptional profiles are not known or not very similar to primary dendritic cells. For MUTZ-3 cells it was successfully shown that they can activate T-cells, which is attributable to the expression of co-stimulatory molecules as CD80 and CD86. Therefore, this cell line is a suitable model for deciphering the molecular mechanism of immune reactions [62].

The THP-1 cell line, which is also commercially available, is a human monocytic leukemia-derived cell line, which can be differentiated to macrophage-like cells after stimulation with phorbol-12-myristate-13-acetate. These cells mimic monocyte-derived macrophages and since their establishment 30 years ago they have become one of the most often used cell lines to replace primary macrophages in *in vitro* models [64]. THP-1 cells are suspension cells which adhere to the bottom of the cell culture flask after stimulation with PMA. During this process PMA induces a cell cycle arrest in the G1 phase via complex mechanisms and an upregulation of several proteins [65]. Furthermore, the cell volume increases, the nucleus becomes more irregular in shape and many phagocytic vacuoles appear in the cell cytoplasm [66]. It has also been shown that THP-1 cells exhibit surface markers typical of macrophages after stimulation with PMA, such as CD14 and TLR2 [67].

By replacing the primary cells in the intestinal *in vitro* model with the above cell lines, it is expected that the model should be more robust and lead to more reproducible results.

The aim of the work presented in the current chapter was therefore to show that both models (the previous model using primary immune cells and the model to be developed in which only cell lines are employed) show the same behavior after inflammation. In order to investigate this, the models were grown until Caco-2 cells formed a confluent monolayer. Afterwards IL-1 $\beta$  was added to the apical compartment to inflame the models. TEER was measured to see if the inflammation was accompanied by opening of tight junctions, which would lead to a decrease of TEER values. It was also important to see if the inflammatory effect was reversible after removal of IL-1 $\beta$ , as was observed in earlier studies with the primary cell-based model. Furthermore, IL-8 release was measured after inflammation and after removal of IL-1 $\beta$ . The ultrastructure of the model was observed via transmission electron microscopy (TEM) and confocal laser scanning microscopy (CLSM) to see if both immune cell types continued to be viable after three weeks in the collagen layer and if the cells were able to move within and out of the collagen, as was shown for the previous model.

Since the Caco-2 clone C2BBE1 needs 21 days to form a confluent monolayer, it was also tried to use the Caco-2 clone HTB37, which grows faster and shows higher TEER values after a shorter time. As this could lead to a higher experimental throughput, the second aim of the following work was to replace clone C2BBE1 by clone HTB37 without changing the inflammation behavior of the model [50].

## **2.2 Materials and Methods**

### **2.2.1 Cell culture**

Caco-2: clone C2BBE1 (passages 60-80) and clone HTB37 (passages 25-45) of the adenocarcinoma cell line were both obtained from the American Type Culture Collection (ATCC) (Rockville, MD). Clone C2BBE1 was grown in Dulbecco's Modified Eagle Medium (DMEM) (Gibco, Carlsbad, CA) supplemented with 10% fetal bovine serum (FBS) and

1% non-essential amino acids (NEAA) (PAA, Pasching, Austria) (this medium will be further referred to as “Caco-2 medium”). Clone HTB37 was grown in Minimum Essential Medium (MEM) (Gibco, Carlsbad, CA) supplemented with 20% FBS, 1% NEAA and 1% sodium pyruvate (PAA, Pasching, Austria). Both C2BBe1 and HBT37 clones were grown in T75 flasks at 37 °C and 5% CO<sub>2</sub>, and medium was changed every second day. Cells were sub-cultured every week with 0.1% trypsin (Sigma, Steinheim, Germany) and 0.02% EDTA (Sigma, Steinheim, Germany). 5x10<sup>5</sup> cells (C2BBe1) or 2x10<sup>5</sup> cells (HTB37) were then seeded in a new T75 flask.

THP-1: this human monocytic cell line was obtained from the Deutsche Sammlung von Mikroorganismen und Zellkulturen (DSMZ) (Braunschweig, Germany). Cells were grown in T75 flasks in Roswell Park Memorial Institute (RPMI) 1640 medium (Gibco, Carlsbad, CA) supplemented with 10% FBS (this medium will be further referred to as “THP-1 medium”) and maintained in similar conditions of temperature and CO<sub>2</sub> as Caco-2 cells. THP-1 cells were differentiated to macrophage like cells by adding 5 ng/ml PMA (Sigma, München, Germany) to the cell culture medium. After 48 h cells were harvested and collected for the co-culture.

MUTZ-3: a human monocytic cell line, which was obtained from DSMZ. Cells were grown in 6 well plates in  $\alpha$ -Minimum Essential Medium ( $\alpha$ -MEM) (Gibco, Carlsbad, CA) supplemented with 20% FBS and 20% conditioned medium from 5637 cells (see below). Cells were maintained in similar conditions as Caco-2 cells, which allowed them to acquire dendritic cell-like characteristics.

5637 cells: a human bladder carcinoma cell line, which was obtained from ATCC. Cells were grown in T75 flasks in RPMI 1640 supplemented with 10% FBS. Medium was collected every second day, filtered and used as conditioned medium to prepare the cell culture medium for MUTZ-3 cells. Before use the conditioned medium was stored at -20°C.

### **2.2.2 Isolation of primary macrophages and dendritic cells**

Blood monocytes were isolated from buffy coats (blood donation service, Saarbrücken, Germany) and differentiated to macrophages and dendritic cells. The peripheral blood mononuclear cells were obtained from buffy coats by Ficoll density gradient centrifugation. Cells were grown in RPMI1640 supplemented with 10% human AB serum (Invitrogen, Carlsbad, CA, USA). After seven days primary macrophages were obtained. Primary dendritic cells were obtained after seven days by cultivating monocytes in the same medium with the addition of 25 ng/ml IL-4 and 50 ng/ml Granulocyte macrophage Colony-Stimulating Factor (GM-CSF).

### **2.2.3 Three dimensional triple culture of epithelial cells, macrophages and dendritic cells**

Differentiated THP-1 cells and MUTZ-3 cells or primary macrophages and dendritic cells were harvested and embedded in an 80% (w/v) solution of type I bovine collagen (Advanced Biomatrix, Tucson, Arizona, USA) with human AB serum and RPMI1640. 150  $\mu$ l of this solution was pipetted into the apical compartment of a transwell filter insert (Corning Incorporated, Acton, MA, USA) with a pore size of 0.4  $\mu$ m and a filter area of 1.12 cm<sup>2</sup>. Cells were incubated at 37 °C and 5% CO<sub>2</sub> until the collagen layer had solidified. Afterwards 6x10<sup>4</sup> Caco-2 cells in 500  $\mu$ l Caco-2 medium with 1% Pen/Strep (PAA, Pasching, Austria) were seeded on top of this collagen layer. 1.5 ml of THP-1 medium with 1% Pen/Strep was added to the basolateral compartment. Medium was changed every second day. Co-cultures with the Caco-2 clone C2BBE1 were grown for 21 days; co-cultures with the Caco-2 clone HTB37 were grown for 11 days. For inflammation 10 ng/ml of IL-1 $\beta$  was added into the apical compartment for 48 h.

#### **2.2.4 Transepithelial electrical resistance (TEER)**

TEER was measured to monitor the confluence of the Caco-2 monolayer. Cells were placed on a heating plate at 37 °C to avoid temperature shock-related TEER fluctuation. TEER was measured with a Chopstick electrode and an epithelial volttohmmeter (EVOM) (World Precision Instruments, Sarasota, USA). Only cell cultures presenting TEER values  $> 400 \Omega \cdot \text{cm}^2$  were used for experiments.

#### **2.2.5 IL-8 measurement**

IL-8 was measured with a bead-based fluorescence activated cell sorter (FACS) array. At several time points after inflammation 50  $\mu\text{l}$  of cell culture supernatant was taken from apical and basolateral compartments of transwells. For measurement, a CBA Flex Set for IL-8 (BD Biosciences, Heidelberg, Germany) was used and samples were prepared in accordance with the manufacturer's protocol. Analysis was done with FCAP array v1.01 cytometric bead array analysis software (BD Biosciences, Heidelberg, Germany).

#### **2.2.6 Transmission electron microscopy (TEM)**

Samples were fixed by adding 2% glutaraldehyde at 37 °C in 200 mM 2-[4-(2-hydroxyethyl)piperazin-1-yl]ethanesulfonic acid (HEPES), pH 7.4, directly to the cell culture medium at a 1:1 ratio. After 5 min the fixative and medium mixture was replaced with 1% glutaraldehyde in HEPES buffer at room temperature (RT) and the samples were incubated overnight at 4 °C. Afterwards transwell inserts were put in a 50 ml falcon tube filled with HEPES buffer, and sent to our collaborators Dr. Urska Repnik and Prof. Dr. Gareth Griffiths from Oslo University, Denmark, for further preparation. For epon embedding, the samples were postfixed with a 2%  $\text{OsO}_4$  (EMA, PA, USA) solution containing 1.5% potassium ferricyanide for 1 h on ice, and stained en bloc with 1.5% aqueous uranyl acetate (EMS, PA, USA) for 30 min. Cells were then dehydrated at

RT using a graded ethanol series and embedded in epoxy resin (Sigma Aldrich; St. Louis, MO, USA). Ultrathin sections of 70-80 nm, perpendicular to the filter plane, were cut with a Leica ultramicrotome Ultracut EM UCT (Leica Microsystems, Austria) and examined with a CM100 transmission electron microscope (FEI, The Netherlands). The images were recorded digitally with a Quemesa TEM CCD camera (Olympus Soft Imaging Solutions, Germany) and iTEM software (Olympus Soft Imaging Solutions, Germany). In addition 2  $\mu$ m thick sections were cut, stained with toluidine blue and analyzed with a widefield Leica DMIRBE microscope and Leica application Suite (LAC) software v 3.8 (both from Leica Microsystems, Germany).

### **2.2.7 Immunostaining for confocal laser scanning microscopy (CLSM)**

THP-1 macrophages or MUTZ-3 dendritic cells were pre-stained with 2  $\mu$ g/ml of fluorescein diacetate (FDA, Sigma Aldrich, St. Louis, MO, USA), a cell-permeant amine-reactive probe, in accordance with the manufacturer's protocol. Afterwards cells were collected and used to seed the co-culture. Triple cultures were fixed with 3% paraformaldehyde (PFA) in phosphate buffered saline (PBS) for 30 min at RT in the apical compartment and quenched with 50 mM  $\text{NH}_4\text{Cl}$ , followed by 30 min incubation with 1% bovine serum albumin (BSA) and 0.05% saponin in PBS. Afterwards the membranes with the collagen layer were transferred into a 24 well cell culture plate for staining. Cells were washed with PBS and incubated with the primary antibody (monoclonal mouse anti-occludin, Zymed, San Francisco, CA), which was diluted 1:200 in PBS, overnight at 4 °C. Afterwards cells were washed with PBS and incubated for 1 h at RT with the secondary antibody (Alexa633 anti-mouse, LifeTechnologies, Darmstadt, Germany), which was diluted 1:400 in PBS. Cells were then washed and incubated for 20 min at RT with DAPI (LifeTechnologies, Darmstadt, Germany) in a concentration of 100 ng/ml. After staining the samples were mounted on slides using fluorescence mounting medium (DAKO,

Glostrup, Denmark). Images were acquired using a confocal laser scanning microscope (Zeiss, Germany) and Zen Software (Zeiss, Germany).

### **2.2.8 Statistical analysis**

Where appropriate, data are presented as mean  $\pm$  standard deviation (SD). One way ANOVA with Holm Sidak test was used to compare results from different treatments at different time points. The ANOVA analysis was done with SigmaPlot 12.5 (Systat Software GmbH, Erkrath, Germany). Significance was assumed at  $p < 0.05$  (\*) or  $p < 0.001$  (\*\*). Individual experiments were performed in triplicate and each experiment was performed twice.

## **2.3 Results**

### **2.3.1 Replacement of primary cells by cell lines**

As stated above, the aim of the current work was to replace the primary immune cells in the already established triple culture model of the inflamed mucosa [50] with cell lines. As epithelial cells, Caco-2 cells, clone C2BBE1, were used, as in the original model. As macrophages, THP-1 cells were treated with PMA for 48 h in order to promote differentiation into macrophage-like cells. During the process of differentiation the cells became adherent (Figure 2.1), and could then be harvested to be used in the co-culture setup. As dendritic cells, MUTZ-3 cells were used in the newly-developed model.

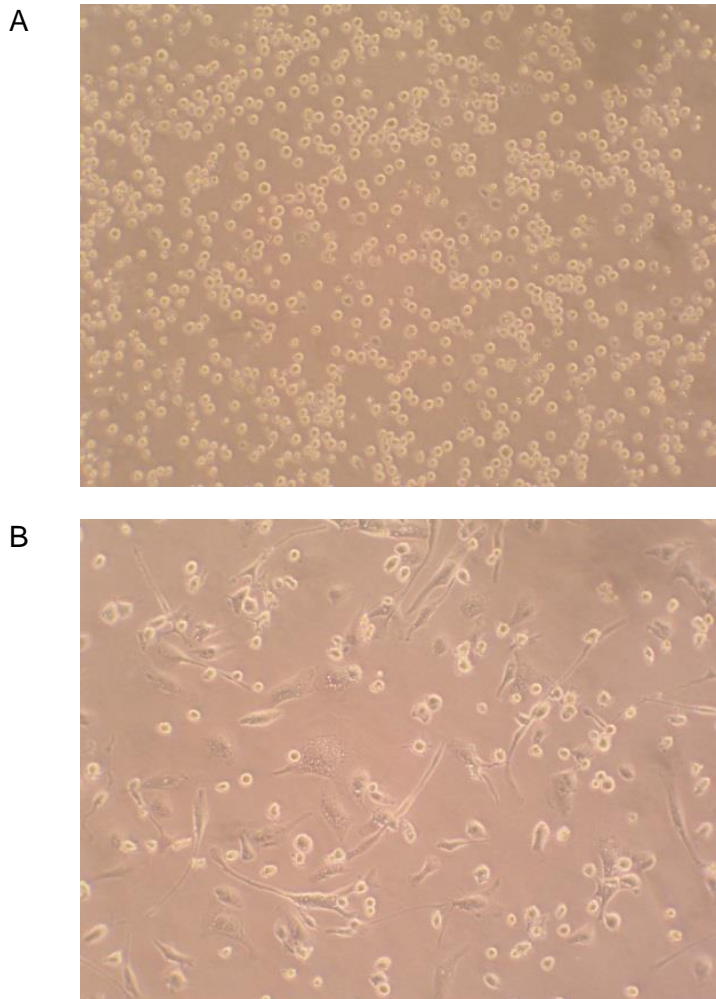
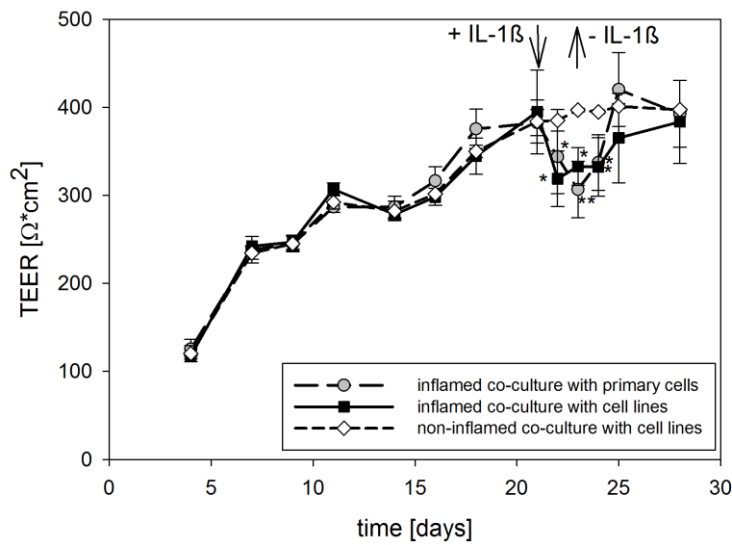


**Figure 2.1: THP-1 cells before (A) and after (B) treatment with PMA.** PMA promoted differentiation to macrophage-like cells was accompanied by an adherence of cells to the bottom of the cell culture flask. Cells are shown in 20-fold magnification.

Both co-culture models were seeded and grown in parallel for 21 days until Caco-2 cells formed a confluent monolayer, which was monitored by measurement of TEER. After 21 days Caco-2 cells reached TEER values between 400 and 450  $\Omega \cdot \text{cm}^2$ . The co-cultures were then inflamed by adding 10 ng/ml of IL-1 $\beta$  into the apical compartment for 48 h. TEER values decreased significantly after this treatment in both triple culture models compared to a non-inflamed control (Figure 2.2A), which is in agreement with earlier studies [50], [68]. To evaluate the reversible effect of inflammation on barrier properties, IL-1 $\beta$  was removed from the co-culture on day 23. In the absence of IL-1 $\beta$ , barrier properties recovered as observed in relation to TEER measurement (Figure 2.2A).

A



B

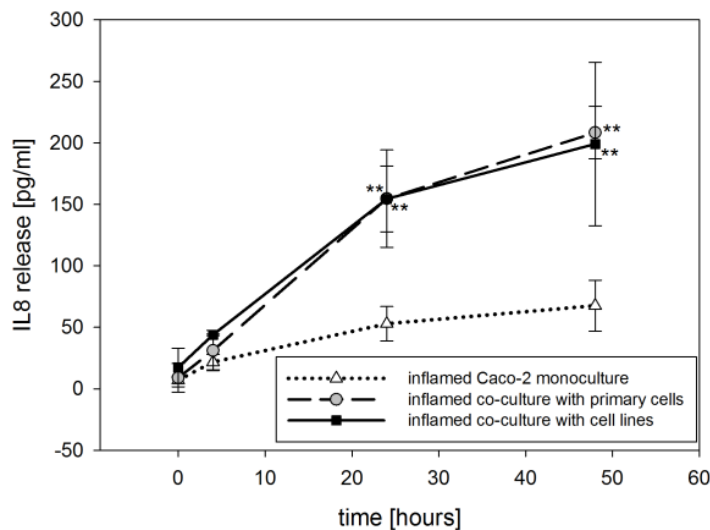


**Figure 2.2: TEER (A) and IL-8 release (B) of co-culture setups after inflammation with IL-1 $\beta$ .** Co-cultures with primary cells and cell lines were grown for three weeks and inflamed at day 21 (+ IL-1 $\beta$ ). At day 23 IL-1 $\beta$  was removed (- IL-1 $\beta$ ). Results of both inflamed co-cultures were compared to TEER values of a non-inflamed co-culture with cell lines (A). IL-8 release was measured in co-cultures with cell lines and primary cells 0, 4, 24 and 48 hours after inflammation with IL-1 $\beta$ . Results were compared to IL-8 release from an inflamed Caco-2 monoculture (B) (mean  $\pm$  SD, n=6 from 2 independent experiments, \* = p<0.05, \*\* = p<0.001).

As an indicator of inflammation in the triple culture models, the pro-inflammatory cytokine IL-8 was measured in the cell culture supernatant. For comparison, the IL-8 release from a Caco-2 monoculture treated with IL-1 $\beta$  was also measured. Results show that in triple culture models, both with cell lines and primary cells, a progressive IL-8 release after inflammation, reaching approximately 200 pg/ml in 48 h, occurred. However, in the Caco-2 monoculture only a slight IL-8 release (50 pg/ml) could be detected even 48 h after stimulation (Figure 2.2B).

To understand whether macrophages and/or dendritic cells are responsible for the production of IL-8 in this experiment, THP-1 and MUTZ-3 cells were seeded either separately or together in the collagen layer, and compared to the 3D co-culture with all three cell lines. Cells were grown for 21 days under the same conditions as the co-culture models (Figure 2.3).

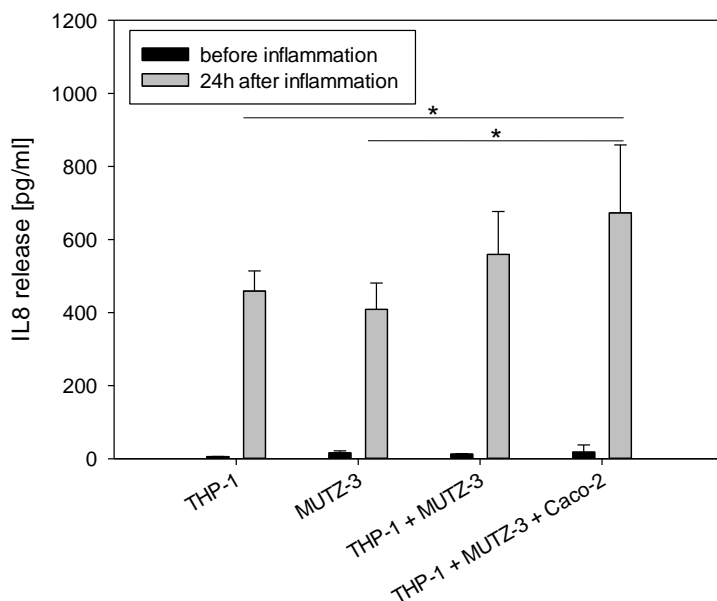


**Figure 2.3: IL-8 release from different combinations of Caco-2, THP-1 and MUTZ-3 cells.** Following 21 days of culture the production of IL-8 was measured, both before and after inflammation with IL-1 $\beta$  (mean  $\pm$  SD, n=3, \* = p<0.05).

It was shown that, when seeded separately in the collagen layer, THP-1 and MUTZ-3 cells were both able to produce approximately 400 pg/ml IL-8 after inflammation with IL-1 $\beta$ . When immune cells were seeded in combination, treatment with IL-1 $\beta$  resulted in an even greater inflammatory response with a release of 600 pg/ml of IL-8. Caco-2 cells alone were also able to produce IL-8 after inflammation with IL-1 $\beta$  (Figure 2.2B), in accordance with Leonard et al [50], while the release of IL-8 was seen to be highest (800 pg/ml) when all three cell types were combined in a co-culture (Figure 2.3). Together these results show that both THP-1 and MUTZ-3 cells contribute to the inflammatory response and that both cell types are viable after 21 days incubation in the collagen.

### **2.3.2 Morphological analysis of the cell line-based triple culture model with TEM and CLSM**

The cell line-based triple culture was also evaluated by transmission electron microscopy (TEM) and confocal laser scanning microscopy (CLSM). TEM pictures (Figure 2.4) showed a well preserved ultrastructure of the triple culture. Macrophages and dendritic cells are distributed within the collagen layer with the Caco-2 monolayer on top. Epithelial cells showed typical microvilli, desmosomes and tight junctions. Furthermore, immune cells in the collagen layer were well preserved and made cell contacts. Macrophages and dendritic cells were located in the collagen layer, as well as on top of the Caco-2 cell monolayer, which provides evidence for the translocation of these immune cells through the epithelial barrier. Both immune cell types were also observed separately. Figure 2.5 shows that these two cell types can be distinguished based on nucleus heterochromatin [69]. Dendritic cells show more condensed heterochromatin than macrophages, which can also be observed in Figure 2.4A.

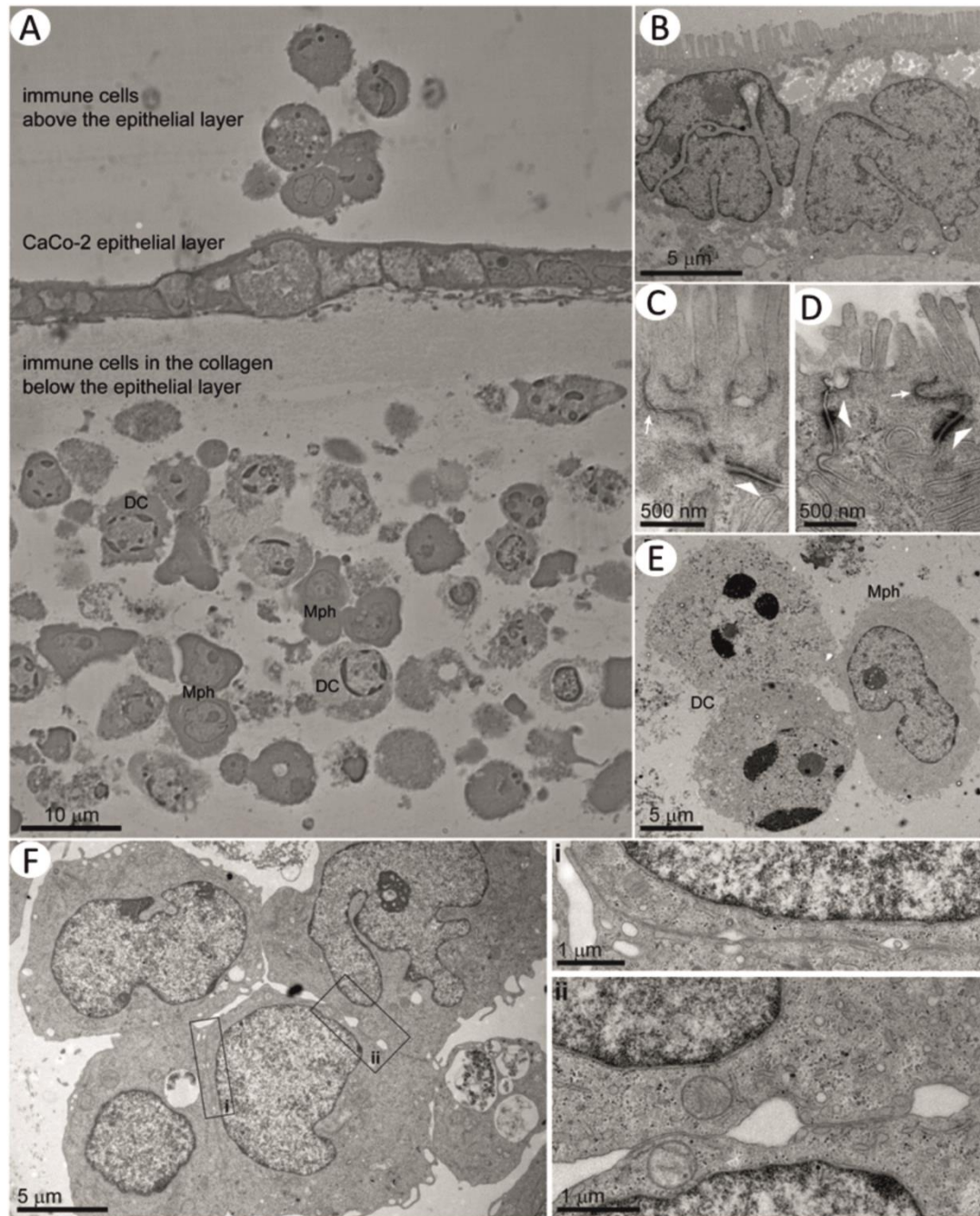


**Figure 2.4: A microscopic overview of the non-inflamed triple culture.** Caco-2 cells seeded on collagen, which contains immune cells. Some immune cells are observed on top of the epithelium (A). Detailed information regarding epithelial cells (B) was also obtained, including visualization of tight junctions (slim arrow) and desmosomes (block arrow) (C,D). Discrete immune cells could also be visualized within the collagen layer (Mph = macrophages, DC = dendritic cells (E)). Interaction between immune cells in the collagen layer were also observed (F, inserts i, ii). (A): 2  $\mu\text{m}$  thick epon section analyzed with a wide field light microscope; (B-F): 70 nm epon sections analyzed with a transmission electron microscope.

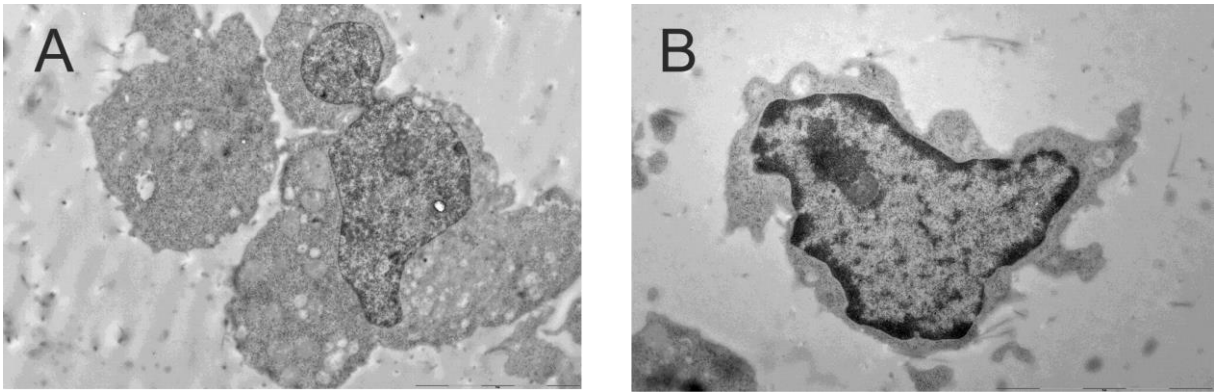


**Figure 2.5: TEM pictures of THP-1 macrophages and MUTZ-3 dendritic cells demonstrating heterochromatin content.** Both macrophages (A) and dendritic cells (B) were seeded separately in the collagen layer of the triple culture and grown for 21 days. Dendritic cells show more heterochromatin in the nucleus than macrophages. 70 nm epon sections analyzed with a transmission electron microscope.

Using CLSM some macrophages and dendritic cells (green) could be detected in the collagen layer and between or on top of the Caco-2 cells within the triple culture setup (Figure 2.6), which is in accordance to the TEM results (Figure 2.4). Furthermore some differences between the inflamed and non-inflamed triple culture could be observed: while the tight junctions (red), which were stained with an anti-occludin antibody, were well preserved in the non-inflamed model (Figure 2.6A/B), a disruption of the tight junctions could be seen in the inflamed culture (Figure 2.6C/D).

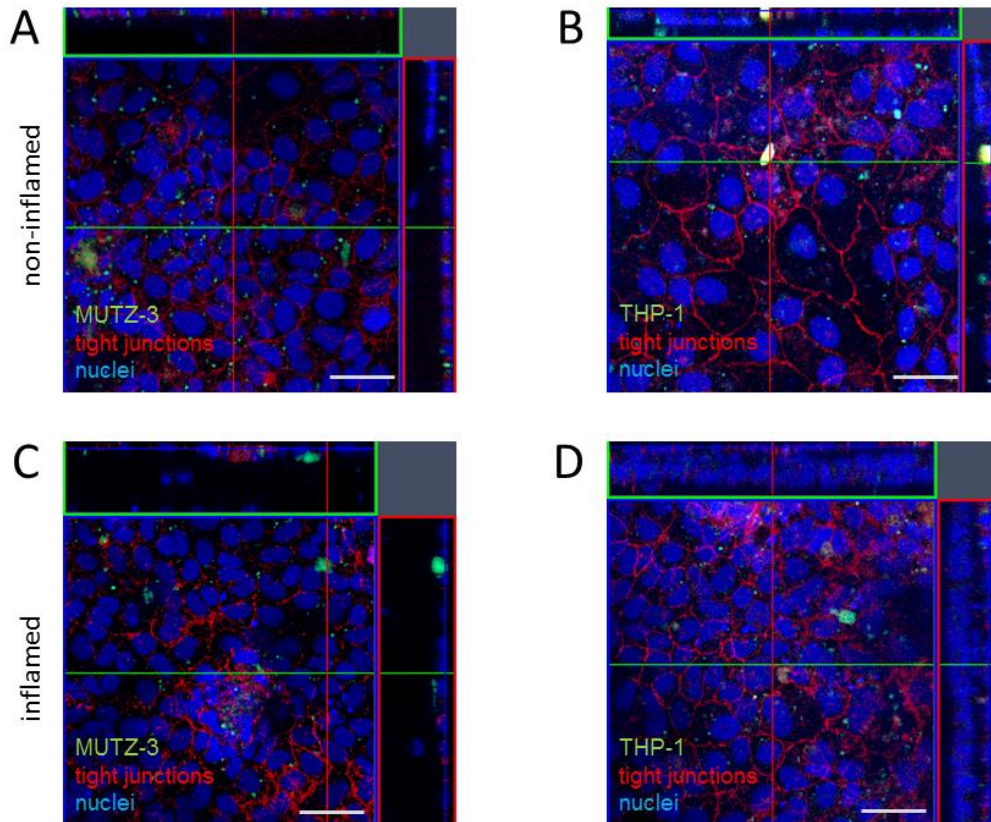


**Figure 2.6: CLSM of non-inflamed and inflamed triple culture.** Z-Stacks of non-inflamed (A,B) and inflamed (C,D) co-cultures; MUTZ-3 cells (A,C) or THP-1 cells (B,D) were pre-stained with FDA (green), while epithelial tight junctions were stained with an anti-occludin antibody (red), cell nuclei are stained with DAPI (blue). Tight junctions in the inflamed co-culture are disrupted (C,D) and not as well defined as in the non-inflamed culture (A,B). Macrophages and dendritic cells (green) can be seen in between or on top of the Caco-2 cells in both inflamed and non-inflamed conditions. Scale bar: 50  $\mu$ m.

### 2.3.3 Improvement of the triple culture model using the Caco-2 clone HTB37

The co-culture with the Caco-2 clone C2BBe1 required 21 days for the cells to form a confluent monolayer and for TEER values to reach a plateau. It was therefore aimed to replace these cells by epithelial cells that grow faster and need less time to form a confluent monolayer. Caco-2 cells from clone HTB37 are known to reach confluence in a shorter period of time. Therefore it was tried to seed these cells on top of the collagen layer instead of the Caco-2 clone C2BBe1. To find the best conditions for the new cell

type, different cell culture media (DMEM with 10% FBS, 1% NEAA and 1% Pen/Strep or MEM with 20% FBS, 1% NEAA, 1% sodium pyruvate and 1% Pen/Strep) and different cell numbers (20000, 40000 and 60000 cells/cm<sup>2</sup>) were used in the co-culture setup and compared to results with Caco-2 C2BBE1. Cells were grown for 21 days and TEER was measured (Figure 2.7).

Results of TEER measurement show that the Caco-2 clone HTB37 developed higher TEER values after a shorter period of time as compared to the Caco-2 clone C2BBE1. Already after 11 days a TEER peak of 1000  $\Omega$ \*cm<sup>2</sup> was reached with HTB37 cells, which was seen to remain at a constant level until day 15. In the light of these results it was decided to use the HTB37 Caco-2 clone for further experiments with the same cell number (60000 cells/cm<sup>2</sup>) and the same cell culture medium (DMEM with 10% FBS, 1% NEAA and 1% Pen/Strep) as the clone used earlier, but with the introduction of IL-1 $\beta$  to induce inflammation after only 11 days. To be sure that the HTB37 cells showed the same behavior after inflammation as the C2BBE1 clone, cells were inflamed after 11 days and TEER and IL-8 release were measured (Figure 2.8).

The co-culture with Caco-2 HTB37 shows the same behavior as the co-culture with C2BBE1: after inflammation with IL-1 $\beta$  TEER values decrease and IL-8 release increases as pro-inflammatory marker. When IL-1 $\beta$  is removed TEER values are stable and IL-8 is decreasing again. So for further experiments it is also possible to use Caco-2 clone HTB37 for the co-culture under the same conditions as Caco-2 clone C2BBE1, but with a shorter growth time.

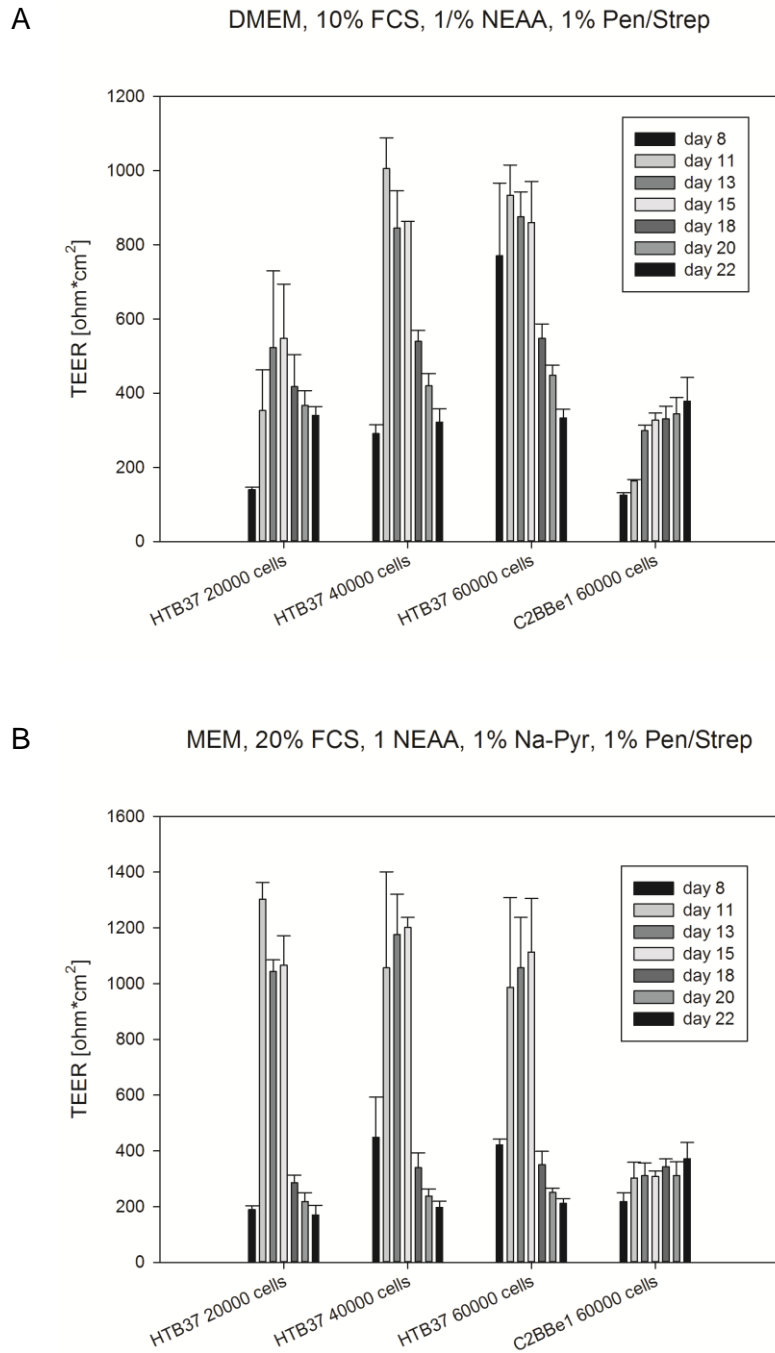
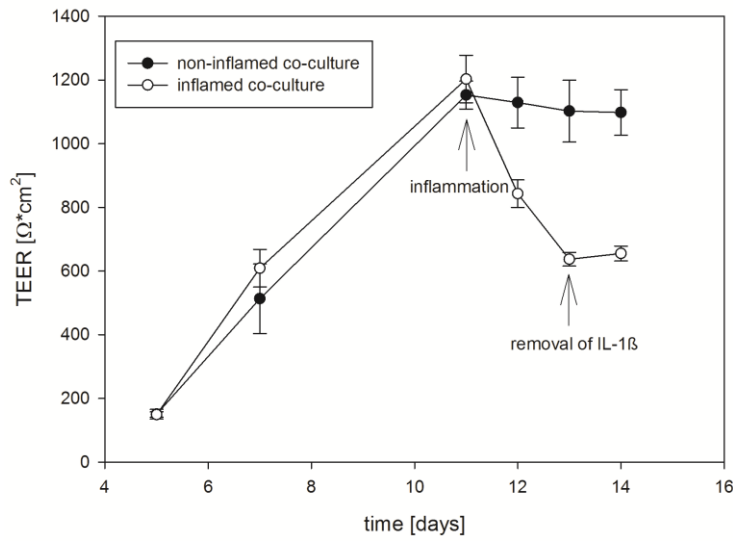


**Figure 2.7: Comparison of co-cultures with Caco-2 clones HTB37 and C2BBE1, using different cell culture media and different cell numbers.** DMEM with 10% FBS, 1% NEAA, 1% Pen/Strep (A) or MEM with 20% FBS, 1% NEAA, 1% sodium pyruvate, 1% Pen/Strep (B) were used as cell culture media. Cells were seeded at 20000, 40000 and 60000 cells/cm<sup>2</sup>; a co-culture with Caco-2 C2BBE1 60000 cells/cm<sup>2</sup> was used as control. All co-cultures were grown for 21 days.

A



B

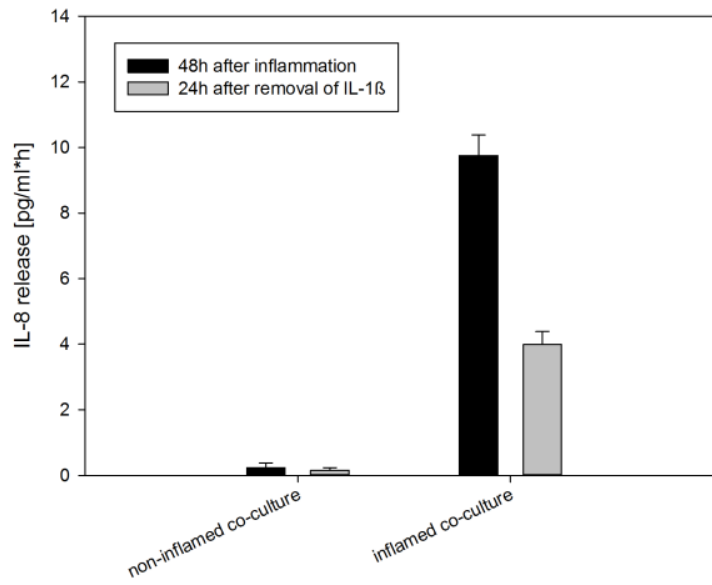


**Figure 2.8: TEER and IL-8 release after inflammation of HTB37 co-culture and comparison to non-inflamed co-culture.** Co-cultures were seeded with the HTB37 Caco-2 cell clone, and allowed to grow for 11 days prior to inflammation.

## 2.4 Discussion

*In vitro* models based on single cell types provide key information regarding particular cell type responses, e.g. to an infectious microorganism. Furthermore, cell monocultures represent an economic and efficient tool for a wide range of experiments. However, all cell culture models consisting only of one cell type do not reflect the complexity of biological host systems with intercellular communication. For instance, all monocultures are unable to reproduce active biological events, such as immune responses to pathogens or particles. As an alternative, co-culture models of multiple cell types, including epithelial cells, have been used to bridge the gap between simplistic *in vitro* models based on single cell types and the complex biological system *in vivo*.

Co-culture models of various biological tissues have been widely accepted [34], [67] for use in several contexts, e.g. to evaluate NP toxicity when exposed to the lungs via inhalation [70], [71]. Regarding the intestinal epithelium, i.e. after oral ingestion, most of the models currently in use focus on co-cultures to study absorption, particle-cell translocation or particle-mucus interactions [41].

Many research groups are working with co-culture models to get more reliable results that can better mimic the *in vivo* situation. Rothen-Rutishauser et al. for example have established an alveolar co-culture model of A549 epithelial cells, human monocyte-derived macrophages and human monocyte derived dendritic cells [34], [67]. In this model different NPs were tested with respect to their toxicity and the results were compared to the same studies in monocultures. Not surprisingly, different results were found for studies conducted co-culture and monoculture, as the lung consists of more than one cell-type. This makes the use of a co-culture model more realistic and representative [68]. A co-culture model of epithelial-like transformed cells (HeLa) together with macrophage-like cells (U937) has also been established by another group to investigate inflammation after treatment with retinoic acid and 1 $\alpha$ ,25-Dihydroxyvitamin D<sub>3</sub>, which induce differentiation of myeloid leukemia cells into granulocytes and macrophages respectively. Macrophages were cultured together with the epithelial cells because they play a very important role in

the innate immune system [70]. It is important to keep this in mind while doing any *in vitro* experiments.

As explained in the introduction of this thesis and mentioned above, several co-culture models of the intestine have also been established. For example there are several models employing Caco-2 cells as epithelial cells, together with mucus-producing HT29 cells as goblet cells and Raji B-cells, which stimulate Caco-2 cells to differentiation into M-cells. In some cases Caco-2 and HT29 cells are seeded on transwell filters and Raji B cells were seeded into the basolateral compartment, whereas in others Caco-2 and HT29 cells are seeded in the basolateral chamber and Raji B cells are added to the apical compartment. It was found that models in the first orientation show a better physiological, functional and reproducible model of the intestinal barrier [38]. Another established co-culture model of the intestine also uses mucus-producing cells. Here Caco-2 cells are cultured together with HT29\_5M21 cells. This model showed a lower permeability than Caco-2 cells in monoculture, which fits better with data from *in vivo* experiments [71]. Another study of an intestinal co-culture system consisting of H4-1 small intestinal epithelial cells co-cultured with TLT macrophages showed that models with macrophages are better protected against pathogens than monocultures [74]. The review by Bermudez-Brito et al. gives many examples for the importance of intestinal co-culture models, especially for models with macrophages and dendritic cells [75].

In the current work we focused on the development and optimization of an intestinal model that could mimic either healthy or inflamed conditions, which makes it an important tool for research on IBD. A co-culture model consisting of Caco-2 cells, macrophages and dendritic cells has been previously developed at our institute by Leonard and colleagues [50]. Macrophages and dendritic cells are used in the model because these are two cell types which are important for antigen possessing and presentation and furthermore for the activation of an immune answer [75]. However due to the expensive and time-consuming procedure of PBMC isolation and, even more importantly, the patient-dependent variability

between the different primary cell samples, it was proposed to improve the established model by replacing the primary cells by cell lines. The cell lines might be an option to establish a more robust and reproducible system. For this purpose several human monocytic cell lines could be used as macrophage-like cells, for example HL-60 [72] or U937 [73]. However, the most commonly used cell line is the monocytic leukemia cell line THP-1 [64]. These cells can be stimulated with PMA to induce differentiation to macrophage-like cells which mimic monocyte-derived macrophages in several aspects and behave more like monocyte-derived macrophages than other cell lines such as HL-60, U937 or KG-1 [66]. The THP-1 cell line has become a common model for macrophages in cell culture systems [74] and was therefore also used in our model. It could be shown that after stimulation with PMA the suspension cells adhered to the bottom of the cell culture flask and showed a macrophage-like shape (Figure 2.1). As dendritic cells the monocytic leukemia cell line MUTZ-3 was used in the model due to its proven suitability for use as dendritic-like cells [79].

After seeding of the revised triple culture model with cell line-derived immune cells, Caco-2 cells formed a confluent monolayer and functional tight junctions after a growth time of three weeks (Figure 2.2). Despite being initially seeded in the underlying collagen layer, it could be seen that macrophages and dendritic cells could interact with Caco-2 cells, being located between them or on top of the epithelium (Figure 2.4, Figure 2.6). Interestingly this interaction did not disrupt the intercellular barrier of the tight junctions as shown by uncompromised TEER value measurements, which could also be observed in the primary cell-based model of Leonard et al. [50]. A possible explanation for this could be that the immune cells are trafficking into or through the Caco-2 cell layer before these start forming a tight barrier. Other studies have shown that THP-1 cells co-cultivated with Caco-2 cells induce epithelial cell death mainly due to TNF- $\alpha$  secretion by THP-1 cells [49]. However, this was not observed in our system. Furthermore, confocal images and TEM studies showed intact tight junctions, especially in the non-inflamed status. Real-time PCR studies, shown in the next chapter of this thesis, also showed that the amount of

TNF- $\alpha$  released from the triple co-culture is quite low, even after inflammation with IL-1 $\beta$  (Figure 3.7E/F); this could be a reason why THP-1 cells do not disturb the epithelial cells in our model.

After IL-1 $\beta$ -induced inflammation, the 3D co-culture model showed a decrease in TEER values (Figure 2.2A). This effect was reversible when IL-1 $\beta$  was removed, which is in agreement with observations of the previous model based on primary cells [50]. Inflammation leads to a loss of the epithelial barrier function due to the opening of tight junctions [76]. Changes in the expression pattern of different tight junction proteins as for example claudin 4, 5 or 8 could be responsible for this effect [77], [78]. Other groups have also reported significantly decreasing TEER values after treatment of Caco-2 cells with the inflammation-inducing agent LPS [79], corroborating our data.

Inflammation of the co-culture resulted in a greater increase of IL-8 release in comparison to the epithelial monoculture (Figure 2.2B), probably as a result of the presence of immune-competent cells in the co-culture. The level of cytokine production was also comparable between models containing cell lines or primary immune cells. MUTZ-3 and THP-1 cells seeded separately already release IL-8 after an inflammable stimulus (Figure 2.3). When they are seeded together the release is even higher although it does not reach the additive level, which shows that the two cell types influence each other in that way that they do not have to produce as much IL-8 as when they are seeded separately.

Many experiments with nanomaterials in co-culture models have shown a clear difference to the results of monocultures [68], [69], [70]. Immune-competent cells may influence epithelial barrier properties during inflammation as shown in studies using endothelial cells [80]; however in our model this was not observed. Nevertheless, immune cells are a very important factor in inflammation models because of the release of pro-inflammatory cytokines to measure the inflammation status.

Following indications that the replacement of primary cells with cell lines did not result in significant changes in the behavior or characteristics of the triple culture model, the next

step was to attempt to further optimize the model by reducing the growth time of the cells prior to model inflammation and/or further use. As mentioned, the Caco-2 clone C2BBe1 cells need 21 days to form a confluent monolayer. Within such a span of time the immune cells within the co-culture could die and in addition, the danger of contamination with bacteria is considerable. Therefore, an alternative Caco-2 clone (HTB37) was used. Previous comparisons of different Caco-2 clones (TC7, PD7, PF11) have shown that some differences may occur, although all the clones are of the same cell line. Several metabolic capabilities such as cell viability or fatty acid and cholesterol uptake were investigated, and it was found that the clones TC7, PD7 and PF11 show different results [81]. As well as different metabolic behavior between clones, it was also shown that different batches from the same clone showed different morphologies [82] necessitating consistent use of the same passage numbers for experiments.

The clone C2BBe1 is always used as Caco-2 cell line in our laboratories - and was also used in the first co-culture model with primary immune cells - which was the reason why it was our first choice. Experiments with the clone HTB37 however showed that these cells need a shorter growth time under the same conditions with the same cell culture medium as previously (containing 10% FBS), and that they build higher TEER values in a shorter time period (Figure 2.7). By using an even higher amount of FBS (20%) in the culture medium, HTB37 cells were seen to grow even faster, however TEER values were seen to decrease at an earlier time point. As higher TEER values in general were seen with HTB37 cells, a greater decrease in TEER values could be observed following inflammation with IL-1 $\beta$ ; as for the previous model utilizing C2BBe1 cells however TEER values were seen to recover after removal of IL-1 $\beta$ . This is seen as a considerable advantage of using HTB37 cells, as the effects of inflammation may be even better monitored. Furthermore, IL-8 release when using HTB37 cells was comparable to that observed in the model using the Caco-2 clone C2BBe1. With the HTB37 Caco-2 clone it is therefore considered that the model is even more useful for high throughput studies because more experiments can be done in less time.

## 2.5 Conclusion

The previously established co-culture model of the inflamed mucosa is a useful *in vitro* model for IBD research because both inflammation of this model with IL-1 $\beta$  and healing of the model following IL-1 $\beta$  removal are possible. The replacement of primary immune cells by the cell lines THP-1 and MUTZ-3, as shown in the current chapter, resulted in a more robust system useful for higher throughput assays, without any effect on the model immunocompetence or epithelial cell differentiation. Furthermore, this cell line-based model has the advantage of being less time consuming to prepare and less variable with respect to model behavior and experimental results than models based on primary cells obtained from blood samples of different patients. By using the Caco-2 clone HTB37 instead of C2BBE1 the growth time of the cells could be reduced from 21 to 11 days, even further increasing the experimental throughput and output capacity. Another improvement is that these Caco-2 cells build higher TEER values, which makes it easier to monitor the inflammation of the model.

---

### 3 Cytotoxicity measurements of nanoparticles in the cell line-based co-culture model

Parts of this chapter have been published in:

**J. Susewind**, C. de Souza Carvalho-Wodarz, U. Repnik, E.-M. Collnot, N. Schneider-Daum, G. W. Griffiths, and C.-M. Lehr, “A 3D co-culture of three human cell lines to model the inflamed intestinal mucosa for safety testing of nanomaterials,” *Nanotoxicology*, vol. 5390, pp. 1–10, 2015.

Julia Susewind made the following contributions to this publication: performed all experiments, analyzed all the data and wrote the manuscript.

### 3.1 Introduction

Engineered nanomaterials (ENs) are commonly employed in food packaging or as additives in various food products, meaning that the chance of unintended human exposure is relatively high. Increased exposure to particulate matter has previously been identified as one of the main environmental factors associated with autoimmune and inflammatory diseases, especially those involving the intestine [83], [84]. For instance, studies show that exposure to microparticles has been linked to the occurrence of IBD, in particular Crohn's disease [85]. Food often contains many non-nutrient microparticles like soil and dust or food additives, which can be taken up by mucosal cells, resulting in inflammatory reactions [86]. NPs can be inhaled, e.g. carbon NPs from laser printers [87], but also swallowed, the latter case being reported to cause diarrhea and histological alterations typical of Crohn's disease [88]. Thus there is an urgent need to understand better the interaction between nanomaterials and the intestinal mucosa, especially in the context of local inflammatory events and diseases.

ENs are also used in innovative drug delivery systems as they can target drugs to their site of action and can protect the cargo from degradation [89]. Therefore, it is essential to thoroughly characterize the safety of ENs. However, the complexity of biological systems makes it difficult to precisely assess the impact of nanomaterials. This holds true in particular for animal models of biological systems, which due to their complexity are essentially "black boxes", difficult to handle and also posing ethical challenges. Therefore, there is a need for advanced cell- and tissue-based *in vitro* models that allow for studying the effects of NPs under well-controlled conditions by monitoring endpoints of clinical relevance. Currently, the enterocyte cell line Caco-2 is a well-established model for the human intestinal barrier. A number of *in vitro* studies have used the Caco-2 cell line to assess cytotoxicity in the GI as well as systemic uptake after oral exposure [90], [91]. However, the complex physiology of the intestinal mucosa is insufficiently modeled with only one cell type, which might explain the limited correlation between *in vivo* and *in vitro* studies achieved to date [92]–[94].

As already mentioned in the previous chapters, one obvious shortcoming of the Caco-2 monoculture model is the lack of immune-competent cells, which are clearly important in the context of inflammatory disorders such as IBD. Interactions between nanomaterials and immune cells can lead to inflammatory reactions with pro-inflammatory cytokine release and cytotoxic effects [47]. NP uptake by immune cells is an important issue related to nanotoxicity. Several NP properties, including the physicochemical properties of size and surface charge, might influence cellular particle uptake. Studies show that particles with cationic or anionic surface charges are more attractive to phagocytes than neutral particles [95], and it is known that particles below 200 nm in diameter show poor uptake by macrophages in comparison to particles between 0.5 and 3  $\mu\text{m}$  in size [96].

Several groups have used *in vitro* cell models to evaluate NP toxicity either in monocultures [90], [91], [97] or in co-cultures [67], [68]. Indeed, *in vitro* models containing two or more types of cells, able to interact with each other and with nanomaterials, seem to be more able to capture the complexity of the *in vivo* situation. As mentioned, our research group has previously established a 3D *in vitro* model of the intestinal mucosa consisting of the Caco-2 intestinal epithelial cell line with primary blood derived dendritic cells and macrophages embedded in a collagen type I gel [50]. This model has been shown to exhibit relevant barrier properties for studying NP translocation. It also appears to reflect typical pathophysiological changes that are observed in the state of inflammation *in vivo*, such as decreased epithelial barrier function, increased production of pro-inflammatory cytokines and an alleviation of such symptoms when anti-inflammatory formulations for the treatment of IBD were applied [51]. However, this model suffered from a relatively high variability and low throughput potential as well as difficulties in standardization, due to its use of primary-derived immune cells. Therefore, the model was modified, as described in the previous chapter, to rather include cell line-derived macrophages and dendritic cells. Such a substitution was not seen to compromise the ability of the model to build an intact permeation-relevant barrier or respond to inflammatory stimuli [103].

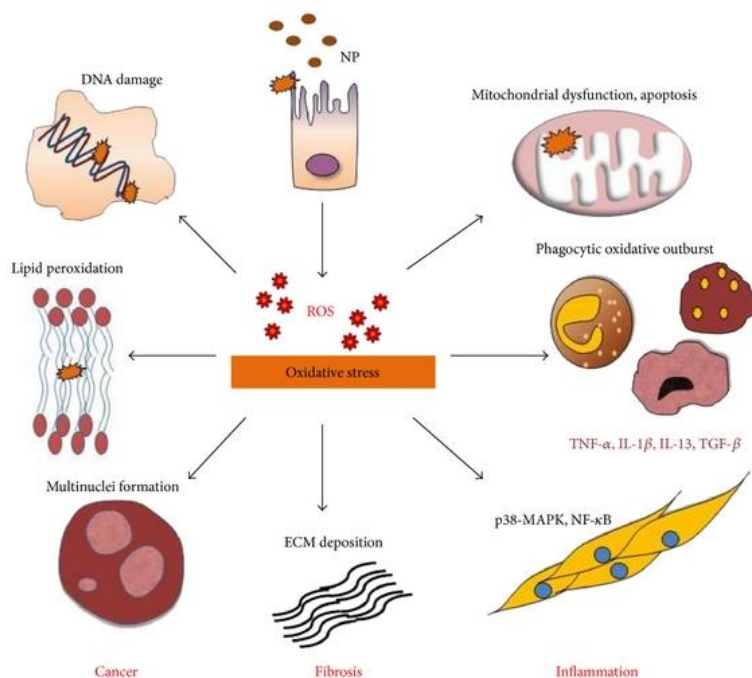


**Figure 3.1: Pathways for NP-induced toxicity** (Manke et al. [104]).

The aim of the work in the current chapter was to use this improved, cell line-based *in vitro* model consisting of Caco-2, THP-1 and MUTZ-3 cells to assess the cytotoxicity of engineered NPs. It is known that NPs from various materials induce oxidative stress in the form of reactive oxygen species (ROS) [105], [106]. ROS generation can lead to e.g. inflammation, cell death or mitochondrial dysfunction as shown in Figure 3.1 [104]. Several of these effects are investigated in our experiments. For this purpose silver (Ag), titanium dioxide (TiO<sub>2</sub>) and gold (Au) NPs were used. These particles were chosen based on their relevance for oral exposure as well as for their use in other toxicological studies: Ag NPs are frequently used in commercial products because of their antimicrobial properties. Such products include cosmetics, textiles and wound dressings, but also food packaging, in which their function is to enhance the shelf life of products. As such they may be released into food and swallowed by humans. A number of studies have described Ag NPs as being able to induce toxicity in a number of different species, and uptake by the intestine has been reported in animal models [98], [99]. As for other

nanomaterials, the toxicity of Ag NPs depends on their concentration and size as uptake of the particles is influenced by both parameters. Furthermore, smaller Ag NPs release more Ag<sup>+</sup> ions, which have been controversially discussed as being the main effectors in Ag NP associated toxicity [100].

TiO<sub>2</sub> NPs are present in many kinds of food, especially sweets such as candies and marshmallows. Children consume more of these kinds of food than adults, therefore having higher exposure rates to such particles [101]. Additionally, TiO<sub>2</sub> NPs serve as whitening agents in toothpastes.

Au NPs may also be included in toothpastes and packaging [102], but nanomedicines/diagnostics and nanoelectronics are more likely sources of application and so exposure. Due to their bright near-infrared fluorescence alone or in combination with e.g. chemotherapeutics in complex theranostic systems, they are used as imaging agents. The toxic potential and uptake pathway of Au NPs remains unclear [103]

## **3.2 Materials and Methods**

### **3.2.1 Nanoparticles (NPs)**

NM300 Ag NPs with a size of < 20 nm, PVP capped, and NM101 TiO<sub>2</sub> NPs with a size of 7-10 nm were purchased from JRC (Joint Research Centre, Ispra, Italy). Au NPs in two different sizes, 15 and 80 nm, were kindly provided by Dr. Wolfgang W. Kreyling, Institute of Lung Biology and Disease, Helmholtz Zentrum, Munich.

### **3.2.2 NP preparation and characterization**

For TiO<sub>2</sub> and Au NPs, stock solutions were prepared by suspending 76 mg of the respective NPs in MilliQ water with 2% FBS to a final concentration of 2.56 mg/ml. Ag NPs were provided at 10% (w/w) dispersed in a viscous mixture of water (75%) with 7% ammonium nitrate as stabilizing agent and 4% Tween20 and polyoxyethylene glycerol

trioleate as emulsifiers. A protocol from the ENPRA project ([www.enpra.eu](http://www.enpra.eu)) was used to prepare a stock solution of Ag NPs. In accordance with this protocol 100 mg of Ag NP solution were dispersed in 38 ml water containing 2% FBS to achieve a final concentration of 2.56 mg/ml. All the stock solutions were sonicated for 15 min in an ultrasonic bath (Bandelin electronic, Berlin, Germany) at 200 W. NPs were then further diluted in Caco-2 medium (described in chapter 2) to achieve concentrations between 0.0001 and 1 mg/ml. Following the dilution in medium, the NPs were sonicated again for 15 min before use in the experiments. For every experiment NPs were freshly dispersed, and the same dispersion protocol was used.

For TiO<sub>2</sub> and Au NPs, the hydrodynamic particle diameter was determined via dynamic light scattering with the Malvern Zetasizer® nano (Malvern Instruments, Herrenberg, Germany). Particle size and polydispersity index (PDI) were determined 0, 1, 2, 4, 6, 8 and 24 h after preparation of the respective dilution. The dilutions were kept at RT protected from light and were sonicated for 15 min before the measurement. Two independent samples were measured three times at each time point to calculate mean and SD.

For Ag NPs size distribution and stability were investigated with a NanoSight® LM10 instrument (Malvern Instruments, Herrenberg, Germany). This measurement is also based on dynamic light scattering, but uses single particle tracking analysis. Two particle concentrations were tested and mean particle diameter and width of the distribution were measured three times.

For TiO<sub>2</sub> and Ag NPs concentrations between 1.25 and 625 µg/cm<sup>2</sup> were tested, for Au NPs concentrations between 0.156 and 80 µg/cm<sup>2</sup> (Table 3.1). These concentrations were used for the following cytotoxicity studies with the different cell culture models.

**Table 3.1: Nanoparticle concentrations employed in cytotoxicity studies with the different cell culture models.**

Ag, TiO <sub>2</sub>		Au	
[µg/cm <sup>2</sup> ]	[µg/ml]	[µg/cm <sup>2</sup> ]	[µg/ml]
625	1000	80	128
312.5	500	40	64
156.25	250	20	32
78.125	125	10	16
39.065	62.5	5	8
19.53	31.25	2.5	4
9.77	15.625	1.25	2
5	8	0.625	1
2.5	4	0.3125	0.5
1.25	2	0.15625	0.25

### 3.2.3 Cell culture

Cells were cultured as described in section 2.2.1. The Caco-2 clone C2BBE1 was used for the following experiments.

### 3.2.4 Triple culture of the intestinal mucosa

The triple culture was set up as described in section 2.2.3. NPs were added to the apical compartment after removal of IL-1 $\beta$ . Cells were incubated with the particles for 24 h as shown in Figure 3.2 until the endpoints were measured.

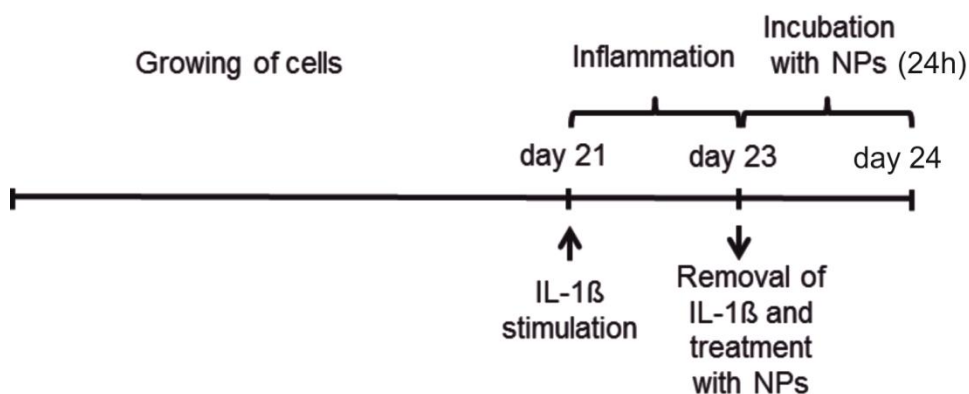


**Figure 3.2: Experimental setup for NP toxicity studies using the triple culture model.**

### **3.2.5 Cell viability measurement via lactate dehydrogenase (LDH) and Alamar Blue assay**

To test NP toxicity, Caco-2 cells were seeded at  $2 \times 10^4$  cells/well in 96 well plates and grown for 7 days. Cells were incubated with various concentrations (Table 3.1) of the different NPs for 24 h at 37 °C and 5% CO<sub>2</sub>. Following this incubation period, 100 µl of the supernatant was collected and LDH release was measured via an LDH detection kit (Roche, Mannheim, Germany), in accordance with the manufacturer's protocol. Briefly, this involved incubation of supernatant samples with the LDH reagent in the dark for 3 min at RT, followed by measurement of excitation at 492 nm with a plate reader (TECAN, Männedorf, Switzerland). For the Alamar Blue assay (which indicated cell metabolic activity), the adherent cells were washed with PBS, and fresh cell culture medium and 10% of Cell Titer Blue Reagent (Promega, Mannheim, Germany) were added. Cells were incubated at 37 °C and 5% CO<sub>2</sub> and the formation of violet Resofurin salt was measured at 590 nm using a plate reader after 30 and 150 min. The specific metabolic activity was calculated as:  $(\text{Abs}_{2h30'} - \text{Abs}_{30'}) / 120'$ . Sample data was normalized to the non-treated medium control.

The viability of the inflamed and non-inflamed triple culture incubated with different concentrations of NPs was also evaluated with LDH and Alamar Blue assays, as described above.

### **3.2.6 Influence of Ag ions on cell viability**

The impact of Ag ions on cell viability was assessed using the LDH assay, as described in section 3.2.5. Caco-2 cells were incubated with AgNO<sub>3</sub>, Ag NPs and supernatant from which intact Ag NPs were removed. Ag NPs with a concentration of 156.25 µg/cm<sup>2</sup> were dispersed in cell culture medium, incubated for 24 h at 37 °C and ultracentrifuged (450,000 g). Supernatant was collected and Caco-2 cells were incubated with this for 24 h. As controls cells were also incubated with Ag NPs and AgNO<sub>3</sub> in equivalent concentrations under similar conditions.

### **3.2.7 Transmission electron microscopy (TEM)**

Inflamed and non-inflamed co-cultures were incubated with Ag NPs in a concentration of 156,25 µg/cm<sup>2</sup> and 15 nm Au NPs in a concentration of 20 µg/cm<sup>2</sup> for 24 h. Afterwards samples were prepared for TEM investigations as described in section 2.2.6.

### **3.2.8 TEER**

TEER measurement as an indicator of cell culture barrier function was performed before and 24 h after the incubation with NPs as described in section 2.2.4.

### **3.2.9 Cytokine measurement (IL-8) on the protein level via FACS**

The production of IL-8 as an indicator of inflammation was measured before and 24 h after the incubation with NPs as described in section 2.2.5.

### **3.2.10 Cytokine measurement (IL-8 and TNF- $\alpha$ ) on the mRNA level via Real-time PCR**

Relative changes in mRNA transcription of the pro-inflammatory marker IL-8 after incubation with different NPs were determined using a quantitative real-time polymerase chain reaction (qRT-PCR). Cells were incubated with NPs for 24 h, collected and lysed. Total RNA was then extracted from the cells with a QIAshredder (Qiagen, Hilden, Germany) and RNeasy Mini Kit (Qiagen, Hilden, Germany) according to the manufacturer's protocol. RNA amount was measured using a photometer (Eppendorf, Hamburg, Germany). A 500  $\mu$ g amount of RNA was then transcribed into cDNA with a QuantiTect Transcription Kit (Qiagen, Hilden, Germany).

Quantitative PCR was conducted using a QuantiTect Probe PCR Kit (Qiagen, Hilden, Germany) according to the manufacturer's instructions. Three replicates were measured for every sample. 35 cycles were measured (10 seconds: 94 °C, 30 seconds: 60 °C);  $\beta$ -actin was used as a housekeeping gene. Sequences of primers and probes employed are shown in Table 3.2.

**Table 3.2: Sequences of primers and probes for quantitative Real-Time PCR**

	Sense	Antisense	Probe
Human $\beta$ -actin	TGC GTG ACA TTA AGG AGA AG	GTC AGG CAG CTC GTA GCT CT	FAM-CAC GGC TGC TTC CAG CTC CTC- BHQ1
Human IL-8	TGC CAG TGA AAC TTC AAG CA	ATT GCA TCT GGC AAC CCT AC	FAM-TCA ACA CTT CAT GTA TTG TGT GGG TCT G-BHQ1
Human TNF $\alpha$	CTC CAC CCA TGT GCT CCT CA	CTC TGG CAG GGG CTC TTG AT	FAM-CAC CAT CAG CCG CAT CGC CGT CTC-BHQ1

### 3.2.11 Statistical analysis

Where appropriate, data are presented as mean  $\pm$  standard deviation (SD). One way ANOVA with Holm Sidak test was used to compare results from different treatments at different time points. The ANOVA analysis was done with SigmaPlot 12.5 (Systat Software GmbH, Erkrath, Germany). Significance was assumed at  $p < 0.05$  (\*) or  $p < 0.001$  (\*\*). Individual experiments were performed in triplicate and each experiment was performed twice. EC50 values were calculated with Sigma Plot 12.5.

### 3.3 Results

#### 3.3.1 NP characterization

Engineered NPs were evaluated according to their dispersion behavior. The two Au NP batches could be easily dispersed in the culture medium at the tested concentrations. The measured hydrodynamic diameter was slightly larger than the nominal diameter supplied by the manufacturer (Table 3.3) with a PDI < 0.1, indicating a narrow size distribution even at high concentrations of 0.1 mg/ml. The particles did not agglomerate in the cell culture medium, but a thin particle corona was likely formed by adsorption of proteins or other components from the Caco-2 medium.

For TiO<sub>2</sub> particles, the dispersibility was very poor in MilliQ water, but could be improved in cell culture medium due to the high FBS/protein concentration and resulting steric stabilization of the particle dispersion. Nevertheless, agglomerates between 700 and 1200 nm were still formed, and measured particle samples showed a high PDI (> 0.4).

Ag NPs could not be evaluated in the Zetasizer via dynamic light scattering due to interference with the laser. Instead the size distribution and stability of the particle dispersion were determined using single particle tracking analysis (NanoSight, Malvern Instruments, Herrenberg, Germany), which employs a different laser wavelength. The mean hydrodynamic diameter of the particles was found to be 120 nm; this value was considerably higher than manufacturer-supplied value < 20 nm, hinting at particle cluster formation together with serum proteins. Particle size distribution was however monomodal, and no agglomeration was observed within 24 h of storage in cell culture medium at 4 °C (Table 3.3).

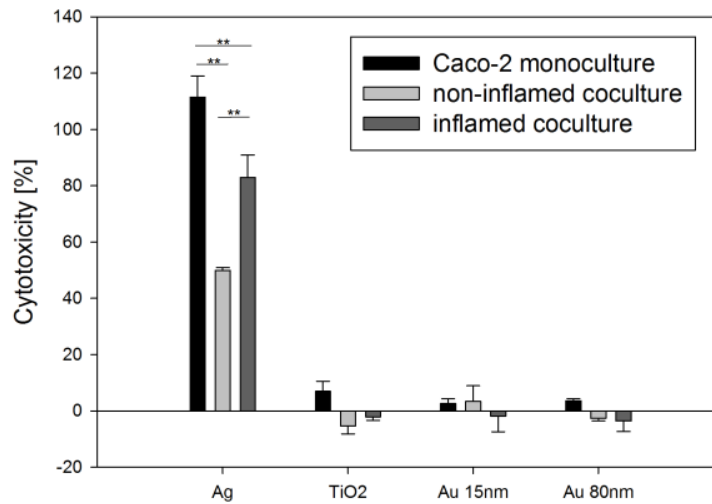
**Table 3.3: Dispersion behavior of ENs in DMEM cell culture medium at 0.1 mg/ml after 1 h of incubation**

NPs	Mean hydrodynamic diameter [nm]	PDI
Au 15	51 ± 6	0.04 ± 0.01
Au 80	116 ± 5	0.04 ± 0.02
TiO <sub>2</sub>	896 ± 133	0.42 ± 0.14
Ag	120 ± 4	NA

### 3.3.2 Cell viability measurement – LDH and Alamar Blue assay

After incubating Caco-2 monocultures and inflamed and non-inflamed co-cultures with the various NP concentrations, cell culture supernatant samples were collected to measure LDH release as an indication of cell damage. Furthermore, NP-treated cells were incubated with fresh medium and Cell Titer Blue reagent was added to measure the metabolic activity of the cells via the Alamar Blue assay. Figure 3.3 shows the results for both assays after incubation of Caco-2 monoculture, inflamed and non-inflamed co-culture for 24 h with 625 µg/cm<sup>2</sup> of Ag and TiO<sub>2</sub> NPs and 80 µg/cm<sup>2</sup> of both 15 nm and 80 nm Au NPs.

A



B

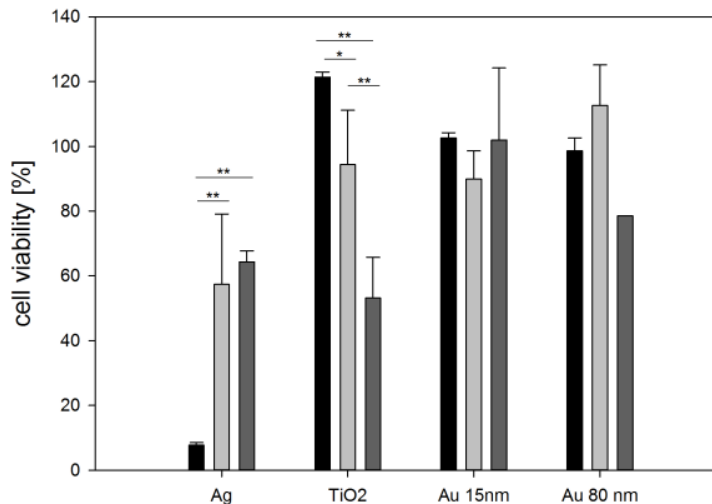


**Figure 3.3: Results of LDH (A) and Alamar Blue (B) assay after incubation of Caco-2 monoculture, inflamed and non-inflamed co-culture with the highest tested NP concentrations (mean  $\pm$  SD, n=6 from 2 independent experiments, \* =  $p < 0.05$ , \*\* =  $p < 0.001$ ).**

Incubation with the highest employed concentration of both types of Au NPs did not affect cell viability and there was no difference between the results of the Caco-2 mono- and co-culture setups, regardless of the state of inflammation. In contrast, the highest employed concentration of Ag NPs induced significant toxicity after 24 h. The Caco-2 monoculture was more sensitive to Ag NPs than the co-culture model. Looking at Figure 3.3A, it looks

like there is a significant influence of the state of co-culture inflammation on Ag NP-induced cytotoxicity, but not in Figure 3.3B. For TiO<sub>2</sub> NPs the LDH assay does not show any toxic effects. However, the results of the Alamar Blue assay show that viability of the cells decreases in the case of the inflamed co-culture.

To further investigate the toxic effects of the Ag NPs, these were studied at various concentrations which are shown in Table 3.1. Based on the results both from the LDH and Alamar Blue assay (Figure 3.4) the Caco-2 monoculture was significantly more susceptible than the co-culture to cytotoxic damage by Ag NPs, while there was at least a slightly increased susceptibility of the inflamed compared to the non-inflamed co-culture. LDH EC<sub>50</sub> values from Caco-2 monoculture (85 µg/cm<sup>2</sup>) and inflamed (216 µg/cm<sup>2</sup>) or non-inflamed (364 µg/cm<sup>2</sup>) co-culture also confirm this result.

The LDH assay was also used to investigate whether the presence of Ag ions was responsible for the toxic effect of Ag NPs (Figure 3.5). Incubation of cells with AgNO<sub>3</sub> containing liberated Ag<sup>+</sup> was confirmed to be equally toxic to Caco-2 cells as Ag NPs. In contrast, no LDH release was measurable in cell cultures treated with the Ag NP-free supernatant, indicating that Ag NP toxicity is not caused by released Ag<sup>+</sup> ions present in cell culture supernatants.

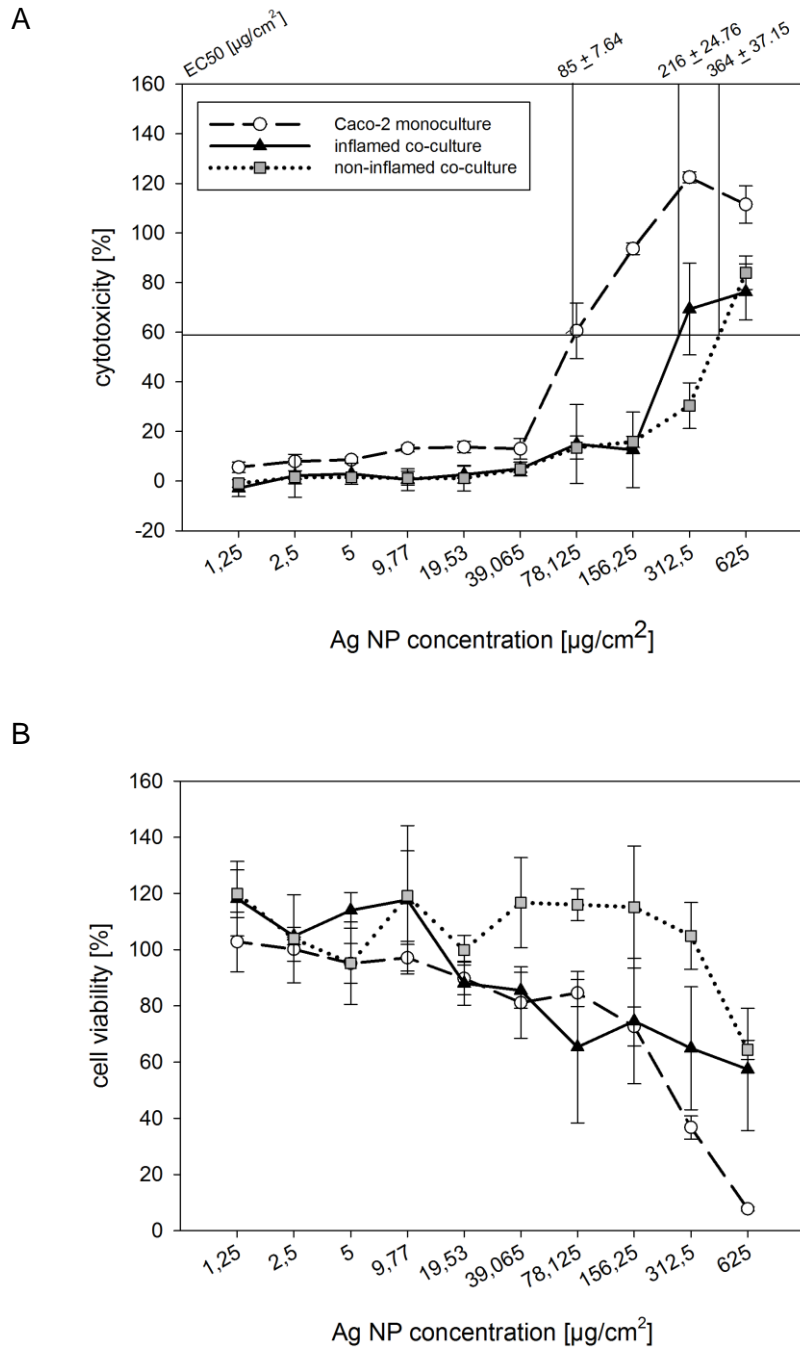


**Figure 3.4: LDH assay and Alamar Blue assay after incubation of Caco-2 monoculture, inflamed and non-inflamed co-culture with different concentrations of Ag NPs.** LDH release (A) and mitochondrial activity (B) were measured for all Ag NP concentrations in all cell culture setups (mean  $\pm$  SD,  $n=6$  from 2 independent experiments).

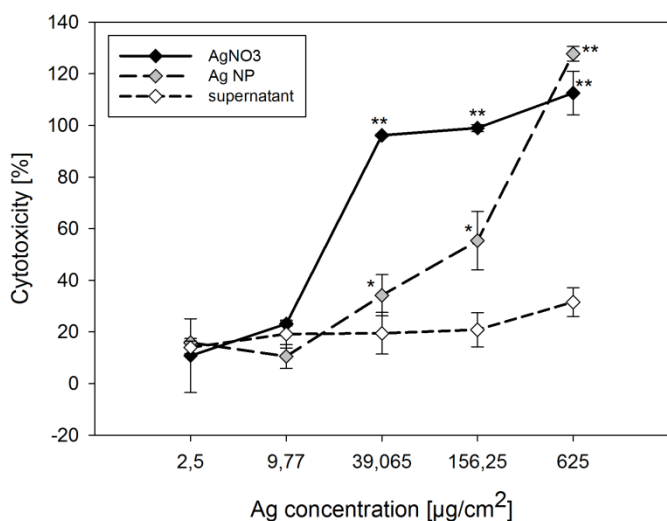


**Figure 3.5: Influence of Ag ions on cell viability.** LDH assay was performed in Caco-2 monoculture incubated with AgNO<sub>3</sub>, Ag NPs and supernatant from which intact Ag NPs were removed (mean  $\pm$  SD, n=3, \* = p<0.05, \*\* = p<0.001 relative to cells incubated with NP-free supernatant).

### 3.3.3 Assessment of Caco-2 cell integrity via TEER measurement

TEER of cell cultures was measured before and 24 h after NP incubation in order to assess the effect of NPs on barrier properties (Figure 3.6). Barrier function was seen to remain intact after incubation with TiO<sub>2</sub> (Figure 3.6B) or Au (Figure 3.6C/D) NPs, even following incubation of cells with high concentrations of NPs. However, in the case of both mono- and co-cultures, treatment of cells with Ag NPs at concentrations greater than or equal to 156.25  $\mu\text{g}/\text{cm}^2$  resulted in disruption of the epithelial barrier, as indicated by a steep drop of the TEER (Figure 3.6A). The monoculture was seen to be the most sensitive to Ag NPs followed by the inflamed and the non-inflamed co-culture, with a decrease in TEER already observable at the even lower concentration of 78.125  $\mu\text{g}/\text{cm}^2$ .

With the highest Ag NP concentration (625  $\mu\text{g}/\text{cm}^2$ ), TEER values showed an abrupt decrease in both mono- and co-cultures, to extremely low levels similar to those exhibited by cells incubated with 1% TritonX, which served as a positive control (data not shown).

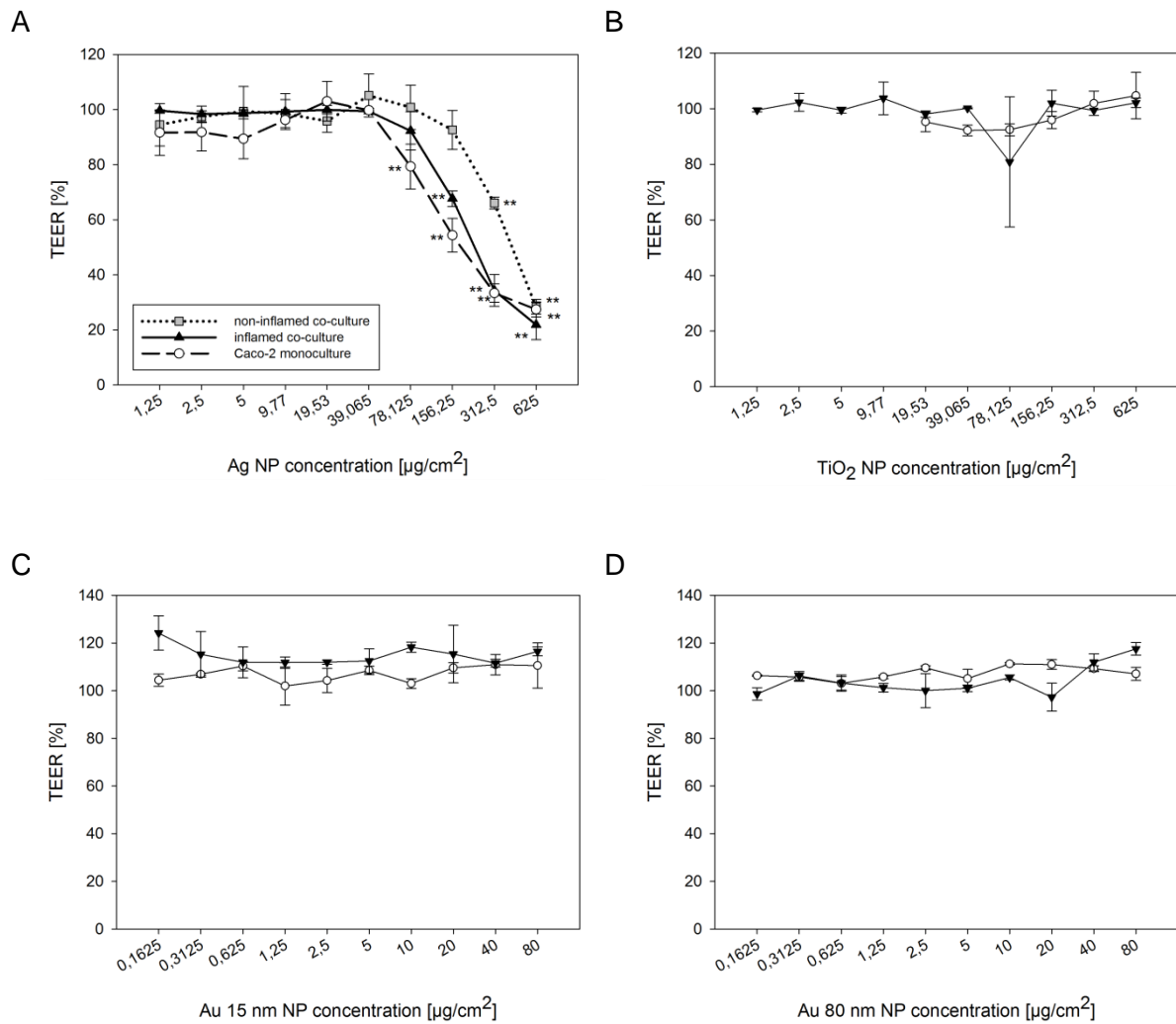


**Figure 3.6: TEER values of Caco-2 monoculture, inflamed and non-inflamed co-culture after incubation with different concentrations of the NPs.** Cells were incubated for 24 h with Ag (A), TiO<sub>2</sub> (B), 15 nm Au (C) and 80 nm Au (D) NPs. TEER was measured before and after incubation. Values are shown as percentage of TEER values after incubation relative to TEER values before incubation with NPs (mean  $\pm$  SD, n=6 from 2 independent experiments, \*\* = p<0.001 relative to TEER values of non-treated controls (not shown)).

### 3.3.4 Impact of NPs on inflammatory response

In order to identify possible sub-lethal but nevertheless potentially damaging effects on the epithelial cells, inflammatory responses were monitored during cellular exposure to NPs by measuring the secretion of pro-inflammatory cytokines. For this purpose the apparently

non-toxic 15 nm Au NPs were chosen for investigation and compared with the evidently more toxic Ag NPs.

Co-cultures as well as Caco-2 monocultures were exposed to Ag and 15 nm Au NPs for 24 h. TiO<sub>2</sub> and 80 nm Au NPs were also initially tested, but production of neither IL-8 nor TNF- $\alpha$  could be detected (data not shown). The inflammatory response to Ag und 15 nm Au NPs was therefore evaluated by monitoring the stimulation of IL-8 on a protein level (Figure 3.7A/B), as well IL-8 (Figure 3.7C/D) and TNF- $\alpha$  (Figure 3.7E/F) on a transcriptional level. In Caco-2 monoculture a slight increase in IL-8 release was only observed with the highest Ag NP concentration employed. However in both the inflamed and non-inflamed co-cultures, IL-8 release was observed already after incubation with the lowest tested concentration of Ag NPs (Figure 3.7A). This indicates that Ag NPs induce inflammatory reactions even at concentrations which are not toxic to the cells. With respect to the relative induction of inflammation with Ag NPs, again, significant differences between the inflamed and non-inflamed co-culture state were observed. Surprisingly the non-inflamed co-culture released more IL-8 than the inflamed one when exposed to Ag NPs. The results with Ag NPs from real-time PCR experiments agreed well with protein expression data (Figure 3.7C). TNF- $\alpha$  measurement showed similar results as seen with IL-8, although a relatively lower expression of TNF- $\alpha$  was observed (Figure 3.7E).

Incubation of Caco-2 cells in monoculture with low concentrations of Au NPs did not induce a significant increase of IL-8 production at any tested concentration. In the co-cultures a considerable release of IL-8 was observed, however the levels were approximately ten times lower than those observed with Ag NPs. Again the stimulation was concentration-dependent, but in this case the inflamed co-cultures released more IL-8 than the healthy ones (Figure 3.7B). In the co-culture models a release of TNF- $\alpha$  was also observed, however this only reached appreciable levels at the highest employed concentration of Au NPs (Figure 3.7F).

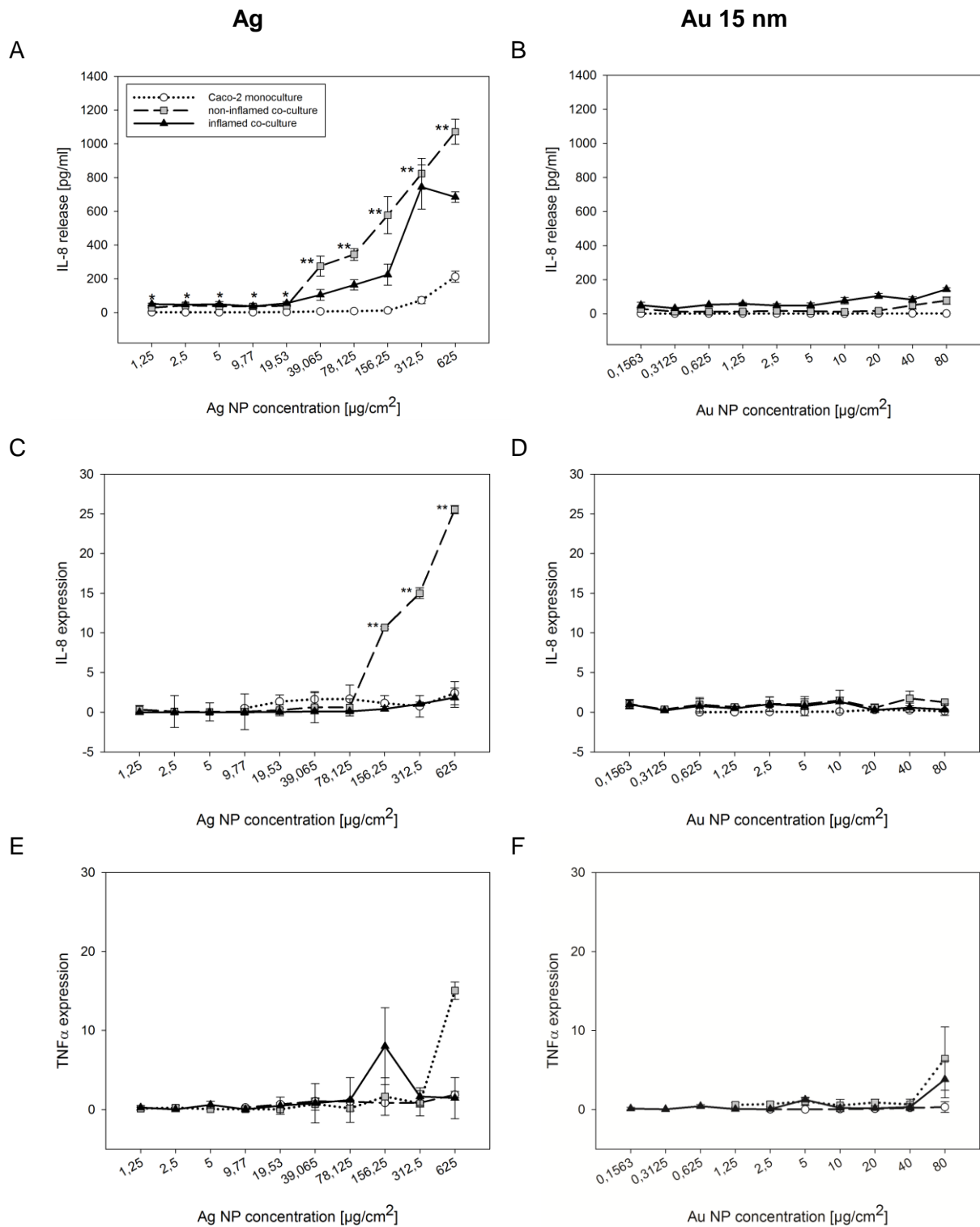


**Figure 3.7: IL-8 release on protein (A,B) and transcriptional level (C,D) and TNF- $\alpha$  release on transcriptional level (E,F) after 24 h incubation of Caco-2 monocultures, inflamed and non-inflamed co-cultures with different concentrations of Ag and Au NPs. Cells were incubated for 24 h with Ag (A/C/E) or 15 nm Au (B/D/F) NPs (mean  $\pm$  SD, n=6 from 2 independent experiments, \* = p<0.05, \*\* = p<0.001).**

### 3.3.5 Uptake of NPs

To evaluate the internalization of NPs, TEM analysis were performed with co-cultures after 24 h incubation with NPs. TiO<sub>2</sub> NPs could not be included in this experimental setup as samples for the TEM have to be cut with a diamond knife, which was not able to cut these particles. TEM images of cells incubated with Ag NPs could not be analyzed with respect to particle uptake, as the used concentration of 156.25 µg/cm<sup>2</sup> of Ag NPs was seen to be toxic (as confirmed by cytotoxicity studies) and resulted in the death of cells in the co-culture set-up. The 15 nm Au NPs were however found to be taken up by the cells. No particles could be found in macrophages or dendritic cells, but it could be shown that the NPs were taken up by Caco-2 cells in the co-culture independent of the state of inflammation (Figure 3.8).

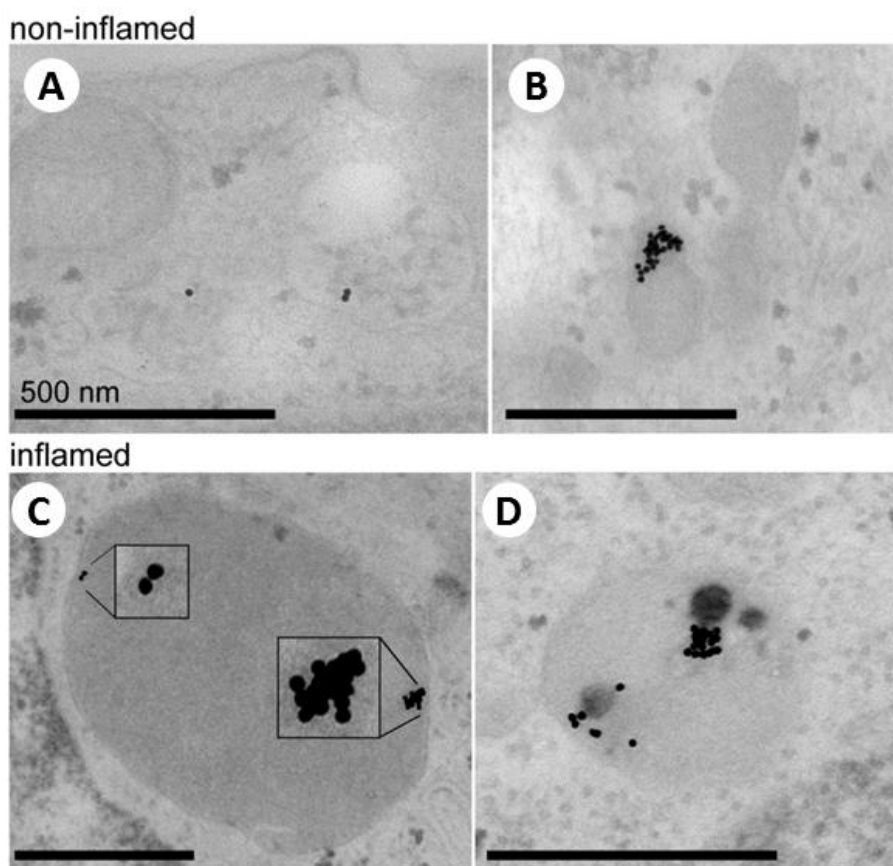


**Figure 3.8:** TEM images of Au NPs (15 nm) uptake by Caco-2 cells in non-inflamed (A,B) and inflamed (C,D) co-culture following 24 h incubation.

### 3.4 Discussion

Assessment of toxicity of nanomaterials is of huge concern, as a significant fraction of the population comes into daily contact with NPs. Furthermore, the field of nanotechnology is advancing at an increase rate, yet still not enough is known about the danger of nanomaterials. Many examples shown in the review by Arora et al. [104] illustrate how important thorough nanotoxicological characterization is, in order to avoid potential adverse effects of nanomaterials. By using appropriate *in vitro* models the toxicity of nanoparticles can be tested and thereby the safety of nanomaterials can be increased.

In the light of the importance of toxicity testing and the use of appropriate, representative models to do this, the aim of the study in this chapter was to investigate the toxicity of different ENs in different cell culture setups. The results from a Caco-2 monoculture and inflamed and non-inflamed co-cultures of the intestinal mucosa were compared to determine if the used co-cultures showed different behavior in presence of the NPs in comparison to the monoculture, and thus potentially provide data more relevant to the *in vivo* situation than the standard Caco-2 monoculture.

Cytotoxicity testing in cell cultures is a very important tool in toxicology [105]. Caco-2 cells are considered to be the most often used model for the human intestine, in the light of their previously mentioned morphological and biochemical similarities to small intestinal enterocytes: they grow in a monolayer, show a cylindrical polarized morphology with microvilli on the apical side and tight junctions between cells, and express small intestinal hydrolase enzymes [106]. As such, Caco-2 cells have been used as a model of the intestinal mucosa in several toxicity studies, not just with NPs, but also with numerous other compounds. However, the *in vitro-in vivo* correlation in these experiments is often not satisfactory [92]–[94]. The limitation of the Caco-2 monoculture is that the interaction between different cell types, as occurs *in vivo*, is missing; for example immune competent cells, which play a very important role in the reaction after exposure to NPs or other toxic compounds, are absent. Therefore, the currently employed co-culture model with Caco-2

cells, macrophages and dendritic cells was established. In this model the influence of immune-competent cells (e.g. possible protection of epithelial cells) on the results of cytotoxicity measurements could be assessed. Another advantage of such a model is that it is possible to induce an inflammation, creating possibilities for testing in relevant disease models as for example IBD.

To assess the toxicity of different ENs, Caco-2 monocultures as well as inflamed and non-inflamed co-cultures were incubated with the NPs for 24 h. Cytotoxicity was measured via membrane damage (LDH release), mitochondrial activity (Alamar Blue assay) and integrity of the cell monolayer (TEER); inflammation was also assessed via measurement of release of pro-inflammatory markers (IL-8 and TNF- $\alpha$ ) on both transcriptional (real-time PCR) and protein (FACS) levels. Some similarities could be seen in Caco-2 monoculture testing in comparison to the inflamed and non-inflamed co-cultures. However, some interesting differences between the cell culture setups were also found.

To explore the possible differences in toxicity triggered by various ENs, we studied the interactions of Au, TiO<sub>2</sub> and Ag NPs with the 3D co-culture and with Caco-2 monolayers. For Au NPs some studies have shown that they are not toxic; however, in contrast, other studies have found a low toxicity of Au NPs [107]–[109]. It is possible that the toxicity depends on the size of the particles [110]. Here two differently-sized Au NPs were used, 15 and 80 nm, but no toxic effect in response to incubation with these NPs was detected in any cell culture model (Figure 3.3). However IL-8 gene expression was slightly increased after exposure to the 15 nm Au NPs in the triple culture models (Figure 3.7). This is in agreement with literature, where it has been shown that Au NPs induce an inflammatory response also in a co-culture model of the human airways [60]. *In vivo* assays have also shown a significant expression of pro-inflammatory markers such as IL-6, IL-1 $\beta$  [111] or, as in our case, TNF- $\alpha$  [60] after treatment with different Au NPs.

Our observations that Au NPs were able to induce inflammatory responses that were evident only in the co-culture models is in agreement with other studies, supporting the

use of more complex *in vitro* systems to investigate in-depth interactions between NPs and biological systems. Differences in responses of co-cultures and monocultures of epithelial cells (H441) and endothelial cells (ISO-HAS-1) [105] have been documented in literature, while further studies have highlighted clear differences between the interaction of nanomaterials with co-culture and monoculture models [71], [84]. It has also been shown previously that a co-culture system with epithelial and immune cells, such as macrophages, dendritic cells or mast cells, can exhibit an amplified inflammatory response following contact with particles in comparison to monoculture models [112]. In our model this amplified effect can be explained by the presence of the macrophages and dendritic cells, which are both responsible for the cytokine release, which was shown in Figure 2.3. The measurement of interleukins as readouts of inflammatory NP interactions with cells allows for the investigation of other cellular responses besides membrane permeability and metabolic activity changes. Indeed, interleukins are important biomarkers for inflammation also in the *in vivo* situation as shown for example in the high release of IL-8 in the GI tract of IBD patients [113]. Therefore the inflammatory response, and cytokine measurement as a reliable endpoint for this, is an important parameter to be addressed in the interaction between NPs and living systems. As such it should be included in safety testing of NPs and nanoparticulate pharmaceuticals, as, as seen in the current work in relation to experiments with Au NPs, potentially harmful inflammatory effects can occur even at subtoxic concentrations.

When the uptake of Au NPs by the cells in the 3D co-culture was evaluated, it was found that these particles were mostly internalized by Caco-2 cells rather than by macrophages (Figure 3.8). This effect could possibly be due to the 24 h incubation time used for the experiment – while the immune cells could have in fact taken up the particles, particle digestion could have already taken place by the time of TEM investigations. Another reason could be that the collagen layer is a limiting factor in the co-culture system. It was shown in the previous chapter that the immune cells are able to move through the collagen to get between or on top of the Caco-2 cells. However, it is not proven if the NPs

are able to similarly get through the collagen layer, meaning that perhaps not many immune cells are able to get in contact with the nanomaterials.

NM101 TiO<sub>2</sub> NPs did not induce any notable toxic effects or inflammation in either monoculture or triple culture models in the current work (Figure 3.3, Figure 3.6, Figure 3.7), which is a good sign since TiO<sub>2</sub> NPs are often found in food or tooth-paste [114] and can easily reach the human intestine. Other studies have shown a low toxicity of differently-sized TiO<sub>2</sub> NPs to mouse macrophages [115] and epithelial lung cells [116] in monoculture models; a study utilizing a co-culture model of the human airway wall with macrophages, dendritic cells and epithelial cells however corroborates our results, as no toxicity or pro-inflammatory reactions after treatment with TiO<sub>2</sub> NPs were observed [60].

NM300 Ag NPs clearly demonstrated toxicity in all cell culture models used in the current work. LDH and Alamar Blue results showed that these particles induced a dose dependent toxicity in Caco-2 cell monocultures and in co-cultures in both healthy and inflamed conditions. However, EC50 values from LDH assays show that the Caco-2 monoculture was more sensitive to the Ag NPs than the co-culture models (Figure 3.4). As a clear interaction between immune-competent cells and Caco-2 cells was observed in the 3D co-culture as evidenced by TEM (Figure 2.4) and CLSM (Figure 2.6) images, it is believed that this interaction might help to reduce the sensitivity to the toxic NPs, compared to the Caco-2 monocultures. It must also be mentioned however that, in spite of a clear toxic effect following treatment with Ag NPs, the sensitivity of the Caco-2 cell monocultures and 3D models to the Ag NP was overall quite low, displaying LC50 values more than 20-100 fold higher than for other cell lines. A research group in Scotland tested the same Ag NPs on C3A cells, a human hepatoblastoma cell line; cytotoxicity measurements showed LC50 values from 2.5 µg/cm<sup>2</sup> (WST-1 assay; LDH assay) to 5 µg/cm<sup>2</sup> (Alamar Blue assay) [117], [118]. This is in contrast to the EC50 value of 85 µg/cm<sup>2</sup> calculated using the LDH assay for the Caco-2 cell monocultures in the current work, and even higher values for the co-culture models. As a point of commonality with

the C3A toxicity investigations however, it was observed in the current work that the Alamar Blue assay was not as sensitive as the LDH assay, and so a lower EC50 value was calculated for the particles with the LDH assay as compared to the Alamar Blue assay (data not shown).

The toxic effect of Ag NPs was also observed as a disruption of barrier function, as indicated by recorded TEER values (Figure 3.6). TEER values decreased after incubation with higher Ag NP concentrations; this considerable decrease correlated well with an increased cell death, as inferred from a high LDH release. Furthermore, TEER profiles indicated that the non-inflamed triple culture was less sensitive to the Ag NPs than the inflamed one, in agreement with the data from LDH and Alamar Blue assays. This suggests that the inflamed triple culture is already in a state of stress resulting from the IL-1 $\beta$  treatment.

The current experiments also showed that IL-8 release was higher in the non-inflamed co-culture than in the already inflamed one after incubation with Ag NPs. This might again be explained by the fact that the inflamed co-culture is already stressed by the inflammation and is not able to release even more IL-8. It may therefore be suggested that the non-inflamed tissue is better protected against effects of toxic materials than the inflamed one as it is capable of releasing more cytokines, and perhaps is therefore better able to initiate activation of the immune system in order to provide protection against the toxic material. A high level of release of IL-8 was also observed in other studies that addressed the toxic potential of Ag NPs in human renal proximal tubule epithelial cells (HK-2) [118], C3A cells [117], and also *in vivo* in mice [119]. Further research groups studying cytotoxicity of Ag NPs *in vivo* found that these particles are mutagenic in mouse lymphoma cells and increase oxidative stress [120]. *In vivo* experiments of other groups showed that after oral uptake, Ag NPs reach the blood circulation and can be found in various other tissues not limited to the intestine [121]. After oral uptake it is possible that most of the NPs are directed to the liver because of its role in drug metabolism [122]. Therefore besides

experiments with intestinal models it would also be useful to test the toxicity of NPs on hepatocytes *in vivo* and *in vitro*. Studies have also been conducted to compare *in vivo-in vitro* correlations utilizing Ag NP toxicity data. The toxicity in human lymphocytes, plants and mice was tested and a very good correlation was found between the different results from *in vitro* and *in vivo* experiments [123]. Gaiser et al. also compared the cytotoxicity of Ag NPs in a hepatocyte cell line (C3A) and in mice. Similar results were found in these experiments with Ag NPs exhibiting cytotoxicity in the cell line and also *in vivo* [118].

So far a proven explanation for Ag NPs showing such a high toxicity is not available. Several studies suggest that released Ag ions are responsible for cytotoxic effects [124], [125]. Hence in the current work, experiments were conducted with particle-free supernatants from Ag NPs following ultracentrifugation (Figure 3.5). No toxic effects could be detected, which shows that released Ag ions are in fact not the reason for the observed cytotoxicity, at least in the current case. This is in line with findings from C3A cell studies which were also not seen to be affected following treatment with particle-free supernatant; cells however demonstrated low viability, inflammation and oxidative stress upon exposure to NM300 Ag NPs [117]. Other studies with the same NM300 Ag NPs showed that less than 1% of the particles were dissolved in the cell culture medium used for experiments, which makes it very unlikely that the toxicity observed was due to the release of Ag ions [118].

While it can be seen from the presented work that the current co-culture model is a very good setup in which to assess toxicity effects, its ability to simulate conditions in either a healthy or inflamed intestine also makes it a potentially very useful tool for IBD studies. A next step in the exploration of the possible applications of the model could therefore focus on efficacy rather than safety testing, and could involve observation of the deposition or healing effect of drug-loaded particles or other formulations. For the treatment of IBD patients it is important to know the deposition behavior of particles or drugs in the tissue. With the current co-culture model this could be determined, and a comparison made

between results in the healthy and inflamed state. It is also possible that the immune cells show an influence on the epithelial barrier properties especially during an inflammation. This was already shown in other studies with inflamed co-culture models for the alveolar region of the lung [80].

### 3.5 Conclusion

The Caco-2 cell line is widely accepted as an accurate model of the normal, healthy intestinal mucosa, but this model cannot mimic the complex interactions between different cell types of the immune system and their influence on overall epithelial layer function. Therefore the co-culture model consisting of Caco-2 cells, THP-1 macrophages and MUTZ-3 dendritic cells was used to better mimic the *in vivo* response.

The cytotoxicity of the various types of NPs was measured in a Caco-2 monoculture and in the developed co-culture model of the intestinal mucosa consisting of macrophages, dendritic cells and epithelial cells, in either an inflamed or non-inflamed state. The differences between healthy and inflamed tissue in terms of barrier permeability further support the importance of a model capable of mimicking diseased conditions, which results in different outcomes during the testing of new formulations. The presence of immune-competent cells as in the current co-culture model is therefore very important in the assessment of NP-cell interactions. Indeed, a release of pro-inflammatory cytokines was noted in current toxicity testing employing the co-culture, but not monoculture models, providing valuable information relating to inflammatory effects - an important endpoint to be considered in safety testing of nanomaterials. Thus, this study provides a new 3D co-culture model of the intestinal mucosa, which can be utilized in either a healthy or inflamed state, suitable for assessment of toxic and inflammatory effects of engineered nanomaterials as well as nanoparticulate pharmaceuticals in the intestine.

---

## 4 Application of the cell line-based co-culture model for efficacy testing of anti-inflammatory formulations

Parts of this chapter will be submitted for publication:

C. Draheim, **J. Susewind**, A. Guillot, B. Loretz, S. Hansen, E.-M. Collnot, C. Villiers, P. Marché, M. Limberger, C.-M. Lehr “PLGA based nano- and microsized particles for inflammatory bowel disease therapy: evaluation of size-dependent accumulation and anti-inflammatory effect in an *in vitro* triple culture model”, *to be submitted*

Julia Susewind made the following contributions to this work: performed all cell culture experiments, measured TEER and IL-8 data, made confocal images, analyzed all data from these experiments and wrote the manuscript.

My colleague Christina Draheim evaluated nanoprecipitation and spray drying methods for the production of particles employed in the current work [135], prepared nanoparticles and microparticles and performed stability and characterization studies.

## 4.1 Introduction

The therapy of IBD, including the chronic and severe forms of Crohn's disease (CD) and ulcerative colitis (UC), is currently limited to the reduction of symptoms rather than being curative [126]. Therapies for IBD symptom reduction also have limits in term of their possible route of application; administration via pellets or tablets for example is often not efficient, as the frequent occurrence of diarrhea in IBD results in an enhanced elimination of orally-administered drug carriers and a limited drug release time [10]. Furthermore, the drug candidates themselves are often immunosuppressive or anti-inflammatory drugs that are required to be taken in daily doses, often leading to severe adverse effects [127]. Drug delivery systems (DDS) that carry the used drugs directly to the inflamed areas of the intestine would therefore be of considerable benefit for patients suffering from IBD – this could provide for an optimized therapy with respect to the limited drug release window, and, compared to a systemic application, such local treatment would allow for a dose reduction which could in term minimize undesired side effects.

Depending on the severity level of CD and UC with particular respect to the degree of inflammation, a reorganization of the intestinal epithelium occurs and ulcerated areas also develop in the intestine [10], [128], [129]. It was shown that the altered intercellular spaces, which occur specifically in the ulcerated areas, are an accessible target for particulate DDS of a suitable size range. Accumulation and prolonged localization of such particles was seen to occur at areas of inflammation, allowing for the release of particle-incorporated active pharmaceutical ingredient (API) specifically in ulcerated regions over an extended time period. Further to this study, Lamprecht et al. reported a size dependent accumulation of non-biodegradable polystyrene NPs in a TNBS colitis mouse model [130]. In contrast to this however, a recent study showed that microparticulate formulations seem to be favorable in terms of accumulation in ulcerated intestinal regions in human patients [131]. More investigations are needed to explain this apparent difference in optimal DDS size for accumulation in murine and human studies. Therefore, in the current

chapter, DDS of the biodegradable and biocompatible polymer polylactic-co-glycolic acid (PLGA) in both nano- and microparticle-size were developed. Two processes were chosen for this purpose: a nanoprecipitation method in order to produce nanoparticles of  $150 \pm 10$  nm, and a nano spray drying technique to fabricate microparticles (MPs) of  $\sim 4$   $\mu$ m in a single step. Both methods were recently established at the Helmholtz Institute for Pharmaceutical Research Saarland (HIPS) and can be scaled-up in one set-up with regards to a development production scale [135].

PLGA is a co-polymer approved by the Food and Drug Administration (FDA) for use in a number of *in vivo* devices and applications, such as in implants and as the major component of surgical sutures. Through hydrolysis of the ester bonds PLGA is degraded in the human body to its two non-toxic components, lactic acid and glycolic acid, which can then be further metabolized in the citric acid cycle [132], [133]. In a 50/50 (wt/wt) ratio of lactic acid to glycolic acid, PLGA exists in an amorphous state; this is optimal for use in DDS, because amorphous PLGA shows the fastest degradation rate and decomposes in the body within two months [95], [96].

As APIs for encapsulation in PLGA-based DDS the drugs budesonide (Bu) and cyclosporine A (CyA) were chosen. They both show anti-inflammatory effects and can be used for IBD therapy. Bu is generally used in a dose of 9 mg per day [136] for oral and rectal treatment of ileal and right colonic CD [137]. In contrast, CyA is often used in fulminant UC intravenously, followed by oral maintenance therapy [138], [137]. Although both APIs are often used for IBD treatment and show a real success in terms of alleviating symptoms, they also lead to several serious side effects [139]. The use of a suitable DDS as described above in order to reduce such side effects is therefore highly desirable. Several studies have already reported on loading of PLGA particles with CyA [142]–[144] as well as with Bu [145], [146] and some promising improvements of IBD therapy could already be shown as a result of the administration of these systems. Nevertheless, to our knowledge, a comprehensive study comparing anti-inflammatory drug-loaded nano- and

microparticles with regards not only to their release kinetics, but also the suitability for inflammation targeting and functional effects, has not yet been performed.

To evaluate the anti-inflammatory efficacy of the developed DDS the use of an *in vitro* cell culture model was preferred, due to the numerous advantages of such models. Firstly as the size-dependent accumulation behavior of DDS is known to show species variability, an advantage of *in vitro* models is that human cell lines can be used to avoid this problem. The analysis in *in vitro* systems is also often easier and faster than in *in vivo* experiments; cell culture models are also less ethically questionable than animal-based testing, and, importantly, provide for a much easier performance of screening studies due to a reduced variation in readout data [51]. Furthermore, *in vitro* models are a first step before such formulations can be tested in animal models. Several cell-based *in vitro* models of the intestine [40], [41], [145] have already been developed, as shown in earlier chapters of this thesis. However, as also discussed, the majority of these models have a focus on application in transport or uptake studies. In contrast, the cell line-based three-dimensional co-culture model developed in this thesis has the advantage over other such models that it does not only show good barrier properties, but can also be inflamed by adding IL-1 $\beta$  to the apical culture compartment. Furthermore, this model contains macrophages and dendritic cells, which are some of the key players in inflammatory reactions. Important markers of inflammation such as increased IL-8 release and decreased TEER values can be detected and measured in this model, as demonstrated in previous chapters of this thesis. This triple culture model therefore has considerable potential as a means to accurately assess the anti-inflammatory efficacy of CyA and Bu PLGA particulate systems. Moreover, the model allows for physiologically-relevant application - DDS can be introduced to the apical compartment of the co-culture model, which mimics the intestinal lumen and therefore is relevant for oral/rectal application; likewise, addition of DDS to the basolateral compartment of the co-culture system allows for stimulation of treatment from the blood side (i.e. parenteral administration). The

relative efficacy of DDS following different routes of application can therefore be compared in this co-culture setup.

In the light of the above, the aim of the study in this chapter was to test developed and optimized PLGA-based DDS for IBD therapy in the co-culture model of the inflamed intestinal mucosa. Both APIs, CyA and Bu, were encapsulated in the PLGA NPs and MPs. The effects of loaded PLGA NPs and MPs were then directly compared in order to improve the understanding of the importance of inflammation targeting and specific release profiles on a successful treatment of IBD. As the two drugs have different physico-chemical properties, it was anticipated that differences in DDS encapsulation efficiencies and release kinetics could be seen. The known difference in pharmacological effects of CyA and Bu was also expected to influence the relative action of API-loaded NPs and MPs during DDS testing. The investigation of the size-dependent DDS accumulation at the site of inflammation, the anti-inflammatory effect of CyA and Bu DDS and the possibility to analyze these factors *in vitro* in the co-culture model were addressed.

## **4.2 Materials and Methods**

### **4.2.1 NP preparation by nanoprecipitation**

NPs were produced by nanoprecipitation as described by Draheim et al. [135] using a HARVARD<sup>®</sup> Ultra PHD pump (Hugo Sachs Elektronik, Germany). PLGA (Resomer RG 503 H; inherent viscosity 0.41 dl/g; Evonik, Darmstadt, Germany) (1.3%, w/v) and Bu (Caesar & Loretz GmbH, Hilden, Germany) or CyA (Fluka) were dissolved in a mixture of acetone/ethanol (16:3, v/v, organic phase). The solution was injected into purified water containing 1% poloxamer 407 (Evonik, Darmstadt, Germany) (w/v) as stabilizer. To determine the maximal loading capacity of NPs, increasing amounts of CyA and Bu were added to the organic phase during particle preparation, while keeping the amount of PLGA used constant. Investigated ratios of API:PLGA (wt/wt) were: 0.5:10, 1:10, 2:10,

3:10, 4:10 in the case of Bu, and additionally 5:10 in the case of CyA. Formed particles were purified and freeze dried using 0.3% (w/v) PVA and trehalose as cryoprotectant.

For imaging the particles following application to the triple culture model, the lipophilic, far-red fluorescent carbocyanine DiD (Invitrogen, Life Technologies GmbH, Darmstadt, Germany) was encapsulated in the NPs following the same protocol. A DiD stock solution (25 mg/ml in ethanol) was directly added at an amount of 10  $\mu$ l per 10 mg of PLGA mixture in acetone:ethanol (16:3, v/v).

#### **4.2.2 PLGA MP preparation by nano spray drying**

A Büchi Nano Spray Dryer B-90 (Büchi Labortechnik GmbH, Essen, Germany) was used for the nano spray drying technique as described by Draheim et al. [135]. For the feeding solution 1.1% PLGA (w/v), sorbitan monostearate (Span 60, 1.6% w/v) as stabilizer and APIs were dissolved in acetone. To determine the optimal loading of MPs, increasing amounts of APIs were employed in the feeding solution, with the same amount of PLGA (110 mg, equal to 1.1% in 10 ml organic phase). Used ratios API:PLGA (w/w) were 0.5:10, 1:10, 1:15, 2:10, 3:10 and 4:10 in the case of Bu, with an additional ratio of 5:10 investigated in the case of CyA. The volume of acetone used for all experiments was 10 ml. Feeding solution was sprayed using a 4  $\mu$ m mesh under ice cooling of the supplied dispersion to prevent heating of the circulating solution.

Particles containing DiD were prepared by directly adding DiD stock solution (25 mg/ml in ethanol) at an amount of 10  $\mu$ l per 10 mg of PLGA to the feeding solution.

### 4.2.3 Determination of particle size and size distribution

#### *Nanoparticles*

Hydrodynamic diameter and PDI were measured by dynamic light scattering (Zetasizer® Nano ZS, Malvern Instruments, UK) in purified water at 25 °C and a fixed angle of 173° in the case of CyA- and Bu-containing NPs; as the fluorescence of DiD loaded particles interferes with the Zetasizer laser, the size distribution of these NPs was characterized by NP tracking analysis (NTA, NanoSight® LM10 HS system, NanoSight Limited, UK) following re-dispersion in purified water. Mean diameter ( $d_{0.5}$ ) and percentile values  $d_{0.1}$  and  $d_{0.9}$  were calculated for NP samples by the NanoSight® software.

The zeta potential was measured for all NPs in purified water using a Zetasizer® Nano ZS (Malvern Instruments, UK)

#### *Microparticles*

Spray dried MPs were characterized by laser diffraction using a Mastersizer® 2000 equipped with a Mastersizer® 2000  $\mu$ P dispersion module (Malvern Instruments, Herrenberg, Germany). Particles were re-dispersed in purified water containing 0.01% PVA under manual shaking for 10 s prior to measurement. Volume mean diameter ( $d_{0.5}$ ), percentile values  $d_{0.1}$  and  $d_{0.9}$  and SD were calculated by the Mastersizer® software. Size distribution (width) is defined in Eq. 1.

$$width = \frac{d_{0.9} - d_{0.1}}{d_{0.5}} \quad (1)$$

### 4.2.4 Determination of encapsulation efficiency and optimal loading

HPLC quantification with a Dionex system (Thermo Fisher GmbH, Idstein, Germany) was used for the quantification of both APIs. The system ran on Chromeleon software version 6.80 SP2. A reversed phase column, LiChrosphere® RP18 column (5  $\mu$ m x 125 mm x 4 mm; Merck KGaA, Germany), and an isocratic elution were used. All

standards were dissolved in a mixture of acetonitrile/phosphate buffer pH 3.0 (1:1, v/v). In case of Bu the mobile phase consisted of a mixture of acetonitrile/phosphate buffer pH 3.0 (2:3, v/v). Oven temperature was set to 30 °C. The retention time was  $4.0 \pm 0.1$  min detecting Bu with UV at 242 nm. The method was linear ( $r^2 > 0.999$ ) between 2.0 µg/ml - 100.0 µg/ml with a lower limit of quantification (LOQ) of 2.0 µg/ml.

In case of CyA, a mixture of phosphate buffer pH 3.0/methanol (1:9, v/v) was used as mobile phase. The retention time was  $2.1 \pm 0.1$  min detecting CyA with UV at 205 nm. The method was linear ( $r^2 > 0.999$ ) between 10.0 µg/ml - 100.0 µg/ml with a LOQ of 6.0 µg/ml.

To determine the amount of encapsulated API, the encapsulation efficiency (EE), an aliquot of API loaded NPs or MPs was dissolved in a mixture of acetonitrile/phosphate buffer pH 3.0 (1:1, v/v) and treated in an ultrasonic bath to disintegrate the PLGA particles. The solution was filtered through a syringe filter with 0.45 µm pore size (CHROMAFIL GF/PET 45/25); the filtrate was collected and analyzed by HPLC to determine the API content.

$$EE = \frac{m(\text{API}_{\text{encapsulated}})}{m(\text{API}_{\text{initial}})} * 100 \quad (2)$$

The EE describes the percentage of encapsulated API referring to the initial mass of API (Eq. 2):  $m(\text{API}_{\text{initial}})$  refers to the weight of API put into the formulation and  $m(\text{API}_{\text{encapsulated}})$  refers to the API measured after the particle dissolution. The optimal loading was determined by encapsulating increasing amounts of both APIs, while keeping the PLGA amount constant. After washing and freeze drying, the EE was determined for NPs and MPs. To determine the actual loading, the mass of encapsulated API was used as seen in Eq. 3, which describes the actual loading as ratio of weight encapsulated API in mg to 100 mg of PLGA as indication for carrier capacity. Eq. 4 describes the theoretical loading which can be calculated from the initial amount of API referring to 100 mg of PLGA.

$$\text{actual loading} = \frac{m(\text{API}_{\text{encapsulated}})}{m(\text{PLGA}_{\text{initial}})} * 100 \quad (3)$$

$$\text{theoretical loading} = \frac{m(\text{API}_{\text{initial}})}{m(\text{PLGA}_{\text{initial}})} * 100 \quad (4)$$

Both actual and theoretical loading were correlated in one graph for NPs or MPs. This representation can be used to determine the optimal theoretical loading that is reached if by increasing the initial API mass the actual loading is not increasing proportionally.

#### 4.2.5 Stability of NPs and MPs in cell culture media

2 mg of blank, CyA- and Bu-loaded NPs and MPs were redispersed in 2 ml of Caco-2 or THP-1 medium (described in section 2.2.1). Particles were incubated for 24 h at 37 °C, with constant shaking at 100 rpm. At various time points (0, 2, 4, 8 and 24 h), 100 µl of the Caco-2 or THP-1 medium-particle suspension was diluted with purified water to 2 ml, in order to avoid light scattering of medium components e.g. proteins during subsequent size analysis. The size and PDI of NPs or MPs was measured as described in section 4.2.3.

#### 4.2.6 *In vitro* drug release

Release profiles of APIs from loaded NPs and MPs were investigated in PBS, pH 6.8 at RT in triplicate. To increase the solubility of CyA, 0.05% Tween 80 (w/v) was added to the PBS release medium. Release studies were performed under sink conditions, which are defined by the United States Pharmacopeia (USP) as being in place when a value no greater than 30% of the API saturation concentration is present in the release medium. Saturation concentrations were determined to be 42.3 µg/ml for CyA and 21.7 µg/ml for Bu; therefore the required mass of NPs or MPs were suspended in 30 ml of the release medium. Release experiments were performed in stock bottles closed with Parafilm®M (BRAND GmbH + CO KG, Germany) to avoid evaporation. The particle suspensions were stirred at 400 rpm at RT for the duration of the experiments. At pre-determined time points 1.5 ml suspension was removed and centrifuged (Hettich Rotina 420 R, Hettich Holding

GmbH & Co. oHG, Germany) at 24400 g at 20 °C for 15 min. 1 ml of the resulting supernatant was removed for analysis by HPLC as described previously. A 1 ml volume of fresh medium was then added to the rest of the supernatant to re-disperse the pellet, which was before replaced in the bulk release medium. Release was cumulatively calculated and normalized to the determined encapsulation efficiency of PLGA particles. The following values were defined for classifying the release of the different formulations:

Fast release: >80% API released after 4 h

Intermediate release: 50-60% API released after 48 h

Slow release: <10% API released after 4 h and <30% after 48 h.

#### **4.2.7 Cell culture**

Cells were maintained as described in section 2.2.1. The Caco-2 clone HTB37 was used for the following experiments.

#### **4.2.8 Triple culture of the inflamed intestinal mucosa**

The triple culture model was seeded as described in section 2.2.3.

Briefly, the co-culture of Caco-2, THP-1 and MUTZ-3 cells was grown until the Caco-2 cells formed a confluent monolayer and TEER values were higher than  $400 \Omega \cdot \text{cm}^2$ . On day 11 cells were inflamed by adding 10 ng/ml IL-1 $\beta$  into the apical compartment of the triple culture. Following two days of incubation, IL-1 $\beta$  was removed and cells were treated with the different particulate formulations or APIs in solution. After 4 (Bu) or 8 (CyA) h the formulations were removed, cells were washed with PBS and fresh cell culture medium was added. TEER values and IL-8 release were measured before and as well as 1, 2 and 3 days after formulation treatment as shown in Figure 4.1.

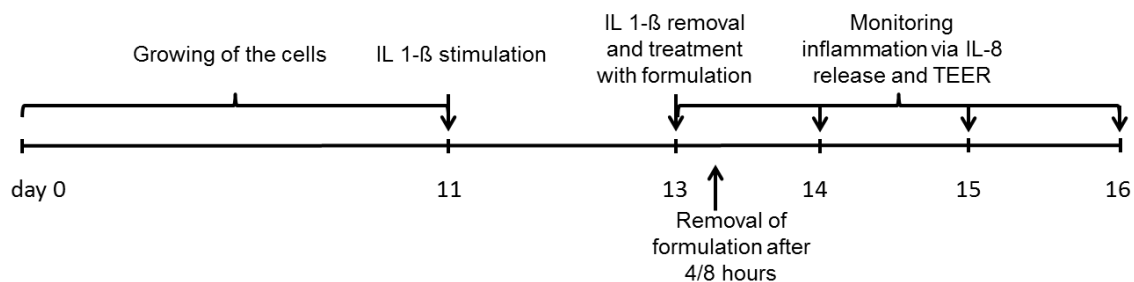


**Figure 4.1: Experimental setup for NP and MP efficacy studies using the triple culture model.**

#### 4.2.9 LDH assay

Assessment of the cytotoxicity of NPs and MPs via LDH measurement was performed as described in section 3.2.5. Caco-2, THP-1 and MUTZ-3 cells were incubated with different concentrations of blank NPs and MPs for 8 h. Afterwards supernatant was collected to measure LDH release.

#### 4.2.10 TEER

TEER measurement was performed as described in section 2.2.4.

#### 4.2.11 IL-8 measurement

IL-8 measurement via FACS was performed as described in section 2.2.5. Analysis was done with FCAP array v3.0 cytometric bead array analysis software (BD Biosciences, Heidelberg, Germany).

#### 4.2.12 Immunostaining of the triple culture for CLSM

Immunostaining was performed as described in section 2.2.7. As secondary antibody Alexa 488 anti-mouse antibody was used, diluted 1:400 in PBS.

#### **4.2.13 Statistical analysis**

Where appropriate, data are presented as mean  $\pm$  standard deviation (SD). One way ANOVA with Holm Sidak test was used to compare results from different treatments at different time points. The ANOVA analysis was done with SigmaPlot 12.5 (Systat Software GmbH, Erkrath, Germany). Significance was assumed at  $p < 0.05$  (\*) or  $p < 0.001$  (\*\*). Individual experiments were performed in triplicate and each experiment was performed twice.

### **4.3 Results**

#### **4.3.1 Encapsulation efficiency and optimal loading**

Particulate DDS should be loaded with the highest possible API content as the DDS itself should only act as a transporter or reservoir for the respective API. In general the loading of API into DDS is a function of lipophilicity of the API, and the polymer used to prepare the DDS [144]. As the PLGA-based DDS were established before [135], their ability to encapsulate the two APIs was now tested. The optimal loading was determined; the values are presented in Figure 4.2A for CyA and in Figure 4.2B for Bu; the line of identity shows an EE of 100% which means that the actual loading would be equal to the theoretical loading.

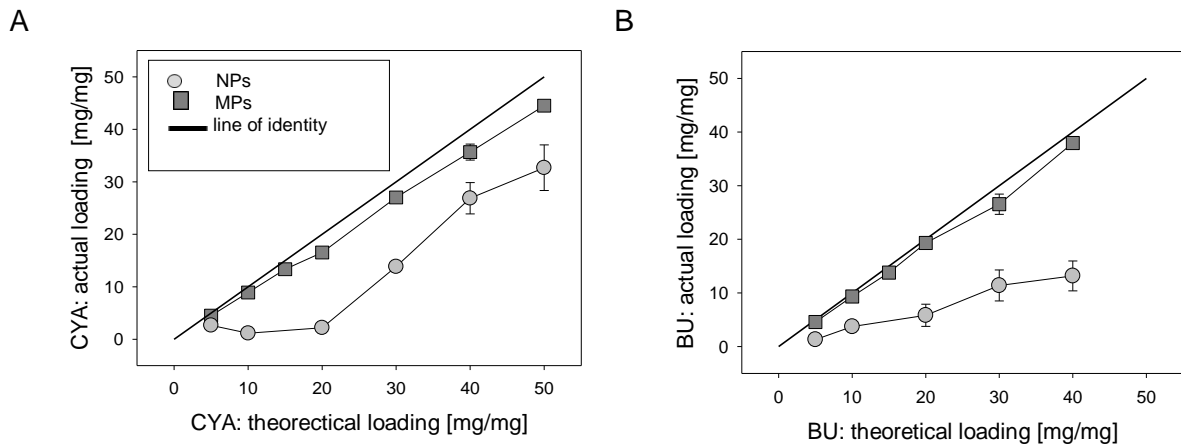


**Figure 4.2: Actual and theoretical loading of CyA-loaded (A) and Bu-loaded (B) NPs and MPs (mean  $\pm$  SD,  $n \geq 3$ ).**

**Table 4.1: Encapsulation efficiency of CyA-loaded NPs and MPs (mean  $\pm$  SD,  $n > 3$ ).**

Ratio	Formulation	
	NP [%]	MP [%]
0.5/10	53.3 $\pm$ 3.8	87.9 $\pm$ 3.3
1/10	11.6 $\pm$ 3.6	92.0 $\pm$ 0.8
2/10	11.0 $\pm$ 0.6	90.9 $\pm$ 3.2
3/10	46.2 $\pm$ 9.2	90.1 $\pm$ 1.5
4/10	67.2 $\pm$ 7.5	89.2 $\pm$ 3.8
5/10	65.4 $\pm$ 8.7	89.0 $\pm$ 0.8

**Table 4.2: Encapsulation efficiency of Bu-loaded NPs and MPs (mean  $\pm$  SD,  $n > 3$ ).**

Ratio	Formulation	
	NP [%]	MP [%]
0.5/10	26.5 $\pm$ 2.5	91.6 $\pm$ 0.2
1/10	36.5 $\pm$ 4.3	91.4 $\pm$ 6.3
2/10	29.7 $\pm$ 9.9	98.3 $\pm$ 5.4
3/10	39.1 $\pm$ 10.3	92.9 $\pm$ 6.6
4/10	34.1 $\pm$ 7.6	94.8 $\pm$ 2.6

For encapsulated CyA in NPs EEs between 11% and 67% were determined (Table 4.1). An optimal loading was fixed at a ratio of 4:10 (CyA:PLGA, w/w), which means an actual loading of 26.8 mg CyA/100 mg PLGA and an EE of 67.2  $\pm$  7.5%. Nearly 100% of the encapsulated CyA was detected for all ratios in the MPs (Table 4.1). The optimal loading

was fixed at the ratio 4:10 keeping the same ratio for NPs and MPs. For the CyA-loaded MPs the optimal loading results in 35.7 mg CyA/ 100 mg PLGA and an EE of  $89.2\% \pm 3.8\%$ .

In the case of Bu encapsulation in NPs, EE values  $< 40\%$  (Table 4.2) were determined for all tested ratios. The optimal loading was fixed at 1:10 resulting in 3.7 mg Bu/100 mg PLGA with an EE of  $36.5\% \pm 4.3\%$  as in higher ratios the variations between different batches were very high. For Bu-loaded MPs SEM images show aggregates at ratios  $> 2:10$  (data not shown) and the optimal loading was fixed at 2:10 resulting in 19.3 mg Bu/100 mg PLGA with an EE of  $98.3\% \pm 5.4\%$ .

#### **4.3.2 Size and size distribution of NPs and MPs**

The size and size distribution of CyA- and Bu-loaded NPs and MPs is summarized in Figure 4.3 and compared to unloaded particles. With respect to NPs, a slight increase in PDI following loading was only observed for CyA-loaded NPs (Figure 4.3A). Nevertheless all loaded particles had a size of  $150 \pm 10$  nm with a narrow size distribution (PDI  $< 0.150$ ). DiD-loaded NPs also showed a size of  $144.7 \pm 7.8$  nm, but with a higher PDI of  $0.81 \pm 0.14$ . The size for blank and loaded NPs increases after freeze drying due to the cryoprotective agent PVA. A negative zeta potential was also determined for all PLGA NPs, as was expected:  $-27.8 \pm 0.61$  mV for blank,  $-18.9 \pm 0.51$  mV for CyA loaded and  $-25.0 \pm 3.91$  mV for Bu-loaded NPs.

The size of all MP formulations was in the low micron size range (Figure 4.3B). Bu-loaded MPs showed a slight increase in size compared to blank and CyA-loaded ones, although these differences are not significant. No appreciable difference in size distribution was determined. DiD-loaded MPs showed a size of  $3.95 \pm 0.13$   $\mu\text{m}$  and a width of  $2.78 \pm 0.10$ .

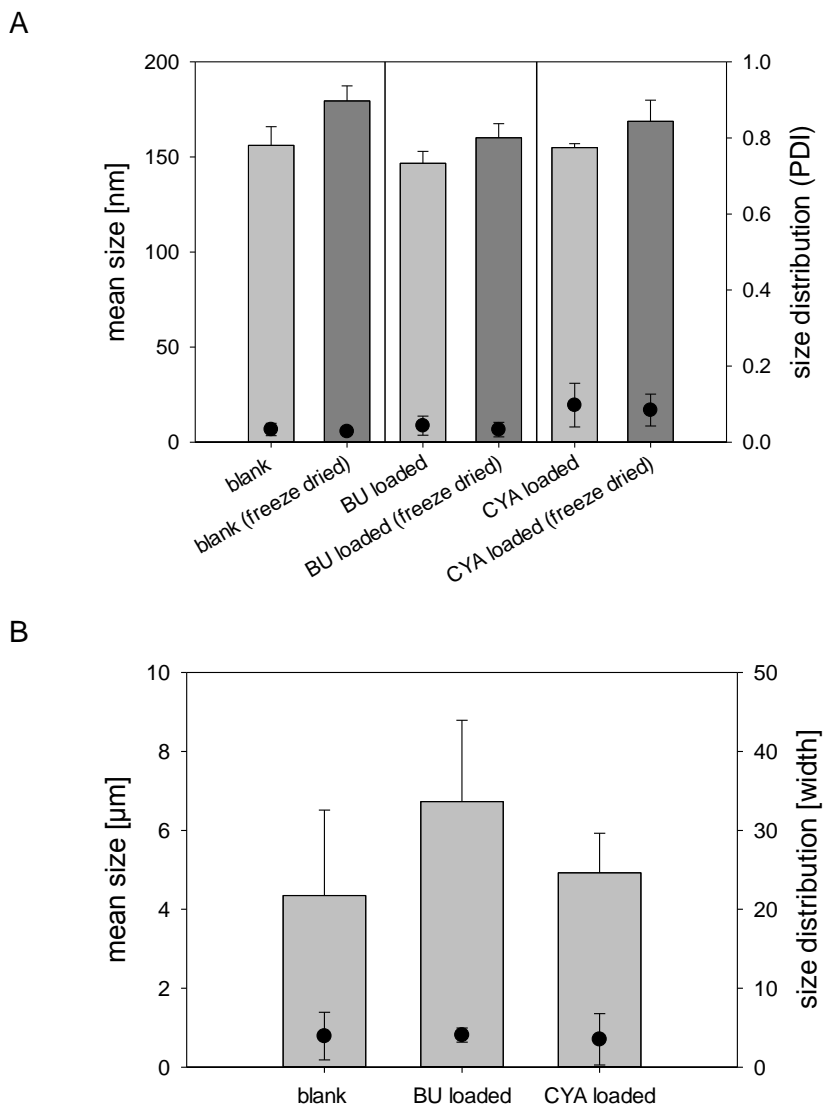


**Figure 4.3: Size and size distribution of NPs (A) and MPs (B).** Blank and API-loaded NPs were measured by dynamic light scattering and blank and loaded MPs were measured by laser light diffraction (mean  $\pm$  SD; n=3).

Batches of both NPs and MPs were visualized by SEM (Figure 4.4) using the optimal loaded particles (section 4.2.4). The images confirm the small size and narrow size distribution of the NPs as seen in dynamic light scattering results, and show that all particles are smooth and spherical in shape. The surface of the MPs however appears rougher possibly caused by Span 60 in the composition.

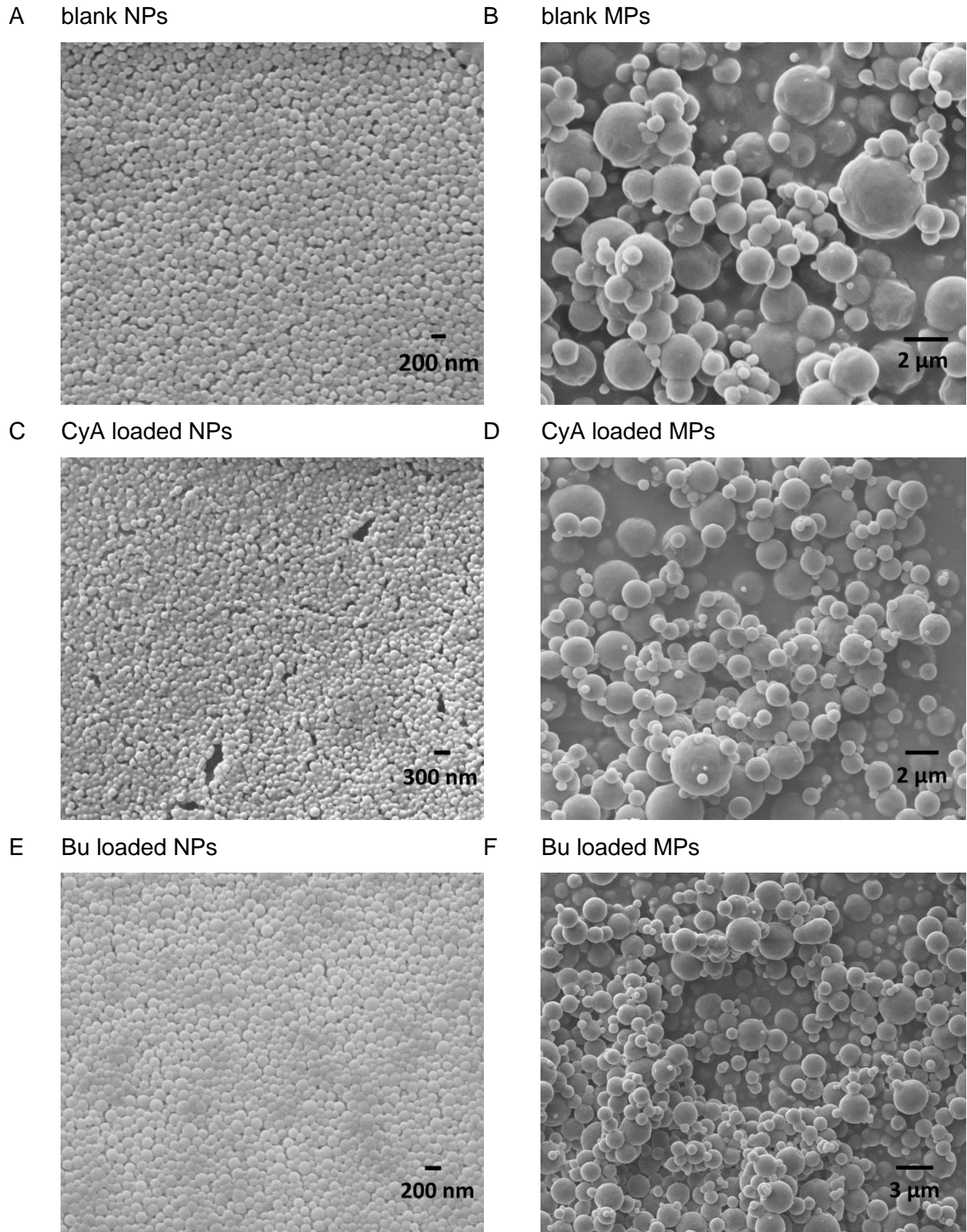


**Figure 4.4: Representative SEM images of blank, CyA- and Bu-loaded NPs and MPs, dispersed in water.**

### 4.3.3 Stability of NPs and MPs in cell culture media

Unloaded, Bu-loaded and CyA-loaded particles were incubated in the cell culture media used in the co-culture setup (Caco-2 and THP-1 medium) for periods up to 24 h, in order to test their physical stability under such conditions. Physical stability was assessed according to size and size distribution. Results are summarized in Figure 4.5 (NPs) and Figure 4.6 (MPs).

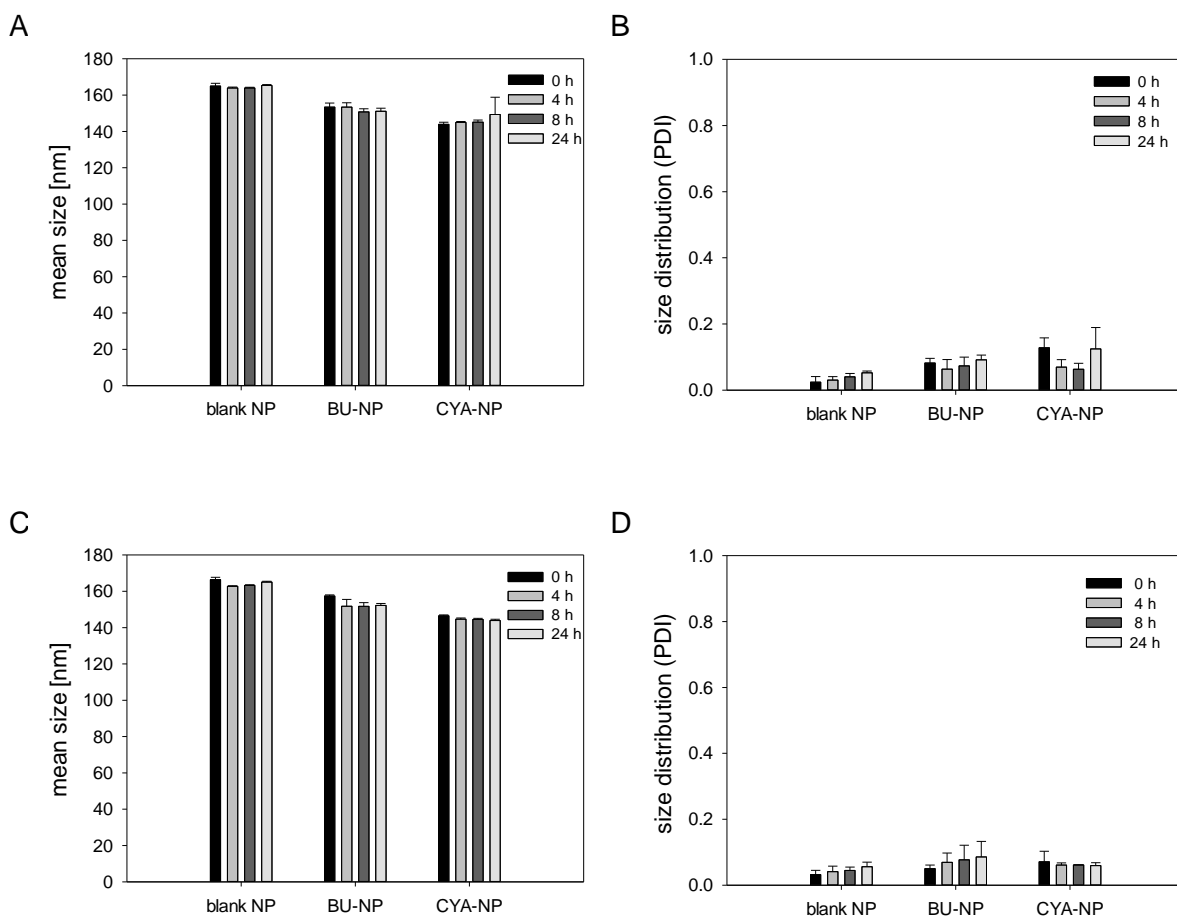


**Figure 4.5: Stability study of NPs in cell culture media over 24 h.** Size and size distribution of NPs incubated in Caco-2 medium (A,B) and in THP-1 medium (C,D) at 37 °C for 4, 8, and 24 h are shown, relative to NPs freshly dispersed in medium (mean  $\pm$  SD; n=3).

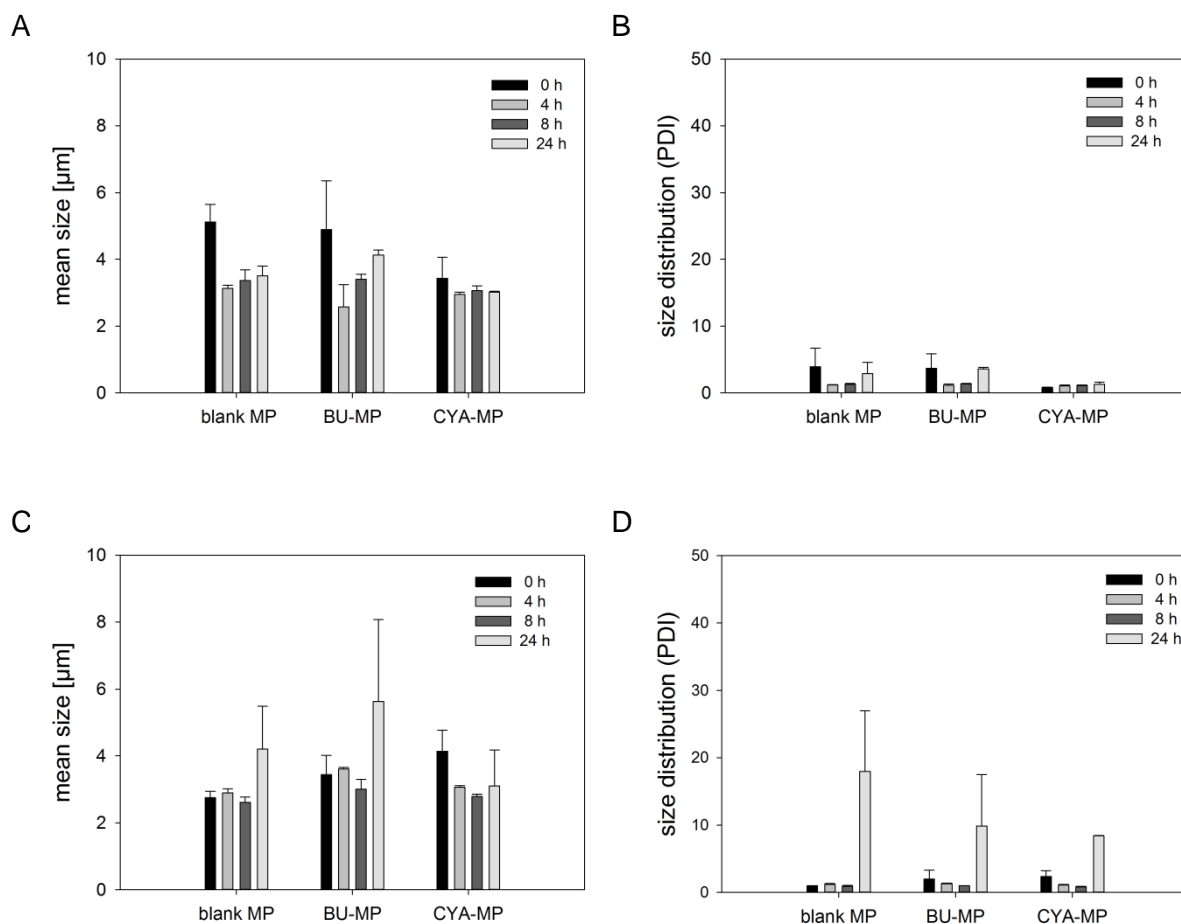


**Figure 4.6: Stability study of MPs in cell culture media over 24 h.** Size and size distribution of MPs incubated in Caco-2 medium (A,B) and in THP-1 medium (C,D) at 37 °C for 4, 8 and 24 h are shown, relative to MPs freshly dispersed in medium (mean  $\pm$  SD; n=3).

All NPs were seen to be stable over 24 h, with no significant changes in size or size distribution observed following incubation in either type of cell culture medium. In the case of MPs, no aggregates of MPs were formed in Caco-2 medium. However, in THP-1 medium size and size distribution increased after 24 h of incubation for all MPs. In the first four hours the size of the MPs decreased due to the Span 60 in the composition which is dispersible in aqueous phases [146].

Incubation times for cell culture experiments are set to 4 h for Bu- and 8 h for CyA-loaded particles. These time points were chosen due to the physiological relevance and the different modes of action of the two APIs. Thus all formulations are stable enough to be tested in the co-culture model.

#### 4.3.4 *In vitro* drug release studies

Drug release from the prepared NPs and MPs was investigated for both APIs. Interestingly, CyA-loaded NPs and MPs showed a different release behavior to Bu-loaded NPs and MPs. CyA-loaded NPs showed a low burst release after 1 h with  $14.03 \pm 2.4\%$  followed by a very slow sustained release, typical of PLGA particles [134]. For CyA-loaded MPs a reduced burst release was shown with  $15.9 \pm 4.3\%$  being released after 1 h followed by a sustained release. After 24 h nearly 100% of the initially entrapped CyA was shown to be released from the MPs (Figure 4.7A).

In case of Bu, the NPs release 80% of the API in 30 min and, therefore, show a strong burst release. Although the particles were washed, Bu could be attached to the surface of the particles or located at the outer edge of the polymeric particles. Contrary to this, the MPs show an intermediate release with a slow and sustained release after 10 h releasing 48% of the encapsulated Bu in 1 h. The release is promising for the investigated approach although 40% retain in the MPs after 24 h (Figure 4.7B).

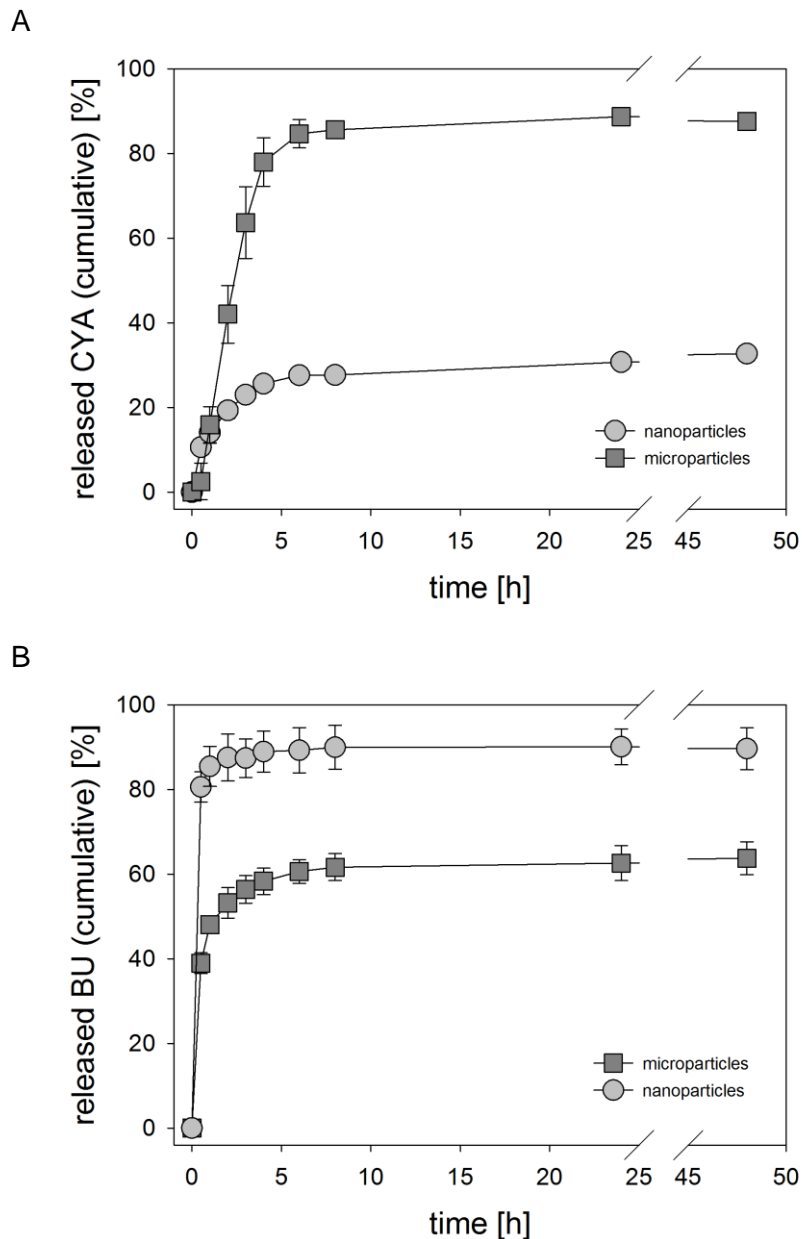


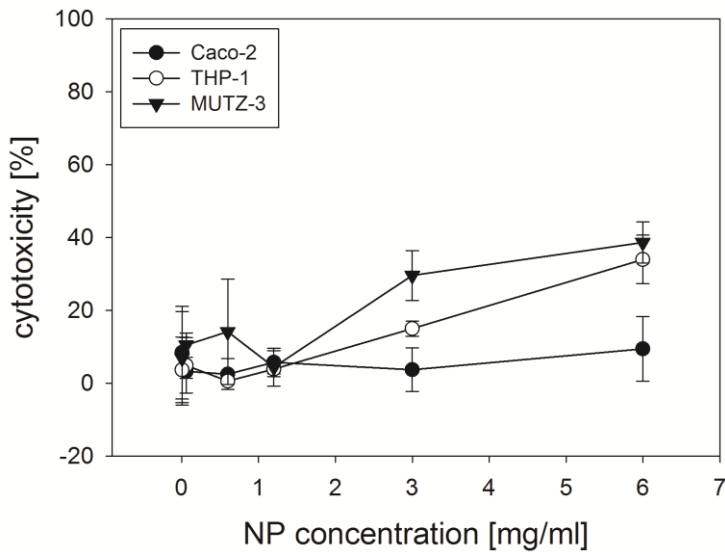
**Figure 4.7: Cumulative *in vitro* release profiles of CyA-loaded MPs and NPs (A) in comparison to Bu-loaded MPs and NPs (B).** Release was monitored in PBS for 48 h (mean  $\pm$  SD, n = 3).

#### 4.3.5 NP and MP cytotoxicity measurements

Before treatment of the inflamed triple culture with the drug loaded NPs and MPs, a cytotoxicity assay was performed to evaluate acceptable particle concentration ranges for the different cell types. All cell types used in the triple culture model (Caco-2, THP-1, MUTZ-3) were seeded separately and incubated for 8 h with different concentrations of blank NPs and MPs to reflect the difference in particle concentration with corresponding

drug dose (Figure 4.8). MPs did not show any toxic effects on the three cell types in the tested concentrations (Figure 4.8B). In contrast, NPs showed 40% toxicity for THP-1 and MUTZ-3 cells at a concentration of 6 mg/ml (Figure 4.8A). The acceptable concentration range for all experiments was therefore set for Bu- and CyA-loaded NPs as 0.006 - 2 mg/ml, and for MPs as 0.0014 - 1.4 mg/ml.

A



B

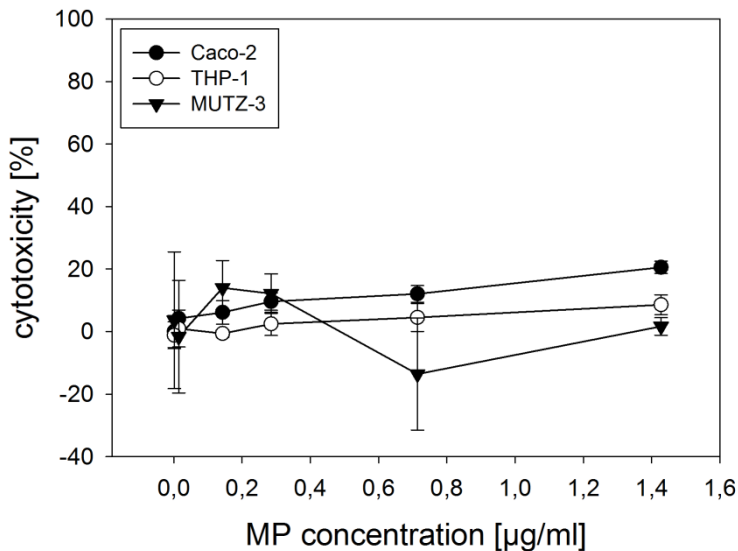


**Figure 4.8: Cytotoxicity assessment of NPs (A) and MPs (B).** Particles were incubated with Caco-2, THP-1 and MUTZ-3 cells in monoculture for 8 h, followed by measurement of LDH release (mean  $\pm$  SD, n = 3).

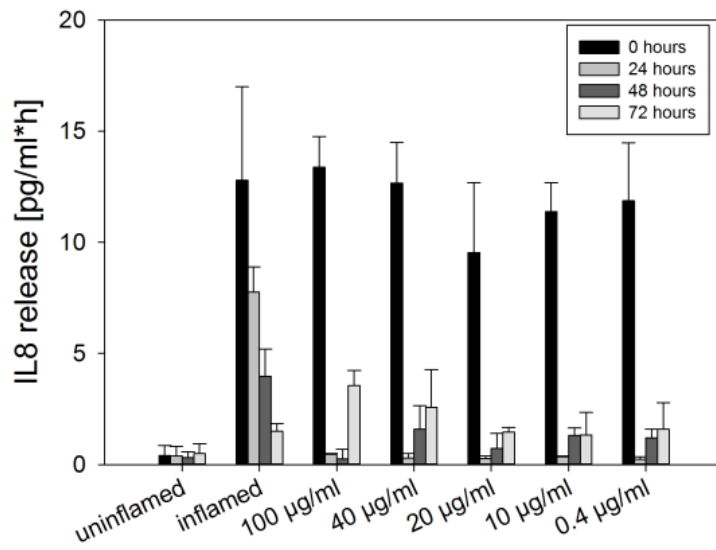
#### 4.3.6 Dose finding experiments with Bu and CyA

Prior to further cell experiments, the optimal Bu- and CyA-concentrations, which showed a meaningful anti-inflammatory effect on the inflamed triple culture model, needed to be established. Therefore, experiments with different concentrations of free CyA and Bu in solution were performed on the inflamed triple culture model, as shown in Figure 4.1, to find the lowest effective anti-inflammatory dose.

All CyA-concentrations showed an anti-inflammatory effect, but no statistical difference between the effects of the different tested concentrations could be observed (Figure 4.9B). After 48 h the release of IL-8 was seen to increase again, because CyA is just effective over a short time period. The rebound increase in IL-8 release was seen to be higher in the co-culture treated with the lowest CyA-concentration of 0.12026 µg/ml; for the other two concentrations tested, the results were comparable. Therefore it was decided to use a concentration of 1.2026 µg/ml CyA for all further experiments. With this concentration the anti-inflammatory effect was seen to be acceptable; this dose also correlated to a particle concentration of 0.014 mg/ml for NPs and 0.008 mg/ml for MPs, which was seen from Figure 4.8 to be low enough to show no toxic effect.

For Bu, all tested concentrations showed similar results: IL-8 release decreased after the treatment (Figure 4.9A). For this API it was therefore decided to take the lowest tested concentration of 0.4 µg Bu/ml which corresponds to 0.024 mg NP/ml and 0.0056 mg MP/ml, for all further experiments.

A



B

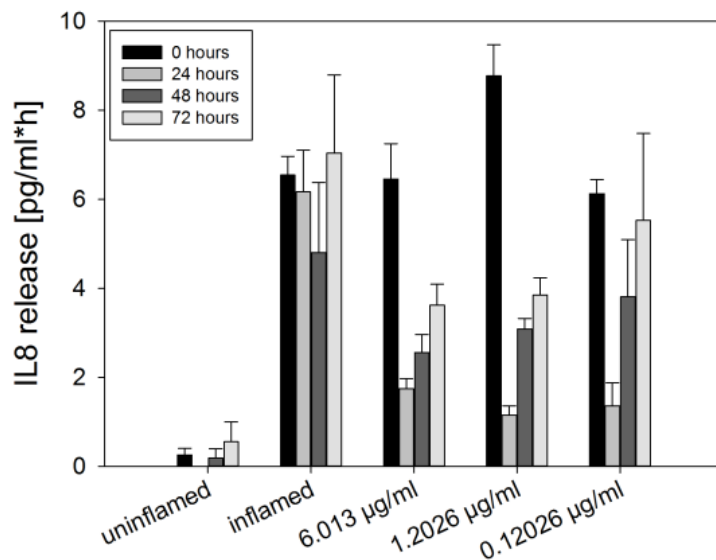
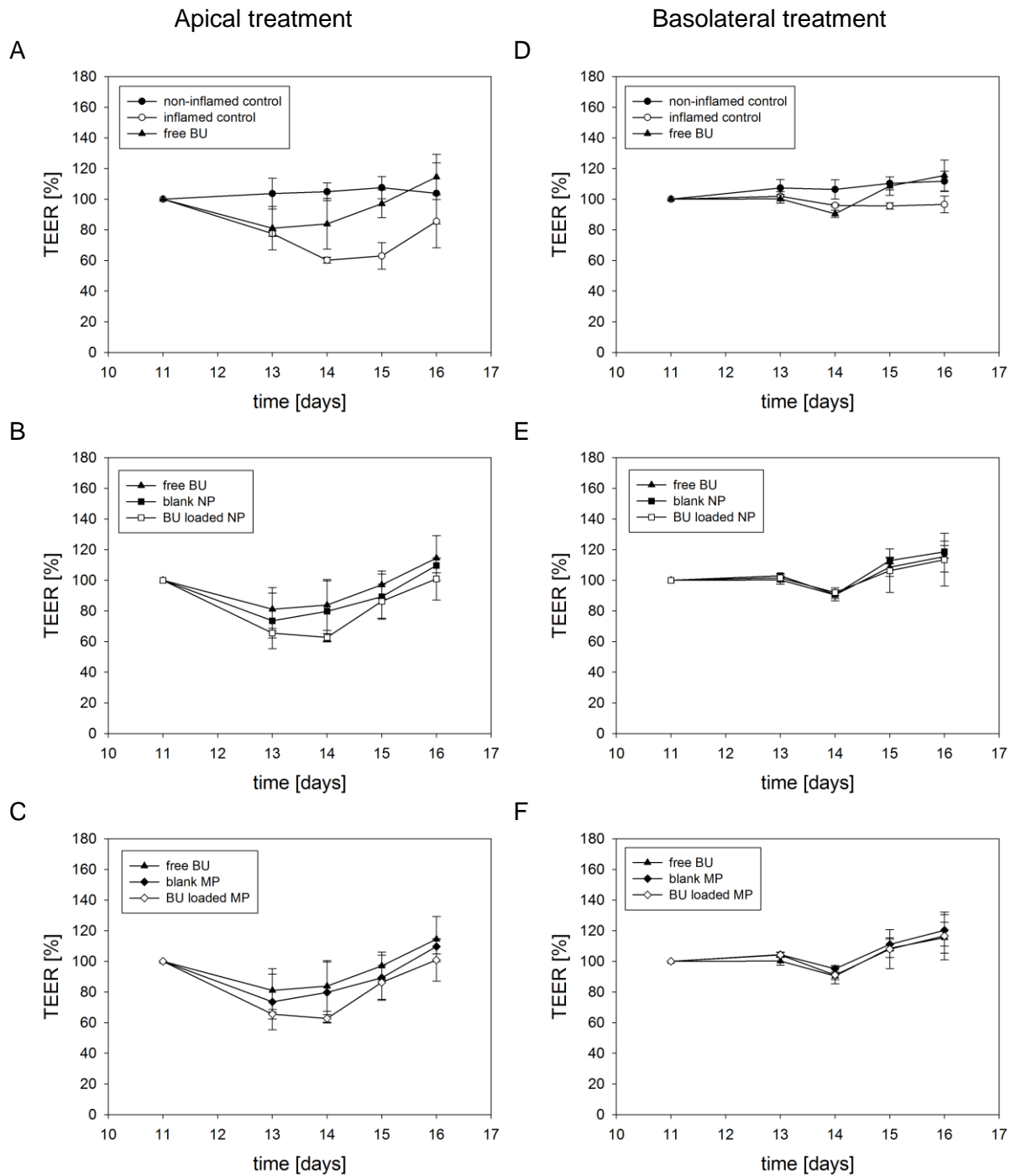


**Figure 4.9: Dose finding studies: IL-8 release from the triple culture model after treatment with free Bu (A) and CyA (B).** The inflamed triple culture was treated with various concentrations of Bu for 4 h and CyA for 8 h. IL-8 production was then measured for a total of 72 h following removal of APIs (mean  $\pm$  SD, n = 3).

#### **4.3.7 Efficacy studies with Bu-loaded NPs and MPs**

The impact of Bu-loaded NPs and MPs was tested following application to either the apical or basolateral compartment of the triple culture model, simulating oral or intravenous administration respectively. Experiments were performed as can be seen in Figure 4.1. As controls non-inflamed and inflamed triple cultures that were not treated with any particles were used. Furthermore, for comparison free Bu solution with the same concentration that was contained in the particles (0.4 µg/ml), was tested, as were blank NPs and MPs. Figure 4.10 shows the results of TEER measurement following apical and basolateral treatment with Bu formulations.

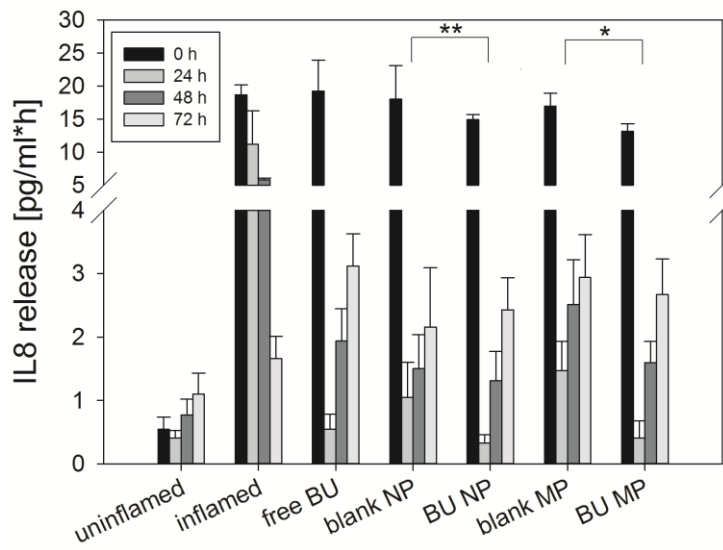
After both apical and basolateral treatment of inflamed co-cultures with Bu in solution and Bu-loaded NP and MP formulations, TEER values were seen to increase back to the initial values observed before the induction of inflammation. This phenomenon indicates a closing of the tight junctions between Caco-2 cells, which were opened because of the inflammation. In comparison, the inflamed non-treated control also showed an increase in TEER following removal of IL-1 $\beta$ , however this occurred more slowly than in the treated cultures. It takes more than three days until TEER values are fully recovered when they are not treated with anti-inflammatory compounds. TEER values were also seen to increase faster after treatment with the blank formulations as in the inflamed untreated culture. No difference could be observed between anti-inflammatory effects of Bu-loaded particles and free Bu solution.



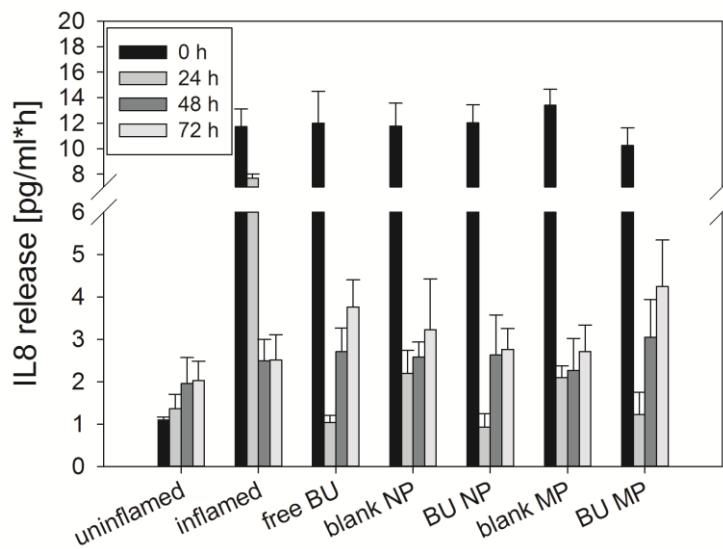
**Figure 4.10: TEER measurement after Bu treatment of the triple culture in the apical (A-C) and basolateral (D-F) compartment.** A,D) untreated inflamed and uninflamed triple cultures; B,E) treatment with Bu-loaded and blank NPs; C,F) treatment with Bu-loaded and blank MPs. As a control result a TEER profile from inflamed triple cultures treated with free Bu solution is added in every graph. Bu concentration = 0.4  $\mu\text{g/ml}$  for solution as well as loaded NP and MP samples. TEER values are expressed as a percentage of values recorded on day 11, prior to inflammation (mean  $\pm$  SD, n = 6 from 2 independent experiments).

Figure 4.11 shows the results of IL-8 release measurements following Bu treatment of the inflamed triple culture. IL-8 release was seen to decrease after the inflamed co-cultures were treated with the drug-loaded NPs and MPs. As already observed from TEER measurements in Figure 4.10, blank particles also showed an effect on the triple culture model, with cells releasing less IL-8 after treatment with unloaded particles. In the case of both drug-loaded and unloaded particle treatment, the decrease in IL-8 release was observed to occur faster in the non-treated inflamed control, confirming an additional anti-inflammatory effect. The greatest anti-inflammatory effect was observed 24 h following treatment in the apical compartment, where significant differences were seen in the IL-8 production of co-cultures treated with blank and drug-loaded particles. No significant difference could be observed in IL-8 production after treatment with Bu-loaded particles or with free Bu solution.

A



B



**Figure 4.11: IL-8 release after apical (A) or basolateral (B) treatment of the inflamed triple culture with different blank and Bu-loaded NPs and MPs.** Bu concentration = 0.4  $\mu\text{g/ml}$  for solution as well as loaded NP and MP samples (mean  $\pm$  SD,  $n = 6$  from 2 independent experiments, \* =  $p < 0.05$ , \*\* =  $p < 0.001$ ).

#### **4.3.8 Efficacy studies with CyA-loaded NPs and MPs**

Due to the different pharmacological mechanism of CyA in comparison to Bu, cells were incubated with the CyA-loaded particles for the longer time period of 8 h. Figure 4.12 shows the results of TEER measurement following apical or basolateral treatment with CyA formulations.

TEER value profiles in response to CyA treatment were seen to show a similar effect to that observed in the Bu particle study: free CyA and CyA in both NPs and MPs induced an increase in TEER values, corresponding to a recovery of barrier properties within the triple culture model. A blank carrier effect was also found here; the TEER values recovered faster after treatment with the blank particles as in case of the inflamed untreated control.

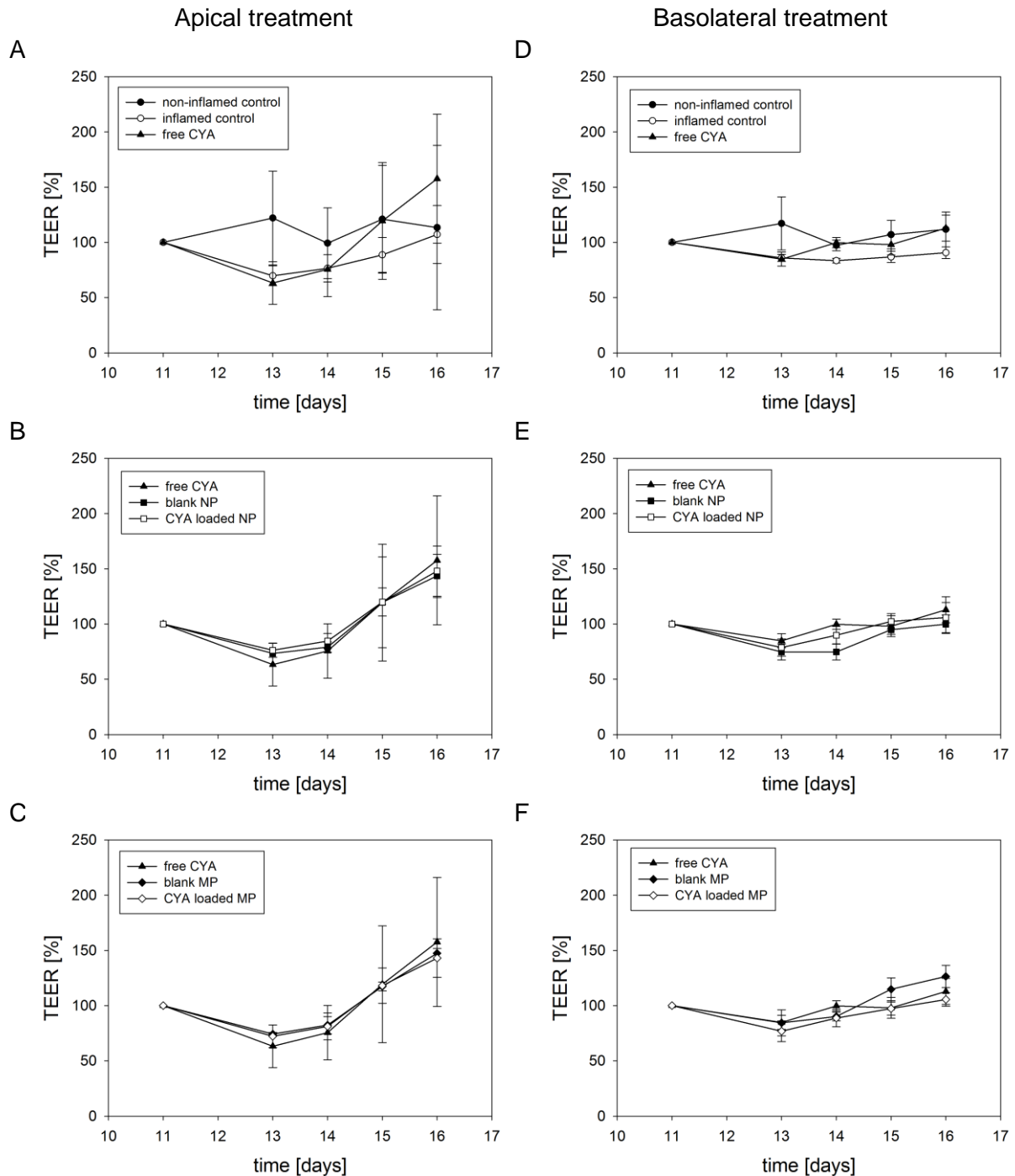
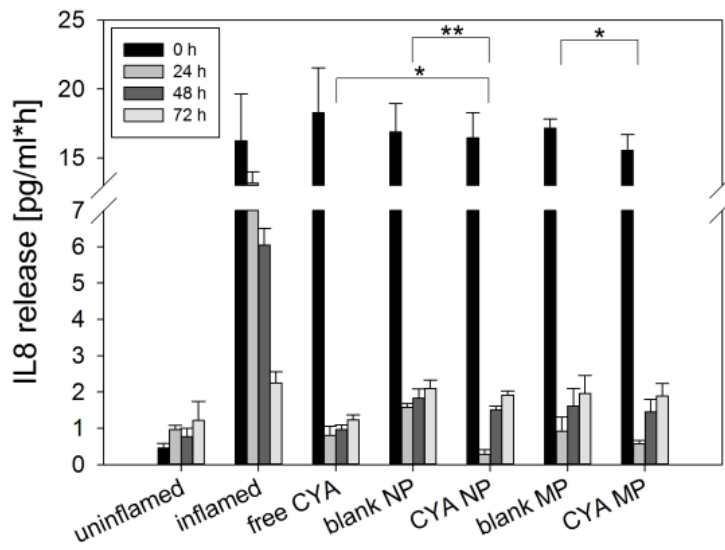


**Figure 4.12: TEER measurement after CyA treatment of the triple culture model in the apical (A-C) and basolateral (D-F) compartment.** A,D) untreated inflamed and uninfamed triple cultures; B,E) treatment with CyA-loaded and blank NPs; C,F) treatment CyA-loaded and blank MPs. As a control result, a TEER profile from inflamed triple cultures treated with free CyA solution is added in every graph. CyA concentration = 1.2026  $\mu\text{g/ml}$  for solution and loaded NP and MP samples. TEER values are expressed as a percentage of values recorded on day 11, prior to inflammation (mean  $\pm$  SD, n = 6 from 2 independent experiments).

A



B

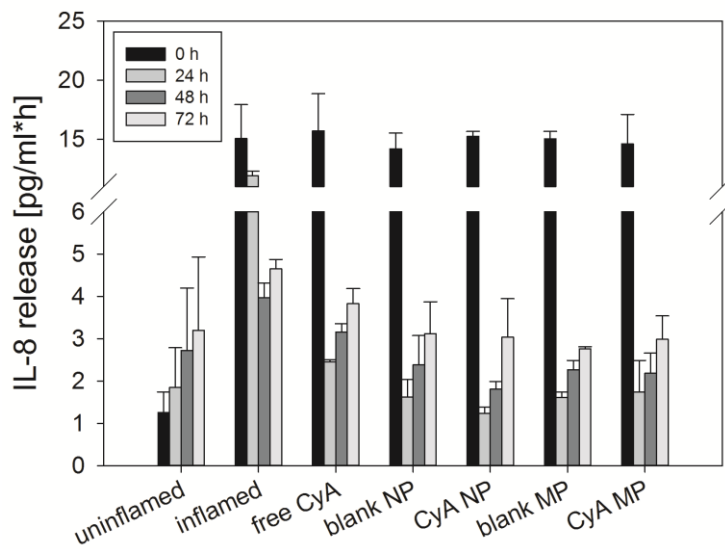


**Figure 4.13: IL-8 release after apical (A) or basolateral (B) treatment of the triple culture with different blank and CyA-loaded NPs and MPs.** CyA concentration = 1.2026  $\mu\text{g/ml}$  for solution and loaded NP and MP samples (mean  $\pm$  SD, n = 6 from 2 independent experiments).

Investigation of IL-8 secretion following CyA treatment (Figure 4.13) showed a comparable effect to that observed with Bu treatment. IL-8 release was seen to decrease after treatment with the different CyA formulations; additionally the effect after treatment in the apical compartment was higher than after treatment in the basolateral compartment.

As in the experiments with Bu, an anti-inflammatory effect of the blank formulations was also observed. However, a significant difference in IL-8 production 24 h after apical treatment with blank as compared to CyA-loaded formulations was determined as it was the same case after treatment with Bu-loaded formulations. Furthermore, after 24 h a significantly higher anti-inflammatory effect of the CyA-loaded NPs in comparison to the free drug solution could be observed.

#### **4.3.9 Deposition of NPs and MPs in the triple culture model**

The inflamed triple culture model was incubated with NPs and MPs loaded with the far-red fluorescent dye DiD, applied to either the apical (Figure 4.14) or the basolateral (Figure 4.15) compartment. The particle concentrations and incubation times were equivalent to those used in the efficacy studies: 0.024 mg/ml NPs and 0.0056 mg/ml MPs with 4 h of incubation in the case of Bu, and 0.014 mg/ml NPs and 0.008 mg/ml MPs with 8 h of incubation for CyA particles.

Confocal images (Figure 4.14) show that NPs as well as MPs were located on top of the Caco-2 cells of the cell culture model when they were incubated in the apical compartment, despite the fact that the cells were washed several times after incubation with the particles. MPs may stick on top of the cells due to their bigger size and as such were seen distributed over the cell borders (Figure 4.14A/C). NPs were in fact taken up by Caco-2 cells. Figure 4.14 B and D show that the NPs were located inside the cells, rather than being located on the cell borders. After basolateral treatment no particles could be found in the co-culture model (Figure 4.15).

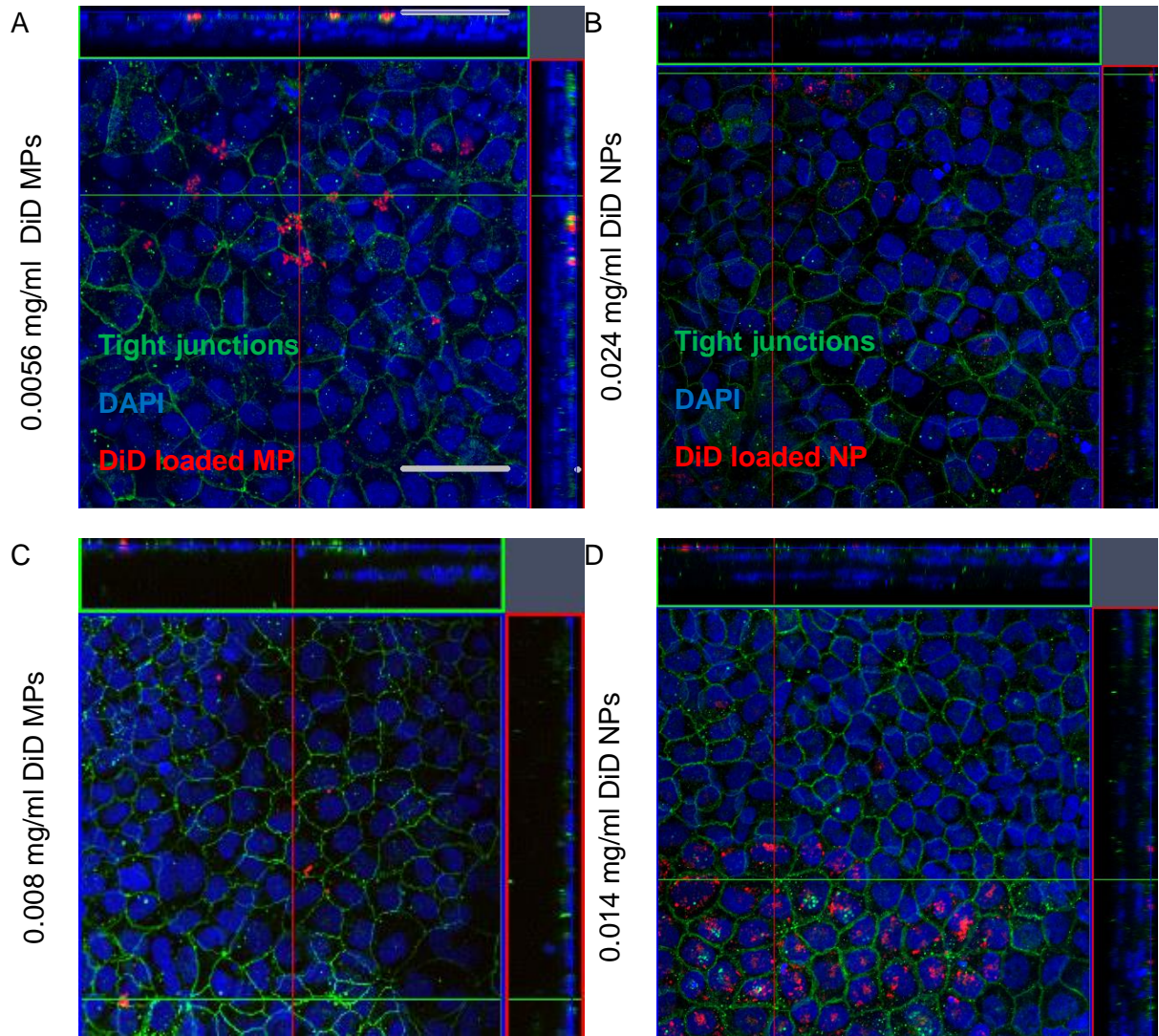


**Figure 4.14: CLSM pictures of the inflamed triple culture incubated with DiD-loaded NPs and MPs in the apical compartment.** A) DiD MPs CyA concentration; B) DiD NPs CyA concentration; C) DiD MPs Bu concentration; D) DiD NPs Bu concentration; scale bar = 50  $\mu\text{m}$ ; blue: DAPI stained nuclei, green: tight junctions stained with anti-occludin antibody, red: DiD loaded particles

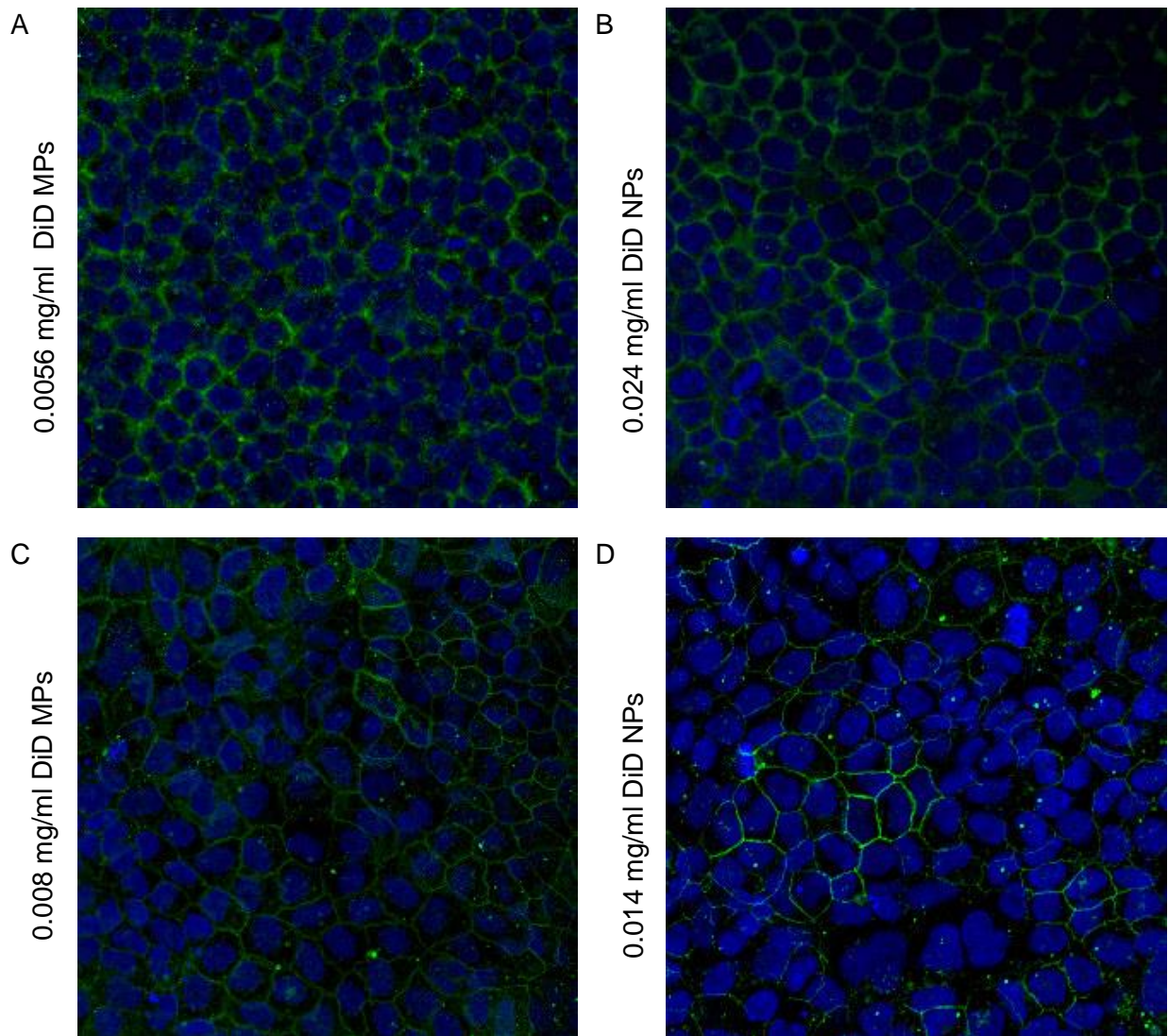


**Figure 4.15: CLSM pictures of the inflamed triple culture incubated with DiD-loaded NPs and MPs in the basolateral compartment** A: DiD MPs CyA concentration; B: DiD NPs CyA concentration; C: DiD MPs Bu concentration; D: DiD NPs Bu concentration; scale bar = 50 μm; blue: DAPI stained nuclei, green: tight junctions stained with anti-occludin antibody, red: DiD loaded particles

#### 4.4 Discussion

DDS can improve the therapy options for IBD patients as they can passively accumulate in inflamed areas of the intestine [130]. By forming a depot at the site of inflammation where treatment is needed, the incidence of systemic adverse effects can be reduced. Studies showed that NPs seem to be favorable for accumulation in inflamed areas in mouse models [130], [147], whereas MPs show a better deposition efficacy in human patients [131]. Such studies showed an enhanced accumulation of MPs in the ulcerated lesions, whereas NPs were only found in traces in the mucosa of patients with CD and UC [131].

Nanoprecipitation is one of the most frequently used methods for the preparation of polymer-based DDS [149], [150], [151]. In comparison to emulsion-diffusion-evaporation methods it shows reduced production times, increased reproducibility and controllability and less production steps [151]. The produced NPs were in suspension and had to be converted into a more stable, storable form by freeze drying. For this process, a suitable cryoprotectant with regards to the prevention of particle aggregation and to the achievement of a maximum stabilization of NPs during freeze drying must be evaluated. In the current work, trehalose was revealed to be the optimal cryoprotectant when used in combination with PVA, which can attach to PLGA NP surfaces [155]. This can result in a slight increase in particle size after freeze drying, as was noted in Figure 4.3. Furthermore we propose that free PVA that is not attached to the surface of the NPs can act as a stabilizer. PVA prevents aggregation during freeze drying as it forms a glassy state at low temperatures [155]. Moreover it forms hydrogen bonds between the polymer and water molecules, contributing to a better particle redispersion [156].

The spray drying technique was used to formulate DDS in a single step process, without the need for extra washing or drying steps [157]. The used novel nano spray drying system was especially developed to produce spray dried products in the sub- or low-micron size range, achieved by a vibrating mesh which transports the feeding solution into

the drying gas flow [158]. Studies performed with this relatively new system have investigated the spray drying of nano-emulsions [157] and of pharmaceutical excipients and proteins [159]. Further studies have focused on the preparation of particles using polymeric wall material and proteins [160] [161] and encapsulation of model drugs in biodegradable polymers [159], [163].

In this study the APIs Bu and CyA were encapsulated in MPs and NPs for the treatment of IBD. The calcineurin inhibitor CyA is commonly administered to UC patients suffering from fulminant colitis that does not respond to intravenous corticosteroids [163]. The therapy is started intravenously for three to five days, and is then typically continued in oral form often in co-medication with corticosteroids and thiopurines for maintenance therapy [137]. CyA therapy is associated with adverse effects for example neurological toxicity, infections, renal dysfunction and hypertension [137]. Bu, a corticosteroid, is a first-line agent for ileal and/or right colonic CD [136], [127]. It is utilized both as oral and local formulation (as foam or enema) [137]. Bu has an extensive first-pass metabolism, reducing the systemic bioavailability to 10 – 15% after oral administration [144], which maximizes its locally available concentration in the distal ileum and proximal colon [128].

*In vitro* release studies are a useful research tool to estimate release kinetics and show comparisons between various DDS samples and batches. PLGA-based DDS show in general a biphasic release profile, starting with a burst release followed by a sustained one [134]. Release of APIs from DDS is driven by three basic mechanisms: a) swelling/erosion, b) diffusion and c) degradation [164]. The produced DDS in this study show an improvement in the release compared to recent studies of CyA-loaded PLGA MPs [143], [166], which revealed a sustained and incomplete drug release over a number of weeks, up to a maximal value of 60% after 50 days [142]. Also for CyA loaded NPs a drug release over three weeks or more was reported, with the use of PLGA 50:50 (lactide:glycolide ratios) showing in general the faster release rates [143], [166]. The *in vitro* release profiles of Bu-loaded DDS in the current work revealed a dramatic burst of

80% for NPs in comparison to 40% for MPs. This shows that Bu is probably more adsorbed at the surface or encapsulated at the outer edge of the particles. It is interesting that the release profiles are so different for NPs as compared to MPs. MPs release might be supported by the stabilizer, which is dispersible in aqueous solutions [146], and by the crystallization processes during MP formation. The spray drying process may produce micro voids in the MPs, supporting water penetration [166], which could explain the faster release of CyA from MPs in comparison to NPs.

A fast release from MPs as seen in the case of CyA could be a benefit for administration as they are supposed to be cleared faster, because the accumulation of particles is size-dependent and NPs are supposed to accumulate at a higher content, building a depot in the inflamed regions [29]. Moreover DDS will not stay in the inflamed areas for an endless time due to for example the regeneration of the epithelium. Lamprecht et al. determined an accumulation of 100 nm polystyrene NPs at  $9.1 \pm 2.8\%$  after four days, which decreased after six and eight days to  $3.4 \pm 2.2\%$  and  $1.9 \pm 1.1\%$ , respectively [130].

The most important point for this study was the investigation of whether the produced particles showed the desired anti-inflammatory effect. Therefore the formulations loaded with CyA and Bu were tested in the cell line-based co-culture model of the inflamed intestinal mucosa by measurement of TEER values and IL-8 release, and it was seen to be persistent enough to allow for the functional evaluation of the anti-inflammatory formulations.

As expected, DDS containing both CyA and Bu showed anti-inflammatory effects in the triple culture model. After treating the inflamed cells with the drug-loaded NPs and MPs in the apical compartment, TEER values increased again in comparison to values seen before inflammation. The self-healing process of the triple culture also leads to a recovery of TEER, which was monitored in the non-treated inflamed control; however this self-healing was seen to take more time than when cells were treated with the formulations. TEER values indicated a strong anti-inflammatory effect of the produced formulations;

however this effect was not precise enough to detect any differences between CyA-loaded particles, Bu-loaded particles or blank NPs and MPs. The pro-inflammatory marker IL-8 was therefore also measured as this is expressed in high amounts in the intestine of IBD patients [113]. IL-8 production proved to be a very important marker for our experiments, with release from the inflamed triple culture models seen to decrease already 24 h after treatment with the different formulations. A rebound release was seen following this initial increase however, because both drugs show an effect just over a short time period.

Results after treatment with Bu NPs and MPs were similar to results following treatment with Bu as free drug. In case of the NPs this is very much expected in consideration of the release profile, which shows that the drug is released very fast from the formulation (Figure 4.7B). In the case of the MPs however, the release profile (Figure 4.7B) shows that after 24 h only approximately 60% of Bu is released and available in free form, which means that the effect of the Bu-loaded MPs could be seen as being better than the effect of the Bu solution, because less API is available. This could be explained by MP accumulation in the model (Figure 4.14), meaning that the encapsulated API is not washed away and can be released over the whole experimental time.

In the case of CyA a significant difference between the effect in terms of IL-8 production of CyA NPs and free drug solution was observed. The release profile (Figure 4.7A) shows that CyA is released more slowly than Bu from the NPs, which means that the released drug can reach the cells over a longer time period. Due to their small size, NPs can be taken up by Caco-2 cells, which could be observed in chapter 2 of this thesis (Figure 3.8). TEM pictures have shown that Caco-2 cells can take up 15 nm Au NPs in vesicles [103]. Although the difference in IL-8 production observed between free drug and drug-loaded MPs was not significant, there is a similar trend as compared to the results from the NPs. Figure 4.14 shows that NPs were found inside the cells, whereas MPs were deposited on top of the cells and are distributed over the cell borders. MPs (~4  $\mu\text{m}$ ) are probably too big to be taken up by the Caco-2 cells; however, they still appear to stick on top of the Caco-2

cells, and so remain at the site of action releasing drug. Furthermore, as indicated from the low TEER values, the tight junctions of the inflamed triple culture are likely to be open (due to lower expression of tight junction proteins ZO-1 and occludin) [76]; the pores created by open tight junctions have been reported to have a size of 58 – 104 nm [167] meaning that, while the MPs are unlikely to be able to pass through they may become trapped and accumulate in these enlarged intercellular spaces. This phenomenon has also been reported by Leonard et al. [68].

Blank formulations also showed an anti-inflammatory effect, which has already been observed in other studies [51], [89]. One reason for this could be the adsorption of soluble signaling parameters involved in the inflammatory cascade of IL-8, to particle surfaces. Another possibility is that blank particles interact with the immune cells within the triple culture, and lead to a response of the immune system with this new stimulus [68]. Further studies have to be performed to show why this effect occurs. However *in vivo* studies have also shown that the released lactate from PLGA leads to wound healing in mice [169], [170], which also shows that PLGA can have a healing and pharmacological effect.

The particles were not only tested in the apical compartment, but also in the basolateral one, which mimics the blood side in the model. Although no significant differences between blank and Bu- and CyA-loaded particles were observed after treatment in the basolateral compartment, the results show the same trend as after apical treatment: drug-loaded particles led to a better effect than blank ones. Confocal images showed that NPs and MPs could however not reach the cells when they were added basolaterally (Figure 4.15). MPs are expected to sediment directly to the bottom of the plate, meaning that their lack of interaction with the cells is not surprising, but NPs also could not reach the apical compartment – this could be due to the barrier of the filter membrane and the collagen layer. Furthermore they were removed by changing the medium during the experiment, which shows that only the released drug was capable of reaching the inflamed cells.

In this study it was shown that the anti-inflammatory effect of drugs can be tested on the developed triple culture model consisting of three cell lines. However, the system also shows certain limitations – while it could be determined whether a tested compound demonstrated an anti-inflammatory effect or not, relative differences in anti-inflammatory function were difficult to distinguish. A further limitation is testing of DDS in the basolateral compartment, which mimics administration via the blood side. It was observed here that DDS cannot reach the cells, either because of sedimentation or due to the barrier action of the transwell filter and collagen layer. Both factors are of course unlikely to occur in the *in vivo* situation. A further deviation from the *in vivo* situation in the current model is the lack of flow behavior. In order to attempt to mimic the flow through the intestine the cells were washed to be sure any non-adherent DDS were removed; however, the model would be even more realistic if there would be a fluid rather than a static system. Nevertheless, *in vitro* testing in this model is closer to the *in vivo* situation than testing with cell monocultures, and the ability to simulate and monitor inflammation in the model through IL-8 measurement offers a comparison to IL-8 production in *in vivo* experiments. Oral DDS could also be tested in the apical compartment and showed realistic results, which gives a promising perspective to the use of produced particles for oral IBD treatment as well as to the model, following further development, for *in vitro* testing for such formulations.

## 4.5 Conclusion

Optimized PLGA-based pharmaceuticals for IBD therapy according to the demands of a scalable and quality controlled production and storage could be successfully loaded with cyclosporine A and budesonide.

The anti-inflammatory effect of these model drugs could be successfully tested on the triple culture model consisting of three cell lines (epithelial cells, macrophages and dendritic cells) using TEER and IL-8 measurement as meaningful markers for inflammation. The investigation of the size-dependent accumulation at the site of inflammation and the anti-inflammatory efficacy was possible following application of DDS from the apical side. Furthermore it could be shown that the co-culture model is a useful tool for this testing because of the reversibility of the inflammable status.

Therefore this model can be considered as a first step for the testing of oral anti-inflammatory drugs before they are tested in animal models, giving a perspective for a reduction in the number of time-consuming and expensive animal tests.

---

## Summary and outlook

The current study has shown the successful replacement of primary immune cells by the cell lines THP-1 and MUTZ-3 in a 3D co-culture model of the intestinal mucosa. After inflammation the model showed the same behavior as the previous, primary immune cell-based setup. The using of cell lines makes this model much easier to seed in a more rapid manner; it also makes the model more reproducible because primary cells were isolated from different persons and showed a higher variability than cell lines.

The model has been proven in the current work to be a useful tool for safety testing of nanomaterials. It could be seen that toxic Ag NPs exerted different effects on the co-culture model in comparison to a Caco-2 monoculture: Caco-2 cells alone were more sensitive to the toxic NPs than the co-culture systems, reinforcing the important role of immune cells in these measurements by virtue of their production of pro-inflammatory cytokines and also their apparent protection of the tissue. It was further shown that cytokine measurement is quite important in order to assess and monitor inflammation, as differences in IL-8 release from the cell cultures after treatment with NPs could be seen that did not correspond to any measurable toxic effects. Additionally cytokine measurements can also be performed in *in vivo* models to be compared to *in vitro* results.

Furthermore the optimized model can also be used to test anti-inflammatory effects of newly developed nano- and microparticulate DDS. By measuring TEER and IL-8 release the anti-inflammatory action of such DDS can be measured within this system. Additionally, the deposition of particles in the model could be investigated by CLSM.

There are still some limitations in the co-culture system which need to be assessed in further work however. The first point for further investigation should be the collagen layer underlying the Caco-2 cells in which the immune cells are embedded. It is still not clear if NPs are able to cross this layer and therefore if all the immune cells can get in contact with the particles. The collagen could also be a hindrance to the testing of anti-

inflammatory compounds applied to the basolateral compartment, as, along with the filter membrane, it forms a physical barrier to compound interaction with the cells. A next step in the model development could therefore be to replace this collagen by another matrix. Furthermore, the system is not so sensitive that differences in the effect of different concentrations of anti-inflammatory compounds can be observed. Regarding these points, the model could still be improved by carrying out further studies.

Nevertheless, though there are points for further consideration, the model has still shown a lot of promise for toxicological testing and also for anti-inflammatory drug efficacy assessment.

---

## References

- [1] T. C. Wallace, F. Guarner, K. Madsen, M. D. Cabana, G. Gibson, E. Hentges, and M. E. Sanders, "Human gut microbiota and its relationship to health and disease.," *Nutr. Rev.*, vol. 69, no. 7, pp. 392–403, Jul. 2011.
- [2] K. J. Maloy and F. Powrie, "Intestinal homeostasis and its breakdown in inflammatory bowel disease.," *Nature*, vol. 474, no. 7351, pp. 298–306, Jun. 2011.
- [3] K. A. Head, J. S. Jurenka, and M. T. Ascp, "Inflammatory Bowel Disease Part I : Ulcerative Colitis – Pathophysiology and Conventional and Alternative Treatment Options," *Altern. Med.*, vol. 8, no. 3, pp. 247–283, 2003.
- [4] J. Cosnes, C. Gower-Rousseau, P. Seksik, and A. Cortot, "Epidemiology and natural history of inflammatory bowel diseases.," *Gastroenterology*, vol. 140, no. 6, pp. 1785–94, May 2011.
- [5] A. Kaser, S. Zeissig, and R. S. Blumberg, "Inflammatory bowel disease.," *Annu. Rev. Immunol.*, vol. 28, pp. 573–621, Jan. 2010.
- [6] M. Fakhoury, R. Negrulj, A. Mooranian, and H. Al-salami, "Inflammatory bowel disease : clinical aspects and treatments," *J. Inflamm. Res.*, pp. 113–120, 2014.
- [7] C. G. Yu and Q. Huang, "Recent progress on the role of gut microbiota in the pathogenesis of inflammatory bowel disease.," *J. Dig. Dis.*, vol. 14, no. 10, pp. 513–7, Oct. 2013.
- [8] R. B. Sartor, "Genetics and environmental interactions shape the intestinal microbiome to promote inflammatory bowel disease versus mucosal homeostasis.," *Gastroenterology*, vol. 139, no. 6, pp. 1816–9, Dec. 2010.
- [9] C. Lautenschläger, C. Schmidt, D. Fischer, and A. Stallmach, "Drug delivery strategies in the therapy of inflammatory bowel disease.," *Adv. Drug Deliv. Rev.*, vol. 71, pp. 58–76, May 2014.
- [10] E.-M. Collnot, H. Ali, and C.-M. Lehr, "Nano- and microparticulate drug carriers for targeting of the inflamed intestinal mucosa.," *J. Control. Release*, vol. 161, no. 2, pp. 235–46, Jul. 2012.
- [11] M. G. Neuman and R. M. Nanau, "Inflammatory bowel disease: role of diet, microbiota, life style.," *Transl. Res.*, vol. 160, no. 1, pp. 29–44, Jul. 2012.
- [12] G. D. Wu, F. D. Bushmanc, and J. D. Lewis, "Diet, the human gut microbiota, and IBD.," *Anaerobe*, vol. 24, pp. 117–20, Dec. 2013.
- [13] C. Ott, A. Taksess, F. Obermeier, E. Schnoy, and M. Müller, "Smoking increases the risk of extraintestinal manifestations in Crohn's disease.," *World J. Gastroenterol.*, vol. 20, no. 34, pp. 12269–76, Sep. 2014.
- [14] H. Roberts, S. N. Rai, J. Pan, J. M. Rao, R. C. Keskey, Z. Kanaan, E. P. Short, E. Mottern, and S. Galandiuk, "Extraintestinal manifestations of inflammatory bowel

- disease and the influence of smoking.," *Digestion*, vol. 90, no. 2, pp. 122–9, Jan. 2014.
- [15] T. Birrenbach and U. Böcker, "Inflammatory Bowel Disease and Smoking," *Inflamm. Bowel Dis.*, vol. 10, no. 6, pp. 848–859, Nov. 2004.
- [16] E. Loftusjr, "Clinical epidemiology of inflammatory bowel disease: incidence, prevalence, and environmental influences," *Gastroenterology*, vol. 126, no. 6, pp. 1504–1517, May 2004.
- [17] J. Karczewski, B. Poniedziałek, P. Rzymiski, A. Rychlewska-Hańczewska, Z. Adamski, and K. Wiktorowicz, "The effect of cigarette smoking on the clinical course of inflammatory bowel disease.," *Przegląd Gastroenterol.*, vol. 9, no. 3, pp. 153–9, Jan. 2014.
- [18] K. a Rao, E. Yazaki, D. F. Evans, and R. Carbon, "Objective evaluation of small bowel and colonic transit time using pH telemetry in athletes with gastrointestinal symptoms.," *Br. J. Sports Med.*, vol. 38, no. 4, pp. 482–7, Aug. 2004.
- [19] J. M. H. Ebden, P. E. Blackshaw, A. C. P. Ins, C. G. Wilson, and R. C. Spiller, "Limited exposure of the healthy distal colon to orally-dosed formulation is further exaggerated in active left-sided ulcerative colitis," *Aliment. Pharmacol. Ther.*, vol. 14, pp. 155–161, 2000.
- [20] N. SG, K. D, R. DS, and E. DF, "Intestinal luminal pH in inflammatory bowel disease : possible determinants and implications for therapy with aminosalicylates and other drugs," *Gut*, vol. 48, pp. 571–577, 2001.
- [21] B. J. Goggins, C. Chaney, G. L. Radford-Smith, J. C. Horvat, and S. Keely, "Hypoxia and Integrin-Mediated Epithelial Restitution during Mucosal Inflammation.," *Front. Immunol.*, vol. 4, no. September, p. 272, Jan. 2013.
- [22] N. a Louis, K. E. Hamilton, G. Canny, L. L. Shekels, S. B. Ho, and S. P. Colgan, "Selective induction of mucin-3 by hypoxia in intestinal epithelia.," *J. Cell. Biochem.*, vol. 99, no. 6, pp. 1616–27, Dec. 2006.
- [23] W. J. Sandborn, B. G. Feagan, and G. R. Lichtenstein, "Medical management of mild to moderate Crohn's disease: evidence-based treatment algorithms for induction and maintenance of remission.," *Aliment. Pharmacol. Ther.*, vol. 26, no. 7, pp. 987–1003, Oct. 2007.
- [24] A. Cassinotti, "Adalimumab for the treatment of Crohn ' s disease," *Biol. Targets Ther.*, vol. 2, no. 4, pp. 763–777, 2008.
- [25] E. M. Collnot, H. Ali, and C. M. Lehr, "Nano- and microparticulate drug carriers for targeting of the inflamed intestinal mucosa," *Journal of Controlled Release*, vol. 161. pp. 235–246, 2012.
- [26] J. C. Hoffmann, N. N. Pawlowski, A. a. Köhl, W. Höhne, and M. Zeitz, "Animal Models of Inflammatory Bowel Disease: An Overview," *Pathobiology*, vol. 70, no. 3, pp. 121–130, 2002.

- [27] J. J. Kim, M. S. Shajib, M. M. Manocha, and W. I. Khan, "Investigating intestinal inflammation in DSS-induced model of IBD.," *J. Vis. Exp.*, no. 60, pp. 1–6, Jan. 2012.
- [28] P. K. Randhawa, K. Singh, N. Singh, and A. S. Jaggi, "A review on chemical-induced inflammatory bowel disease models in rodents.," *Korean J. Physiol. Pharmacol.*, vol. 18, no. 4, pp. 279–88, Aug. 2014.
- [29] E. Viennois, M. T. Baker, B. Xiao, L. Wang, H. Laroui, and D. Merlin, "Longitudinal study of circulating protein biomarkers in inflammatory bowel disease.," *J. Proteomics*, vol. 112, Sep. 2014.
- [30] Y. Sambuy, I. De Angelis, G. Ranaldi, M. L. Scarino, a Stammati, and F. Zucco, "The Caco-2 cell line as a model of the intestinal barrier: influence of cell and culture-related factors on Caco-2 cell functional characteristics.," *Cell Biol. Toxicol.*, vol. 21, no. 1, pp. 1–26, Jan. 2005.
- [31] I. Chantret, A. Barbat, E. Dussaulx, M. G. Brattain, and A. Zweibaum, "Epithelial Polarity, Villin Expression, and Enterocytic Differentiation of Cultured Human Colon Carcinoma Cells: A Survey of Twenty Cell Lines Epithelial Polarity , Villin Expression , and Enterocytic Differentiation of Cultured Human Colon Carcinoma C.," *Cancer Res.*, vol. 48, pp. 1936–1942, 1988.
- [32] P. E. R. Artursson, "Epithelial Transport of Drugs in Cell Culture . I: A Model for Studying the Passive Diffusion of Drugs over Intestinal," *J. Pharm. Sci.*, vol. 79, no. 6, pp. 476–482, 2000.
- [33] I. Hubatsch, E. G. E. Ragnarsson, and P. Artursson, "Determination of drug permeability and prediction of drug absorption in Caco-2 monolayers.," *Nat. Protoc.*, vol. 2, no. 9, pp. 2111–9, Jan. 2007.
- [34] B. M. Rothen-Rutishauser, S. G. Kiama, and P. Gehr, "A three-dimensional cellular model of the human respiratory tract to study the interaction with particles.," *Am. J. Respir. Cell Mol. Biol.*, vol. 32, no. 4, pp. 281–9, Apr. 2005.
- [35] A. D. Lehmann, N. Daum, M. Bur, C.-M. Lehr, P. Gehr, and B. M. Rothen-Rutishauser, "An in vitro triple cell co-culture model with primary cells mimicking the human alveolar epithelial barrier.," *Eur. J. Pharm. Biopharm.*, vol. 77, no. 3, pp. 398–406, Apr. 2011.
- [36] A. des Rieux, E. G. E. Ragnarsson, E. Gullberg, V. Pr at, Y.-J. Schneider, and P. Artursson, "Transport of nanoparticles across an in vitro model of the human intestinal follicle associated epithelium.," *Eur. J. Pharm. Sci.*, vol. 25, no. 4–5, pp. 455–65, 2005.
- [37] A. des Rieux, V. Fievez, I. Th ate, J. Mast, V. Pr at, and Y.-J. Schneider, "An improved in vitro model of human intestinal follicle-associated epithelium to study nanoparticle transport by M cells.," *Eur. J. Pharm. Sci.*, vol. 30, no. 5, pp. 380–91, Apr. 2007.
- [38] F. Antunes, F. Andrade, F. Ara ujo, D. Ferreira, and B. Sarmiento, "Establishment of a triple co-culture in vitro cell models to study intestinal absorption of peptide drugs.," *Eur. J. Pharm. Biopharm.*, vol. 83, no. 3, pp. 427–35, Apr. 2013.

- [39] F. Araújo and B. Sarmiento, "Towards the characterization of an in vitro triple co-culture intestine cell model for permeability studies.," *Int. J. Pharm.*, vol. 458, no. 1, pp. 128–34, Dec. 2013.
- [40] A. Béduneau, C. Tempesta, S. Fimbel, Y. Pellequer, V. Jannin, F. Demarne, and A. Lamprecht, "A tunable Caco-2/HT29-MTX co-culture model mimicking variable permeabilities of the human intestine obtained by an original seeding procedure.," *Eur. J. Pharm. Biopharm.*, vol. 87, no. 2, pp. 290–8, Jul. 2014.
- [41] C. Schimpel, B. Teubl, M. Absenger, C. Meindl, E. Fröhlich, G. Leitinger, A. Zimmer, and E. Roblegg, "Development of an Advanced Intestinal in Vitro Triple Culture Permeability Model To Study Transport of Nanoparticles.," *Mol. Pharm.*, vol. 11, pp. 808–818, Feb. 2014.
- [42] L. Le Hégarat, S. Huet, and V. Fessard, "A co-culture system of human intestinal Caco-2 cells and lymphoblastoid TK6 cells for investigating the genotoxicity of oral compounds.," *Mutagenesis*, vol. 27, no. 6, pp. 631–6, Nov. 2012.
- [43] T. Tanoue, Y. Nishitani, K. Kanazawa, T. Hashimoto, and M. Mizuno, "In vitro model to estimate gut inflammation using co-cultured Caco-2 and RAW264.7 cells.," *Biochem. Biophys. Res. Commun.*, vol. 374, no. 3, pp. 565–9, Sep. 2008.
- [44] D. Haller, C. Bode, W. P. Hammes, A. M. A. Pfeifer, E. J. V Schi, and S. Blum, "Non-pathogenic bacteria elicit a differential cytokine response by intestinal epithelial cell / leucocyte co-cultures," *Gut*, vol. 47, pp. 79–87, 2000.
- [45] S. Holland-Cunz, S. Bainsczyk, C. Hagl, E. Wink, T. Wedel, W. Back, and K. H. Schäfer, "Three-dimensional co-culture model of enterocytes and primary enteric neuronal tissue.," *Pediatr. Surg. Int.*, vol. 20, no. 4, pp. 233–7, Apr. 2004.
- [46] M. Calatayud, J. V Gimeno-Alcañiz, V. Devesa, and D. Vélez, "Proinflammatory effect of trivalent arsenical species in a co-culture of Caco-2 cells and peripheral blood mononuclear cells.," *Arch. Toxicol.*, May 2014.
- [47] G. Bisping, N. Lügering, S. Lütke-Brintrup, H. Pauels, G. Schürmann, W. Domschke, and T. Kucharzik, "Patients with inflammatory bowel disease ( IBD ) reveal increased induction capacity of intracellular interferon-gamma ( IFN- g ) in peripheral CD8 1 lymphocytes co-cultured with intestinal epithelial cells," *Clin. Exp. Immunol.*, vol. 123, pp. 1–8, 2001.
- [48] L. Willemsen, C. Schreurs, H. Kroes, E. Spillenaar Bilgen, S. van Deventer, and E. van Tol, "A Coculture Model Mimicking the Intestinal Mucosa Reveals a Regulatory Role for Myofibroblasts in Immune-Mediated Barrier Disruption," *Dig. Dis. sciences*, vol. 47, no. 10, pp. 2316–2324, 2002.
- [49] H. Satsu, Y. Ishimoto, T. Nakano, T. Mochizuki, T. Iwanaga, and M. Shimizu, "Induction by activated macrophage-like THP-1 cells of apoptotic and necrotic cell death in intestinal epithelial Caco-2 monolayers via tumor necrosis factor-alpha.," *Exp. Cell Res.*, vol. 312, no. 19, pp. 3909–19, Nov. 2006.
- [50] F. Leonard, E. Collnot, and C. Lehr, "articles A Three-Dimensional Coculture of Enterocytes , Monocytes and Dendritic Cells To Model Inflamed Intestinal Mucosa in Vitro," vol. 7, no. 6, pp. 2103–2119, 2010.

- [51] F. Leonard, H. Ali, E. Collnot, B. J. Crielaard, T. Lammers, G. Storm, and C.-M. Lehr, "Screening of Budesonide Nanoformulations for Treatment of Inflammatory Bowel Disease in an Inflamed 3D Cell-Culture Model," *ALTEX*, vol. 3, no. 29, pp. 275–285, 2012.
- [52] "Nanoscience and nanotechnologies : opportunities and uncertainties," *R. Soc.*, no. July, 2004.
- [53] N. Khlebtsov and L. Dykman, "Biodistribution and toxicity of engineered gold nanoparticles: a review of in vitro and in vivo studies.," *Chem. Soc. Rev.*, vol. 40, no. 3, pp. 1647–71, Mar. 2011.
- [54] C. Som, P. Wick, H. Krug, and B. Nowack, "Environmental and health effects of nanomaterials in nanotextiles and façade coatings.," *Environ. Int.*, vol. 37, no. 6, pp. 1131–42, Aug. 2011.
- [55] J. Lee, S. Mahendra, and P. J. J. Alvarez, "Nanomaterials in the Construction Industry : A Review of Their Applications," *ACS Nano*, vol. 4, no. 7, 2010.
- [56] B. a Magnuson, T. S. Jonaitis, and J. W. Card, "A brief review of the occurrence, use, and safety of food-related nanomaterials.," *J. Food Sci.*, vol. 76, no. 6, pp. R126–33, Aug. 2011.
- [57] M. Pinto, S. Robine-Leon, M.-D. Appay, M. Kedinger, N. Triadou, E. Dussaulx, B. Lacroix, P. Simon-assmann, K. Haffen, J. Fogh, and A. Zweibaum, "Enterocyte-like Differentiation and Polarization," *Biol. Cell*, vol. 47, no. 323, pp. 323–330, 1983.
- [58] M. D. Peterson and M. S. Mooseker, "Characterization of the enterocyte-like brush border cytoskeleton of the C2 BBe clones of the human intestinal cell line , Caco-2," *J. Cell Sci.*, vol. 102, pp. 581–600, 1992.
- [59] M. a Dobrovolskaia and S. E. McNeil, "Immunological properties of engineered nanomaterials.," *Nat. Nanotechnol.*, vol. 2, no. 8, pp. 469–78, Aug. 2007.
- [60] B. Rothen-Rutishauser, C. Mühlfeld, F. Blank, C. Musso, and P. Gehr, "Translocation of particles and inflammatory responses after exposure to fine particles and nanoparticles in an epithelial airway model," *Part. Fibre Toxicol.*, vol. 4, no. 1, p. 9, 2007.
- [61] C. Berges, C. Naujokat, S. Tinapp, H. Wieczorek, A. Höh, M. Sadeghi, G. Opelz, and V. Daniel, "A cell line model for the differentiation of human dendritic cells," *Biochem. Biophys. Res. Commun.*, vol. 333, pp. 896–907, 2005.
- [62] K. Larsson, M. Lindstedt, and C. a K. Borrebaeck, "Functional and transcriptional profiling of MUTZ-3, a myeloid cell line acting as a model for dendritic cells.," *Immunology*, vol. 117, no. 2, pp. 156–66, Feb. 2006.
- [63] S. F. G. van Helden, F. N. van Leeuwen, and C. G. Figdor, "Human and murine model cell lines for dendritic cell biology evaluated.," *Immunol. Lett.*, vol. 117, pp. 191–197, 2008.
- [64] Z. Qin, "The use of THP-1 cells as a model for mimicking the function and regulation of monocytes and macrophages in the vasculature.," *Atherosclerosis*, vol. 221, no. 1, pp. 2–11, Mar. 2012.

- [65] K. Traore, M. a. Trush, M. George, E. W. Spannhake, W. Anderson, and A. Asseffa, "Signal transduction of phorbol 12-myristate 13-acetate (PMA)-induced growth inhibition of human monocytic leukemia THP-1 cells is reactive oxygen dependent," *Leuk. Res.*, vol. 29, pp. 863–879, 2005.
- [66] J. Auwerx, "The human leukemia cell line, THP-1: A multifaceted model for the study of monocyte-macrophage differentiation," *Experientia*, vol. 47, pp. 22–31, 1991.
- [67] M. Daigneault, J. a Preston, H. M. Marriott, M. K. B. Whyte, and D. H. Dockrell, "The identification of markers of macrophage differentiation in PMA-stimulated THP-1 cells and monocyte-derived macrophages.," *PLoS One*, vol. 5, no. 1, p. e8668, Jan. 2010.
- [68] F. Leonard, H. Ali, E.-M. Collnot, B. J. Crielaard, T. Lammers, G. Storm, and C.-M. Lehr, "Screening of budesonide nanoformulations for treatment of inflammatory bowel disease in an inflamed 3D cell-culture model.," *ALTEX*, vol. 29, no. 3, pp. 275–85, Jan. 2012.
- [69] R. M. Steinmann and Z. A. Cohn, "Identification of a Novel Cell Type in Peripheral Lymphoid Organs of," *J. Immunol.*, vol. 137, pp. 1142–1162, 2014.
- [70] B. Rothen-rutishauser, L. Müller, F. Blank, C. Brandenberger, C. Mühlfeld, and P. Gehr, "A Newly Developed In Vitro Model of the Human Epithelial Airway Barrier to Study the Toxic Potential of Nanoparticles," *ALTEX*, vol. 25, no. 8, pp. 191–196, 2008.
- [71] L. Muller, M. Riediker, P. Wick, M. Mohr, P. Gehr, and B. Rothen-rutishauser, "Oxidative stress and inflammation response after nanoparticle exposure: differences between human lung cell monocultures and an advanced three-dimensional model of the human epithelial airways," *J. R. Soc. Interface*, vol. 7, no. July 2009, pp. 27–40, 2010.
- [72] C. Bodet, F. Chandad, and D. Grenier, "Inflammatory responses of a macrophage/epithelial cell co-culture model to mono and mixed infections with *Porphyromonas gingivalis*, *Treponema denticola*, and *Tannerella forsythia*," *Microbes Infect.*, vol. 8, no. 1, pp. 27–35, Jan. 2006.
- [73] G. Nollevaux, C. Devillé, B. El Moualij, W. Zorzi, P. Deloyer, Y.-J. Schneider, O. Peulen, and G. Dandrifosse, "Development of a serum-free co-culture of human intestinal epithelium cell-lines (Caco-2/HT29-5M21).," *BMC Cell Biol.*, vol. 7, p. 20, Jan. 2006.
- [74] M. Trapecar, A. Goropevsek, M. Gorenjak, L. Gradisnik, and M. Slak Rupnik, "A co-culture model of the developing small intestine offers new insight in the early immunomodulation of enterocytes and macrophages by *Lactobacillus* spp. through STAT1 and NF- $\kappa$ B p65 translocation.," *PLoS One*, vol. 9, no. 1, p. e86297, Jan. 2014.
- [75] M. Bermudez-Brito, J. Plaza-Díaz, L. Fontana, S. Muñoz-Quezada, and A. Gil, "In vitro cell and tissue models for studying host-microbe interactions: a review.," *Br. J. Nutr.*, vol. 109 Suppl , pp. S27–34, 2013.

- [76] H. Takahashi, Y. Hatta, N. Iriyama, Y. Hasegawa, H. Uchida, M. Nakagawa, M. Makishima, J. Takeuchi, and M. Takei, "Induced Differentiation of Human Myeloid Leukemia Cells into M2 Macrophages by Combined Treatment with Retinoic Acid and 1 $\alpha$ ,25-Dihydroxyvitamin D3.," *PLoS One*, vol. 9, no. 11, p. e113722, Jan. 2014.
- [77] S. A. Olofinsae, B. O. Ibeh, and J. Ahluwalia, "Increased oxygen consumption observed in phorbol 12-myristate 13-acetate stimulated human cultured promonocytic U937 cell lines treated with calcitriol and retinoic acid.," *Asian Pac. J. Trop. Med.*, vol. 7S1, no. Suppl 1, pp. S272–7, Sep. 2014.
- [78] W. Chanput, J. J. Mes, and H. J. Wichers, "THP-1 cell line: An in vitro cell model for immune modulation approach.," *Int. Immunopharmacol.*, vol. 23, no. 1, pp. 37–45, Aug. 2014.
- [79] A. J. Masterson, C. C. Sombroek, T. D. De Gruijl, Y. M. F. Graus, H. J. J. Van Der Vliet, M. Lougheed, A. J. M. Van Den Eertwegh, H. M. Pinedo, and R. J. Scheper, "Brief report MUTZ-3 , a human cell line model for the cytokine-induced differentiation of dendritic cells from CD34<sup>+</sup> precursors," *Bloodjournal*, vol. 100, no. 2, pp. 701–704, 2015.
- [80] N. Bertiaux-Vandaële, S. B. Youmba, L. Belmonte, S. Leclaire, M. Antonietti, G. Gourcerol, A.-M. Leroi, P. Déchelotte, J.-F. Ménard, P. Ducrotté, and M. Coëffier, "The expression and the cellular distribution of the tight junction proteins are altered in irritable bowel syndrome patients with differences according to the disease subtype.," *Am. J. Gastroenterol.*, vol. 106, no. 12, pp. 2165–73, Dec. 2011.
- [81] J. D. Schulzke, S. Ploeger, M. Amasheh, A. Fromm, S. Zeissig, H. Troeger, J. Richter, C. Bojarski, M. Schumann, and M. Fromm, "Epithelial tight junctions in intestinal inflammation.," *Ann. N. Y. Acad. Sci.*, vol. 1165, pp. 294–300, May 2009.
- [82] S. Zeissig, N. Bürgel, D. Günzel, J. Richter, J. Mankertz, U. Wahnschaffe, a J. Kroesen, M. Zeitz, M. Fromm, and J.-D. Schulzke, "Changes in expression and distribution of claudin 2, 5 and 8 lead to discontinuous tight junctions and barrier dysfunction in active Crohn's disease.," *Gut*, vol. 56, no. 1, pp. 61–72, Jan. 2007.
- [83] S. Guo, R. Al-Sadi, H. M. Said, and T. Y. Ma, "Lipopolysaccharide causes an increase in intestinal tight junction permeability in vitro and in vivo by inducing enterocyte membrane expression and localization of TLR-4 and CD14.," *Am. J. Pathol.*, vol. 182, no. 2, pp. 375–87, Feb. 2013.
- [84] A. D. Lehmann, F. Blank, O. Baum, P. Gehr, and B. M. Rothen-Rutishauser, "Diesel exhaust particles modulate the tight junction protein occludin in lung cells in vitro.," *Part. Fibre Toxicol.*, vol. 6, p. 26, Jan. 2009.
- [85] M. I. Hermanns, J. Kasper, P. Dubruel, C. Pohl, C. Uboldi, V. Vermeersch, S. Fuchs, R. E. Unger, and C. J. Kirkpatrick, "An impaired alveolar-capillary barrier in vitro: effect of proinflammatory cytokines and consequences on nanocarrier interaction," *Interface*, vol. 7, no. September 2009, pp. 41–54, 2010.
- [86] S. Salvini, M. Charbonnier, C. Defoort, C. Alquier, and D. Lairon, "Functional characterization of three clones of the human intestinal Caco-2 cell line for dietary lipid processing," *Br. J. Nutr.*, vol. 87, no. 03, p. 211, Mar. 2007.

- [87] G. Herold, G. Rogler, D. Rogler, and E. F. Stange, "Morphology of Caco-2 cells varies in different cell batches," *Vitr. cell*, vol. 18, no. May, pp. 289–291, 1994.
- [88] D. 2014 Alexis, NE, Huang, YC, Rappold, AG, Kehrl, H, Devlin, R & Peden, "Patients with asthma demonstrate airway inflammation after exposure to concentrated ambient particulate matter," *Am J Respir Crit Care Med*, vol. 190, no. 2, pp. 235–237, 2014.
- [89] L. Kish, N. Hotte, G. G. Kaplan, R. Vincent, R. Tso, M. Gänzle, K. P. Rioux, A. Thiesen, H. W. Barkema, E. Wine, and K. L. Madsen, "Environmental particulate matter induces murine intestinal inflammatory responses and alters the gut microbiome.," *PLoS One*, vol. 8, no. 4, p. e62220, Jan. 2013.
- [90] J. J. Powell, N. Faria, E. Thomas-McKay, and L. C. Pele, "Origin and fate of dietary nanoparticles and microparticles in the gastrointestinal tract.," *J. Autoimmun.*, vol. 34, no. 3, pp. J226–33, May 2010.
- [91] N. Mahmud and D. G. Weir, "The urban diet and Crohn's disease: is there a relationship?," *Eur. J. Gastroenterol. Hepatol.*, vol. 13, no. 2, pp. 93–95, Feb. 2001.
- [92] D. Theegarten, S. Boukercha, S. Philippou, and O. Anhenn, "Submesothelial deposition of carbon nanoparticles after toner exposition: case report.," *Diagn. Pathol.*, vol. 5, no. 1, p. 77, Jan. 2010.
- [93] B. K. Gaiser, T. F. Fernandes, M. Jepson, J. R. Lead, C. R. Tyler, and V. Stone, "Assessing exposure, uptake and toxicity of silver and cerium dioxide nanoparticles from contaminated environments.," *Environ. Health*, vol. 8 Suppl 1, p. S2, Jan. 2009.
- [94] A. Beloqui, R. Coco, P. B. Memvanga, B. Ucakar, A. des Rieux, and V. Pr eat, "pH-sensitive nanoparticles for colonic delivery of curcumin in inflammatory bowel disease.," *Int. J. Pharm.*, vol. 473, no. 1–2, pp. 203–12, Oct. 2014.
- [95] M. Fisichella, F. Berenguer, G. Steinmetz, M. Auffan, J. Rose, and O. Prat, "Intestinal toxicity evaluation of TiO<sub>2</sub> degraded surface-treated nanoparticles: a combined physico-chemical and toxicogenomics approach in caco-2 cells.," *Part. Fibre Toxicol.*, vol. 9, no. 1, p. 18, Jan. 2012.
- [96] B. a Koeneman, Y. Zhang, P. Westerhoff, Y. Chen, J. C. Crittenden, and D. G. Capco, "Toxicity and cellular responses of intestinal cells exposed to titanium dioxide.," *Cell Biol. Toxicol.*, vol. 26, no. 3, pp. 225–38, Jun. 2010.
- [97] F. F oger, a Kopf, B. Loretz, K. Albrecht, and a Bernkop-Schn urch, "Correlation of in vitro and in vivo models for the oral absorption of peptide drugs.," *Amino Acids*, vol. 35, no. 1, pp. 233–41, Jun. 2008.
- [98] A. Frick, H. Mo, and E. Wirbitzki, "Biopharmaceutical characterization of oral immediate release drug products . In vitro / in vivo comparison of phenoxymethylpenicillin potassium , glimepiride and levofloxacin," *Eur. J. Biopharm.*, vol. 46, pp. 305–311, 1998.
- [99] E. Walter, S. Janich, B. Roessler, H. JM, and G. Amidon, "HT29-MTX / Caco-2 Cocultures as an in Vitro Model for the Intestinal Epithelium : In Vitro – in Vivo

- Correlation with Permeability Data from Rats and Humans,” *J. Pharm. Sci.*, vol. 85, no. 10, pp. 1070–1076, 1996.
- [100] V. Ayala, A. P. Herrera, M. Latorre-Esteves, M. Torres-Lugo, and C. Rinaldi, “Effect of surface charge on the colloidal stability and in vitro uptake of carboxymethyl dextran-coated iron oxide nanoparticles.,” *J. Nanopart. Res.*, vol. 15, no. 8, p. 1874, Aug. 2013.
- [101] M. Desjardins and G. Griffiths, “Phagocytosis: latex leads the way,” *Curr. Opin. Cell Biol.*, vol. 15, no. 4, pp. 498–503, Aug. 2003.
- [102] B. K. Gaiser, S. Hirn, A. Kermanizadeh, N. Kanase, K. Fytianos, A. Wenk, N. Haberl, A. Brunelli, W. G. Kreyling, and V. Stone, “Effects of silver nanoparticles on the liver and hepatocytes in vitro.,” *Toxicol. Sci.*, vol. 131, no. 2, pp. 537–47, Feb. 2013.
- [103] J. Susewind, C. de Souza Carvalho-Wodarz, U. Repnik, E.-M. Collnot, N. Schneider-Daum, G. W. Griffiths, and C.-M. Lehr, “A 3D co-culture of three human cell lines to model the inflamed intestinal mucosa for safety testing of nanomaterials,” *Nanotoxicology*, vol. 5390, pp. 1–10, 2015.
- [104] A. Manke, L. Wang, and Y. Rojanasakul, “Mechanisms of nanoparticle-induced oxidative stress and toxicity,” *Biomed Res. Int.*, vol. 2013, 2013.
- [105] J. C. Bonner, “Lung fibrotic responses to particle exposure.,” *Toxicol. Pathol.*, vol. 35, pp. 148–153, 2007.
- [106] V. Vallyathan and X. Shi, “The role of oxygen free radicals in occupational and environmental lung diseases.,” *Environ. Health Perspect.*, vol. 105 Suppl , no. February, pp. 165–177, 1997.
- [107] C. Beer, R. Foldbjerg, Y. Hayashi, D. S. Sutherland, and H. Autrup, “Toxicity of silver nanoparticles - nanoparticle or silver ion?,” *Toxicol. Lett.*, vol. 208, no. 3, pp. 286–92, Feb. 2012.
- [108] K. Loeschner, N. Hadrup, K. Qvortrup, A. Larsen, X. Gao, U. Vogel, A. Mortensen, H. R. Lam, and E. H. Larsen, “Distribution of silver in rats following 28 days of repeated oral exposure to silver nanoparticles or silver acetate.,” *Part. Fibre Toxicol.*, vol. 8, no. 1, p. 18, Jan. 2011.
- [109] M. V. D. Z. Park, A. M. Neigh, J. P. Vermeulen, L. J. J. de la Fonteyne, H. W. Verharen, J. J. Briedé, H. van Loveren, and W. H. de Jong, “The effect of particle size on the cytotoxicity, inflammation, developmental toxicity and genotoxicity of silver nanoparticles.,” *Biomaterials*, vol. 32, no. 36, pp. 9810–7, Dec. 2011.
- [110] A. Weir, P. Westerhoff, L. Fabricius, and N. von Goetz, “Titanium Dioxide Nanoparticles in Food and Personal Care Products,” *Environ. Sci. Technol.*, vol. 46, no. 4, pp. 2242–2250, 2013.
- [111] E. Fröhlich and E. Roblegg, “Models for oral uptake of nanoparticles in consumer products,” *Toxicology*, vol. 291, pp. 10–17, 2012.

- [112] T. Mironava, M. Hadjiargyrou, M. Simon, V. Jurukovski, and M. H. Rafailovich, "Gold nanoparticles cellular toxicity and recovery: effect of size, concentration and exposure time.," *Nanotoxicology*, vol. 4, no. 1, pp. 120–37, Mar. 2010.
- [113] S. Arora, J. M. Rajwade, and K. M. Paknikar, "Nanotoxicology and in vitro studies: the need of the hour.," *Toxicol. Appl. Pharmacol.*, vol. 258, no. 2, pp. 151–65, Jan. 2012.
- [114] J. Kasper, M. I. Hermanns, C. Bantz, M. Maskos, R. Stauber, C. Pohl, R. E. Unger, and J. C. Kirkpatrick, "Inflammatory and cytotoxic responses of an alveolar-capillary coculture model to silica nanoparticles: comparison with conventional monocultures.," *Part. Fibre Toxicol.*, vol. 8, no. 1, p. 6, Jan. 2011.
- [115] E. Cabré and E. Domènech, "Impact of environmental and dietary factors on the course of inflammatory bowel disease.," *World J. Gastroenterol.*, vol. 18, no. 29, pp. 3814–22, Aug. 2012.
- [116] T. A. Kuhlbusch, C. Asbach, H. Fissan, D. Göhler, and M. Stintz, "Nanoparticle exposure at nanotechnology workplaces: a review.," *Part. Fibre Toxicol.*, vol. 8, no. 1, p. 22, Jan. 2011.
- [117] J. H. Sung, J. H. Ji, J. D. Park, M. Y. Song, K. S. Song, H. R. Ryu, J. U. Yoon, K. S. Jeon, J. Jeong, B. S. Han, Y. H. Chung, H. K. Chang, J. H. Lee, D. W. Kim, B. J. Kelman, and I. J. Yu, "Subchronic inhalation toxicity of gold nanoparticles.," *Part. Fibre Toxicol.*, vol. 8, p. 16, Jan. 2011.
- [118] F. Perreault, S. P. Melegari, C. F. Fuzinato, N. Bogdan, M. Morin, R. Popovic, and W. G. Matias, "Toxicity of PAMAM-Coated Gold Nanoparticles in Different Unicellular Models Franc," *Environ. Toxicol.*, vol. 29, no. 3, pp. 1–9, 2012.
- [119] X.-D. Zhang, D. Wu, X. Shen, P.-X. Liu, N. Yang, B. Zhao, H. Zhang, Y.-M. Sun, L.-A. Zhang, and F.-Y. Fan, "Size-dependent in vivo toxicity of PEG-coated gold nanoparticles.," *Int. J. Nanomedicine*, vol. 6, pp. 2071–81, Jan. 2011.
- [120] W.-S. Cho, S. Kim, B. S. Han, W. C. Son, and J. Jeong, "Comparison of gene expression profiles in mice liver following intravenous injection of 4 and 100 nm-sized PEG-coated gold nanoparticles.," *Toxicol. Lett.*, vol. 191, no. 1, pp. 96–102, Dec. 2009.
- [121] E. Alfaro-Moreno, T. S. Nawrot, B. M. Vanaudenaerde, M. F. Hoylaerts, J. a Vanoirbeek, B. Nemery, and P. H. M. Hoet, "Co-cultures of multiple cell types mimic pulmonary cell communication in response to urban PM10.," *Eur. Respir. J.*, vol. 32, no. 5, pp. 1184–94, Nov. 2008.
- [122] G. Múzes, B. Molnár, Z. Tulassay, and F. Sipos, "Changes of the cytokine profile in inflammatory bowel diseases," vol. 18, no. 41, pp. 5848–5861, 2012.
- [123] A. Weir, P. Westerhoff, L. Fabricius, K. Hristovski, and N. von Goetz, "Titanium dioxide nanoparticles in food and personal care products.," *Environ. Sci. Technol.*, vol. 46, no. 4, pp. 2242–50, Feb. 2012.
- [124] J. Zhang, W. Song, J. Guo, J. Zhang, Z. Sun, L. Li, F. Ding, and M. Gao, "Cytotoxicity of different sized TiO<sub>2</sub> nanoparticles in mouse macrophages.," *Toxicol. Ind. Health*, vol. 29, no. 6, pp. 523–33, Jul. 2013.

- [125] I.-L. Hsiao and Y.-J. Huang, "Effects of various physicochemical characteristics on the toxicities of ZnO and TiO nanoparticles toward human lung epithelial cells.," *Sci. Total Environ.*, vol. 409, no. 7, pp. 1219–28, Mar. 2011.
- [126] A. Kermanizadeh, G. Pojana, B. K. Gaiser, R. Birkedal, D. Bilanicová, H. Wallin, K. A. Jensen, B. Sellergren, G. R. Hutchison, A. Marcomini, and V. Stone, "In vitro assessment of engineered nanomaterials using a hepatocyte cell line: cytotoxicity, pro-inflammatory cytokines and functional markers.," *Nanotoxicology*, vol. 7, no. 3, pp. 301–13, May 2013.
- [127] A. Kermanizadeh, S. Vranic, S. Boland, K. Moreau, A. Baeza-squiban, B. K. Gaiser, L. A. Andrzejczuk, and V. Stone, "An in vitro assessment of panel of engineered nanomaterials using a human renal cell line : oxidative stress and genotoxicity," *BMC Nephrol.*, vol. 14, no. 96, 2013.
- [128] B. K. Gaiser, T. F. Fernandes, M. a Jepson, J. R. Lead, C. R. Tyler, M. Baalousha, A. Biswas, G. J. Britton, P. a Cole, B. D. Johnston, Y. Ju-Nam, P. Rosenkranz, T. M. Scown, and V. Stone, "Interspecies comparisons on the uptake and toxicity of silver and cerium dioxide nanoparticles.," *Environ. Toxicol. Chem.*, vol. 31, no. 1, pp. 144–54, Jan. 2012.
- [129] N. Mei, Y. Zhang, Y. Chen, X. Guo, W. Ding, S. F. Ali, A. S. Biris, P. Rice, M. M. Moore, and T. Chen, "Silver Nanoparticle-Induced Mutations and Oxidative Stress in Mouse Lymphoma Cells," *Environ. Mol. Mutagen.*, vol. 53, no. 6, pp. 409 – 419, 2012.
- [130] Y. S. Kim, M. Y. Song, J. D. Park, K. S. Song, H. R. Ryu, Y. H. Chung, H. K. Chang, J. H. Lee, K. H. Oh, B. J. Kelman, I. K. Hwang, and I. J. Yu, "Subchronic oral toxicity of silver nanoparticles.," *Part. Fibre Toxicol.*, vol. 7, p. 20, Jan. 2010.
- [131] H. J. Johnston, G. Hutchison, F. M. Christensen, S. Peters, S. Hankin, and V. Stone, "A review of the in vivo and in vitro toxicity of silver and gold particulates: particle attributes and biological mechanisms responsible for the observed toxicity.," *Crit. Rev. Toxicol.*, vol. 40, no. 4, pp. 328–46, Apr. 2010.
- [132] M. Ghosh, M. J. S. Sinha, A. Chakraborty, S. K. Mallick, M. Bandyopadhyay, and A. Mukherjee, "In vitro and in vivo genotoxicity of silver nanoparticles.," *Mutat. Res.*, vol. 749, no. 1–2, pp. 60–9, Dec. 2012.
- [133] K. M. Newton, H. L. Puppala, C. L. Kitchens, V. L. Colvin, and S. J. Klaine, "Silver nanoparticle toxicity to *Daphnia magna* is a function of dissolved silver concentration.," *Environ. Toxicol. Chem.*, vol. 32, no. 10, pp. 2356–64, Oct. 2013.
- [134] Y.-J. Lee, J. Kim, J. Oh, S. Bae, S. Lee, I. S. Hong, and S.-H. Kim, "Ion-release kinetics and ecotoxicity effects of silver nanoparticles.," *Environ. Toxicol. Chem.*, vol. 31, no. 1, pp. 155–9, Jan. 2012.
- [135] C. Draheim, F. de Crécy, S. Hansen, E.-M. Collnot, and C.-M. Lehr, "A Design of Experiment Study of Nanoprecipitation and Nano Spray Drying as Processes to Prepare PLGA Nano- and Microparticles with Defined Sizes and Size Distributions," *Pharm. Res.*, 2015.

- [136] P. L. Kozuch and S. B. Hanauer, "Treatment of inflammatory bowel disease: a review of medical therapy.," *World J. Gastroenterol.*, vol. 14, no. 3, pp. 354–77, Jan. 2008.
- [137] F. Grimpen and P. Pavli, "Advances in the management of inflammatory bowel disease.," *Intern. Med. J.*, vol. 40, no. 4, pp. 258–64, Apr. 2010.
- [138] N. J. Talley, M. T. Abreu, J.-P. Achkar, C. N. Bernstein, M. C. Dubinsky, S. B. Hanauer, S. V Kane, W. J. Sandborn, T. a Ullman, and P. Moayyedi, "An evidence-based systematic review on medical therapies for inflammatory bowel disease.," *Am. J. Gastroenterol.*, vol. 106 Suppl , no. S1, pp. S2–25; quiz S26, Apr. 2011.
- [139] S. B. Hanauer, "Inflammatory bowel disease: epidemiology, pathogenesis, and therapeutic opportunities.," *Inflamm. Bowel Dis.*, vol. 12 Suppl 1, no. January, pp. S3–9, Jan. 2006.
- [140] A. Lamprecht, U. Schäfer, and C. M. Lehr, "Size-dependent bioadhesion of micro- and nanoparticulate carriers to the inflamed colonic mucosa.," *Pharm. Res.*, vol. 18, no. 6, pp. 788–93, Jun. 2001.
- [141] C. Schmidt, C. Lautenschlaeger, E.-M. Collnot, M. Schumann, C. Bojarski, J.-D. Schulzke, C.-M. Lehr, and A. Stallmach, "Nano- and microscaled particles for drug targeting to inflamed intestinal mucosa – a first in vivo study in human patients," *J. Control. Release*, pp. 1–7, Nov. 2012.
- [142] F. Danhier, E. Ansorena, J. M. Silva, R. Coco, A. Le Breton, and V. Pr at, "PLGA-based nanoparticles: an overview of biomedical applications.," *J. Control. Release*, vol. 161, no. 2, pp. 505–22, Jul. 2012.
- [143] M. L. Hans and A. M. Lowman, "Biodegradable nanoparticles for drug delivery and targeting," *Curr. Opin. Solid State Mater. Sci.*, vol. 6, no. September, pp. 319–327, 2002.
- [144] H. K. Makadia and S. J. Siegel, "Poly Lactic-co-Glycolic Acid (PLGA) as Biodegradable Controlled Drug Delivery Carrier," *Polymers (Basel)*, vol. 3, no. 3, pp. 1377–1397, Aug. 2011.
- [145] N. Wang and X. S. Wu, "Synthesis, characterization, biodegradation, and drug delivery application of biodegradable lactic/glycolic acid oligomers: Part II. Biodegradation and drug delivery application," *J. Biomater. Sci. Polym. Ed.*, vol. 9, no. 1, pp. 75–87, Jan. 1998.
- [146] G. G. Greenberg, B. G. Feagan, F. Martin, L. R. Sutherland, A. B. R. Thomson, N. Williams, L.-G. Nilsson, and T. Persson, "Oral budesonide for active Crohn's disease," *N. Engl. J. Med.*, vol. 331, no. 13, pp. 836–841, 1994.
- [147] K. Herrlinger, B. Wittig, and E. F. Stange, "Chronic inflammatory intestinal diseases. Pathophysiology and therapy," *Internist (Berl)*, vol. 50, no. 10, pp. 1229–46; quiz 1247, Oct. 2009.
- [148] a Kornbluth, "Cyclosporine in inflammatory bowel disease.," *Curr. Gastroenterol. Rep.*, vol. 1, no. 6, pp. 486–90, Dec. 1999.

- [149] M. Clark, J.-F. Colombel, B. C. Feagan, R. N. Fedorak, S. B. Hanauer, M. a Kamm, L. Mayer, C. Regueiro, P. Rutgeerts, W. J. Sandborn, B. E. Sands, S. Schreiber, S. Targan, S. Travis, and S. Vermeire, "American gastroenterological association consensus development conference on the use of biologics in the treatment of inflammatory bowel disease, June 21-23, 2006.," *Gastroenterology*, vol. 133, no. 1, pp. 312–39, Jul. 2007.
- [150] R. C. Rowe, P. J. Sheskey, and M. E. Quinn, *Handbook of Pharmaceutical Excipients*, 6th ed. Pharmaceutical Press, 2009, pp. 675–678.
- [151] A. Lamprecht, N. Ubrich, H. Yamamoto, U. Schäfer, H. Takeuchi, P. Maincent, Y. Kawashima, and C. M. Lehr, "Biodegradable nanoparticles for targeted drug delivery in treatment of inflammatory bowel disease.," *J. Pharmacol. Exp. Ther.*, vol. 299, no. 2, pp. 775–81, Nov. 2001.
- [152] N. Anton, J.-P. Benoit, and P. Saulnier, "Design and production of nanoparticles formulated from nano-emulsion templates-a review.," *J. Control. Release*, vol. 128, no. 3, pp. 185–99, Jun. 2008.
- [153] C. E. Mora-Huertas, H. Fessi, and A. Elaissari, "Influence of process and formulation parameters on the formation of submicron particles by solvent displacement and emulsification-diffusion methods critical comparison.," *Adv. Colloid Interface Sci.*, vol. 163, no. 2, pp. 90–122, Apr. 2011.
- [154] A. N. and B. S. Fessi H, Puisieux F, Devissaguet J Ph, "Nanocapsule formation by interfacial polymer deposition following solvent displacement," *Int. J. Pharm.*, vol. 55, pp. 1–4, 1989.
- [155] S. Galindo-Rodríguez, F. Puel, S. Briançon, E. Allémann, E. Doelker, and H. Fessi, "Comparative scale-up of three methods for producing ibuprofen-loaded nanoparticles.," *Eur. J. Pharm. Sci.*, vol. 25, no. 4–5, pp. 357–67, 2005.
- [156] W. Abdelwahed, G. Degobert, and H. Fessi, "A pilot study of freeze drying of poly(epsilon-caprolactone) nanocapsules stabilized by poly(vinyl alcohol): formulation and process optimization.," *Int. J. Pharm.*, vol. 309, no. 1–2, pp. 178–88, Feb. 2006.
- [157] H. Takeuchi, H. Yamamoto, T. Toyoda, H. Toyobuku, T. Hino, and Y. Kawashima, "Physical stability of size controlled small unilamellar liposomes coated with a modified polyvinyl alcohol," *Int. J. Pharm.*, vol. 164, no. 1–2, pp. 103–111, Apr. 1998.
- [158] X. Li, N. Anton, C. Arpagaus, F. Bellesteix, and T. F. Vandamme, "Nanoparticles by spray drying using innovative new technology: The Büchi Nano Spray Dryer B-90.," *J. Control. Release*, vol. 147, no. 2, pp. 304–310, Jul. 2010.
- [159] N. Schafroth, C. Arpagaus, U. Y. Jadhav, S. Makne, and D. Douroumis, "Nano and microparticle engineering of water insoluble drugs using a novel spray-drying process.," *Colloids Surf. B. Biointerfaces*, vol. 90, pp. 8–15, Feb. 2012.
- [160] N. Schafroth and M. Meuri, "SPRAY-DRYING OF LACTOSE: A REVIEW," *Eur. Ind. Pharm.*, no. 15, pp. 4–8, 2012.

- [161] K. Bürki, I. Jeon, C. Arpagaus, and G. Betz, "New insights into respirable protein powder preparation using a nano spray dryer.," *Int. J. Pharm.*, vol. 408, no. 1–2, pp. 248–56, Apr. 2011.
- [162] S. H. Lee, D. Heng, W. K. Ng, H.-K. Chan, and R. B. H. Tan, "Nano spray drying: a novel method for preparing protein nanoparticles for protein therapy.," *Int. J. Pharm.*, vol. 403, no. 1–2, pp. 192–200, Jan. 2011.
- [163] M. Beck-Broichsitter, C. Schweiger, T. Schmehl, T. Gessler, W. Seeger, and T. Kissel, "Characterization of novel spray-dried polymeric particles for controlled pulmonary drug delivery.," *J. Control. Release*, vol. 158, no. 2, pp. 329–35, Mar. 2012.
- [164] A. C. Ford, W. J. Sandborn, K. J. Khan, S. B. Hanauer, N. J. Talley, and P. Moayyedi, "Efficacy of biological therapies in inflammatory bowel disease: systematic review and meta-analysis.," *Am. J. Gastroenterol.*, vol. 106, no. 4, pp. 644–59, quiz 660, Apr. 2011.
- [165] H. Ali, E.-M. Collnot, M. Windbergs, and C.-M. Lehr, "Nanomedicines for the treatment of inflammatory bowel diseases," *Eur. J. Nanomedicine*, vol. 5, no. 1, pp. 23–38, Jan. 2013.
- [166] J. Cheng, B. a Teply, I. Sherifi, J. Sung, G. Luther, F. X. Gu, E. Levy-Nissenbaum, A. F. Radovic-Moreno, R. Langer, and O. C. Farokhzad, "Formulation of functionalized PLGA-PEG nanoparticles for in vivo targeted drug delivery.," *Biomaterials*, vol. 28, no. 5, pp. 869–76, Feb. 2007.
- [167] Y. Li, K. J. Zhu, J. X. Zhang, H. L. Jiang, J. H. Liu, Y. L. Hao, H. Yasuda, A. Ichimaru, and K. Yamamoto, "In vitro and in vivo studies of cyclosporin A-loaded microspheres based on copolymers of lactide and epsilon-caprolactone: comparison with conventional PLGA microspheres.," *Int. J. Pharm.*, vol. 295, no. 1–2, pp. 67–76, May 2005.
- [168] J. L. Italia, D. K. Bhatt, V. Bhardwaj, K. Tikoo, and M. N. V. R. Kumar, "PLGA nanoparticles for oral delivery of cyclosporine: nephrotoxicity and pharmacokinetic studies in comparison to Sandimmune Neoral.," *J. Control. Release*, vol. 119, no. 2, pp. 197–206, Jun. 2007.
- [169] T. Urata, K. Arimori, and H. Nakano, "Modification of release rates of cyclosporin A from poly(L-lactic acid) microspheres by fatty acid esters and in-vivo evaluation of the microspheres.," *J. Control. Release*, vol. 58, no. 2, pp. 133–41, Mar. 1999.
- [170] J. Linnankoski and J. Ma, "Paracellular Porosity and Pore Size of the Human Intestinal Epithelium in Tissue and Cell Culture Models," vol. 99, no. 4, pp. 2166–2175, 2010.
- [171] P. E. Porporato, V. L. Payen, C. J. De Saedeleer, V. Pr eat, J.-P. Thissen, O. Feron, and P. Sonveaux, "Lactate stimulates angiogenesis and accelerates the healing of superficial and ischemic wounds in mice.," *Angiogenesis*, vol. 15, no. 4, pp. 581–92, Dec. 2012.
- [172] K. K. Chereddy, R. Coco, P. B. Memvanga, B. Ucar, A. des Rieux, G. Vandermeulen, and V. Pr eat, "Combined effect of PLGA and curcumin on wound healing activity.," *J. Control. Release*, vol. 171, no. 2, pp. 208–15, Oct. 2013.

---

## Abbreviations

ADME	Absorption, distribution, metabolism and excretion
ATCC	American Type Culture Collection
API	Active pharmaceutical ingredient
Ag	Silver
Au	Gold
Bu	Budesonide
CD	Crohn´s disease
CLSM	Confocal laser scanning microscopy
CyA	Cyclosporine A
DAPI	4',6-Diamidin-2-phenylindol
DDS	Drug delivery system
DMEM	Dulbecco´s Modified Eagle Medium
DSMZ	Deutsche Sammlung von Mikroorganismen und Zellkulturen
DSS	Dextran sodium sulfate
EC50	Half maximal effective concentration
EE	Encapsulation efficiency
EN	Engineered nanomaterials
EVOM	Epithelial volttohmmeter
FACS	Fluorescence activated cell sorter
FBS	Fetal bovine serum
FDA	Fluorescein diacetate
GI	Gastrointestinal
GM-CFS	Granulocyte macrophage colony stimulating factor
HEPES	4-(2-hydroxyethyl)-1-piperazineethanesulfonic acid
IBD	Inflammatory bowel disease
IL	Interleukin
LDH	Lactate dehydrogenase

LPS	Lipopolysaccharide
MEM	Minimum Essential Medium
MP	Microparticles
NEAA	Non-essential amino acids
NP	Nanoparticles
PBMCs	Peripheral blood mononuclear cells
PBS	Phosphate buffered saline
PDI	Poly dispersity index
PFA	Paraformaldehyde
PLGA	poly (lactic-co-glycolic acid)
PVA	Poly vinyl alcohol
ROS	Reactive oxygen species
RPMI	Roswell Park Memorial Institute
RT	Room temperature
SD	Standard deviation
SEM	Scanning electron microscopy
TEER	Transepithelial electrical resistance
TEM	Transmission electron microscopy
TiO <sub>2</sub>	Titanium dioxide
TNBS	2, 4, 6-Trinitrobenzene sulfonic acid
TNF	Tumor necrosis factor
UC	Ulcerative colitis

---

## List of publications

### Research papers:

**J. Susewind**, C. de Souza Carvalho-Wodarz, U. Repnik, E.-M. Collnot, N. Schneider-Daum, G. W. Griffiths, and C.-M. Lehr, "A 3D co-culture of three human cell lines to model the inflamed intestinal mucosa for safety testing of nanomaterials" *Nanotoxicology*, vol. 5390, pp. 1–10, 2015.

B. Mostaghaci, **J. Susewind**, G. Kickelbick, C.-M. Lehr, B. Loretz, „Transfection System of Amino-functionalized Calcium Phosphate Nanoparticles: in-vitro Efficacy, Biodegradability and Immunogenicity study" *ACS Applied Materials & Interfaces*, vol 7, pp 5124-33, 2015

C. Draheim\*, **J. Susewind\***, A. Guillot, B. Loretz, S. Hansen, E.-M. Collnot, C. Villiers, P. Marché, M. Limberger, C.-M. Lehr: "PLGA based nano- and microsized particles for inflammatory bowel disease therapy: evaluation of size-dependent accumulation and anti-inflammatory effect in an *in vitro* triple culture model" *prepared for submission*

### Book chapter:

E.-M. Collnot, **J. Susewind**, C.-M. Lehr: "Advanced *in vitro* Models of the Intestinal Mucosa for Drug Delivery Studies" 2013 in *Haycock, Ahluwalia, Wilkinson: "Cellular in vitro Testing"*

### Poster:

C. Draheim\*, **J. Susewind\***, F. de Crecy, B. Loretz, C. de Souza Carvalho, N. Daum, E.-M. Collnot, S. Hansen, C.-M. Lehr: „Evaluation of PLGA based drug delivery systems for the therapy of inflammatory bowel disease in a 3 D cell-culture model" 10th International Conference and Workshop on Biological Barriers, February 2014, Saarbücken, Germany

**J. Susewind**, E.-M. Collnot, C.-M. Lehr: "An inflamed and non-inflamed triple culture model of the intestinal mucosa to assess cytotoxicity of engineered nanoparticles" AAPS Annual Meeting and Exposition, October 2012, Chicago, IL, USA

**J. Susewind**, E.-M. Collnot, C.-M. Lehr: “An inflamed and non-inflamed triple culture model of the intestinal mucosa to assess cytotoxicity of engineered nanoparticles” 9th International Conference and Workshop on Biological Barriers, March 2012, Saarbücken, Germany

**J. Susewind**, T. Sbrana, M. Favre, A. Ahluwalia, E.-M. Collnot, C.-M. Lehr: “The InLiveTox system – A novel microfluidic in vitro test system” New Developments in Cell-Based In-Vitro Testing and 3rd Annual Quasi-Vivo® User Group Meeting, May 2011, Saarbrücken, Germany

**Oral presentations:**

**J. Susewind**, C. Draheim, C. de Souza Carvalho, B. Loretz, C.-M. Lehr.: “*In vitro* triple culture of inflamed human intestine as a model to investigate nanoparticle safety and efficacy” 9th World Congress on Alternatives and Animal Use in the Life Sciences, August 2014, Prague, Czech Republic

**J. Susewind**, E.-M. Collnot, C.-M. Lehr: “An inflamed and non-inflamed triple culture model of the intestinal mucosa to assess cytotoxicity of engineered nanoparticles” Dechema 3D cell culture, March 2012, Zurich, Switzerland

\* The authors have equally contributed to the work

---

## Curriculum Vitae

### Personal information

<b>Name</b>	Julia Susewind
<b>Date of birth</b>	29.07.1981
<b>Address</b>	Blumenstraße 32, 66111 Saarbrücken
<b>Place of birth</b>	Saarbrücken, Germany

### PhD thesis

<b>06.2010 – 10.2014</b>	Department of Biopharmaceutics and Pharmaceutical Technology, Saarland University <i>Title: “A cell line-based co-culture model of the inflamed intestinal mucosa and its application for safety and efficacy testing of nanomaterials”</i>
--------------------------	--

### Internship

<b>01. – 06.2010</b>	Pharmacelsus GmbH, Saarbrücken, Germany
----------------------	---

### Diploma thesis

<b>01. – 11.2009</b>	Department of Epigenetics, Saarland University <i>Title: “Expression der DNA-Methyltransferasen in der Spaltheife Schizosaccharomyces pombe und Nachweis ihrer Enzymaktivität in vitro“</i>
----------------------	--

### Undergraduate study

<b>2004 – 2009</b>	Study of human and molecular biology, Saarland University
<b>2002 – 2004</b>	Study of chemistry, Saarland University

### School

<b>1992 – 2002</b>	Secondary high school “Gymnasium am Schloss”
<b>1988 – 1992</b>	Basic primary school “Rastpfuhl”

---

## Danksagung

An dieser Stelle möchte ich bei Herrn Prof. Dr. Claus-Michael Lehr für die Bereitstellung des interessanten Themas und die Betreuung meiner Doktorarbeit bedanken. Des Weiteren bedanke ich mich bei Herrn Prof. Dr. Manfred Schmitt für die Anfertigung des Zweitgutachtens sowie bei der gesamten Prüfungskommission.

Ebenfalls bedanken möchte ich mich bei Dr. Eva-Maria Collnot, die mich in den ersten beiden Jahren meiner Promotion betreut hat, und in dieser Zeit immer mit Rat und Tat zur Seite stand und bei Krankheitsfällen auch mal selbst bei Laborarbeiten ausgeholfen hat. Auch wenn nach ihrem Berufswechsel alles etwas schwierig war, habe ich in den ersten beiden Jahren viel von ihr gelernt wovon ich später profitieren konnte.

Danke an Dr. Sarah Gordon für das Korrekturlesen und an Dr. Cristiane de Souza Carvalho-Wodarz für die Betreuung im letzten Jahr. (Thanks to Dr. Sarah Gordon for proof reading and to Dr. Cristiane Carvalho de Souza for supervising me during the last year). Vielen Dank auch an Dr. Brigitta Loretz, die neben der Betreuung ihrer eigenen Doktoranden auch immer ein offenes Ohr für mich hatte und mir bei vielen Problemen helfen konnte.

Vielen Dank an Dr. Urska Repnik und Prof. Dr. Gareth Griffiths der Oslo University für das Anfertigen der TEM Bilder von meinem Zellkulturmodell.

Danke auch an Dr. Wolfgang W. Kreyling vom Helmholtz Zentrum München für das Bereitstellen der Au Nanopartikel.

Ein riesengroßes Dankeschön geht auch an das Techniker-Team: Chiara de Rossi für ihre Unterstützung am Konfokalmikroskop, Marijas Jurisic für die Hilfe bei den nicht immer so spannenden FACS-Messungen und beim Umgang mit Herrn Riedel, Heike Stumpf für die Isolation der Primärzellen und natürlich Petra König, weil sie mir eine unendlich große Hilfe in der Zellkultur war, mich bei allen Rückschlägen wieder

aufgebaut hat und immer für das ein oder andere Gespräch über unsere Katzen zur Verfügung stand.

Ein großer Dank geht auch an die beste Büropartnerin Christina Draheim, die sich tapfer mit mir durch die letzten Monate gekämpft hat. Danke fürs gute Kollegin-, Freundin-, Shoppingberaterin- und Seelsorgerin-sein!

Danke auch an meine Mitdoktoranden und Freunde, vor allem Chrissi, Florian, Emad, Stephanie, Sandra S., Jenny, Sandra G., Anne und Lutz für Kaffee-, Eis- und Mittagspausen und viele lustige Wochenenden. Und an alle Katzenfreunde am Institut für lustige Geschichten über Lucy, Djego, Marie und Co. und für die vielen geteilten Zooplus Bestellungen.

Ein riesengroßes Dankeschön an meinen Freund Simon, den ich ohne die Arbeit an diesem Institut gar nicht kennengelernt hätte, und der trotz eigenem Doktorarbeitsstress gerade in den letzten Monaten immer für mich da war, mich von der Arbeit ablenken konnte und mir bei dem ein oder anderen PC-Problem geholfen hat.

Ein besonderer Dank geht an meine Mutter Verena Susewind und meine Schwester Daniela Susewind, weil sie immer für mich da sind und mich bei allem unterstützen.

---

This work was financially supported by the project “Intestinal, Liver and Vascular Nanoparticle Toxicity *InLiveTox*” and by the EuroNanoMed project “Delivering Nanopharmaceuticals through Biological Barriers *BIBA*”.

“With magic, you can turn a frog into a prince. With science, you can turn a frog into a Ph.D and you still have the frog you started with.”

Terry Pratchett, *The Science of Discworld: A Novel*